

**THE FEASIBILITY OF QUADRUPOLE DIP IMAGING WITH PMRI: FOCUS
ON MULTIPLE SCLEROSIS**

A Senior Honors Thesis

by

EDWARD HILTON JETER

Submitted to the Office of Honors Programs
& Academic Scholarships
Texas A & M University
in partial fulfillment of the requirements of the

UNIVERSITY UNDERGRADUATE
RESEARCH FELLOWS

April 2001

Group: Engineering

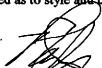
**THE FEASIBILITY OF QUADRUPOLE DIP IMAGING WITH PMRI: FOCUS
ON MULTIPLE SCLEROSIS**

A Senior Honors Thesis
by
EDWARD HILTON JETER

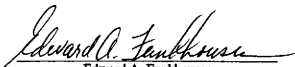
Submitted to the Office of Honors Programs
& Academic Scholarships
Texas A & M University
in partial fulfillment of the requirements of the

UNIVERSITY UNDERGRADUATE
RESEARCH FELLOWS

Approved as to style and content by:



Patrick N. Morgan
(Fellows Advisor)



Edward A. Funkhouser
(Executive Director)

April 2001
Group: Engineering

ABSTRACT

The Feasibility of Quadrupole Dip Imaging with PMRI:

Focus on Multiple Sclerosis. (April 2001)

Edward Hilton Jeter
Department of Electrical Engineering
Texas A & M University

Fellows Advisor: Dr. Patrick N. Morgan
Department of Electrical Engineering

Magnetic Resonance (MR) techniques provide valuable information for the diagnosis, monitoring, treatment, and study of many diseases. However, limitations on the sensitivity and specificity warrant the development of new imaging techniques. Quadrupole Dip Imaging (QDI) is a novel MR technique based on the magnitude of the quadrupole dip in the T_1 dispersion profile of substances containing rotationally immobilized proteins. The implementation of QDI requires field-cycled (FC) relaxometry. Prepolarized MRI (PMRI) could potentially provide a low-cost way to conduct FC experiments and thus implement QDI. I have conducted a literature review and analysis to predict the value of using QDI to study Multiple Sclerosis (MS), to determine the feasibility of implementing QDI with PMRI, and to identify obstacles to successful penetration of the technology to the clinical environment. QDI could potentially be used to non-invasively create protein density maps *in vivo*, which could provide clinically valuable information on the histopathological substrate of MS that is not available through present imaging techniques. It appears that this information will be most valuable for studies of the development and nature of the diseases instead of for diagnosis and disease monitoring. Factors that will affect the development and dissemination of QDI with PMRI include the development of PMRI T_1 -measuring pulse sequences that are robust to inhomogeneity and field ramping, the inherently small signal and dynamic range of QDI, and MR hardware acquisition trends towards high-field devices. QDI with PMRI will probably maintain or exceed conventional MRI safety, patient tolerance, and cost. I have also conducted experiments that demonstrate that PMRI can, in fact, be used to create dispersion profiles. Using the home-made PMRI scanner at the Magnetic Resonance Systems Laboratory at Texas A&M I have verified the linearity of SNR with increasing prepolarizing field strength and demonstrated qualitatively the feasibility of T_1 measurement at different field strengths for CuSO_4 (aq) and Bovine Serum Albumin/glutaraldehyde phantoms.

ACKNOWLEDGEMENTS

I am very grateful for Dr. Steve Wright, the director of the Magnetic Resonance Systems Laboratory, for his making the lab and his students available to me. At the lab Hyokwon Nam, Mary McDougall, Dan Spence, and in particular Dave Brown, provided invaluable insight, assistance, and encouragement and were incredibly patient as I struggled up the learning curve. Dr. Andy LiWang of the Department of Biochemistry and Biophysics helped me to understand the requirements for preparing protein gels and made his lab and students available to me. John Vakonakis, one of Dr. LiWang's students, helped me to prepare the gels. Dr. Robert Bryant of the University of Virginia also provided advice and encouragement on the gels. The Office of Honors Programs and Academic Scholarships, The Engineering Academic Programs Office, and the Department of Electrical Engineering at Texas A&M University provided administrative support and valuable funding. My roommates, Keith Collins, Ernie Clawson, Chad Kidder, and Kenneth Parker, have been tolerant as I have kept odd hours, scattered scribbles and journal articles about the apartment, and asked for rides to the lab and computer help at all hours. Most especially I am grateful to Dr. Patrick N. Morgan for his patience, insight, and energy.

TABLE OF CONTENTS

	Page
ABSTRACT.....	iii
ACKNOWLEDGEMENTS.....	iv
TABLE OF CONTENTS.....	v
LIST OF FIGURES.....	vi
CHAPTER	
I INTRODUCTION.....	1
II MEDICAL IMAGING.....	3
III MAGNETIC RESONANCE IMAGING.....	8
IV RELAXOMETRY WITH PREPOLARIZED MRI.....	14
V RELAXOMETRY OF PROTEIN SYSTEMS.....	26
VI QUADRUPOLE INTERACTIONS IN PROTEIN SYSTEMS.....	32
VII QUADRUPOLE DIP IMAGING WITH PMRI.....	38
VIII QDI FOR MULTIPLE SCLEROSIS.....	55
IX EXPERIMENTAL DEMONSTRATION OF PMRI RELAXOMETRY.....	68
X SUMMARY AND CONCLUSIONS.....	78
REFERENCES.....	80
VITA.....	98

TABLE OF FIGURES

FIGURE		Page
1	Two-pulse PMRI Sequence and Magnetization	14
2	Comparison of 1, 2, and 4 Parameter Models for Protein Relaxation Rate	31
3	Two-pulse PMRI Sequence and Magnetization	71
4	Magnetization versus Source Voltage in Electromagnet.....	72
5	Signal Amplitude after Prepolarizing Pulse	74
6	Inversion Recovery of CuSO_4 at 0.6 T and 0.16 T	74
7	Inversion Recovery of BSA at 0.06 T and 0.16 T.....	75

CHAPTER I

INTRODUCTION

The focus of this research is to develop medical imaging techniques that are more specific and less expensive than current techniques. In recent years Magnetic Resonance Imaging (MRI) has become a powerful imaging tool for diagnosis, treatment monitoring, and research in various pathologies. Its excellent soft-tissue contrast, safety, and 3D imaging capabilities make it an invaluable medical tool. However, its high cost, insensitivity, and lack of specificity in certain conditions lead us to seek improvements in the technology and methodology. Prepolarized MRI (PMRI) is a novel imaging technique that is significantly less expensive than current MRI hardware and facilitates the measurement of dispersion profiles. With these capabilities it should be possible to measure quadrupole dipoles and potentially implement a new form of imaging—Quadrupole Dip Imaging (QDI)—whose contrast is based on the magnitude of the quadrupole dip in a rotationally immobilized protein-containing sample. The quadrupole dip magnitude has recently been shown to be proportional to protein concentration. Thus, QDI implemented with PMRI could provide non-invasive maps of protein concentrations in tissue.

This research has two main purposes: (1) to develop an analysis of the potential benefits and pitfalls in attempting to implement QDI with PMRI in a clinical setting and (2) to provide empirical evidence that demonstrate that it is, in fact, feasible to implement QDI with PMRI. In chapters I–VII I will review briefly the MRI mechanism and its application, PMRI's development and architecture, the quadrupole interaction, and magnetic resonance phenomena in protein/water systems and will consider how these topics affect the potential capabilities and requirements for implementing QDI protein concentration mapping with PMRI. In an attempt to focus my study of the value of QDI I have chosen to use Multiple Sclerosis (MS) as a case study. Using the potential capabilities and constraints that I developed in the preceding chapters, in Chapter VIII I will review briefly the histopathological and clinical characteristics of MS and analyze potential benefits for its study arising from QDI implemented with

PMRI. In Chapter IX I will describe methods, results, and implications of experiments that I have conducted to demonstrate the practical feasibility of implementing QDI with PMRI. Throughout the thesis I will take a clinical perspective—that is, I will focus on what happens and how it can be useful clinically instead of focusing on why it happens from a theoretical viewpoint. In that spirit, I will only concern myself with the frequency range that is relevant for protein QDI—2.5 to 3.5 MHz and physiological temperature, pH, etc.

CHAPTER II

MEDICAL IMAGING

Introduction

At the risk of being trivial I will begin with a brief discussion of medical imaging. Medical imaging is a subset of the more inclusive field of what might be called "medical measurement," which concerns itself with gathering information from the body for medical purposes. Imaging refers to visualizing some portion of the interior of the body, while techniques such as the electroencephalogram provide invaluable information but no spatial localization—no pictures. Medical imaging is a relatively new development on the medical front, beginning in 1895 with Roentgen's discovery of X-rays. As a field, however, it has experienced explosive growth and diversification, with imaging modalities based on a variety of physical phenomenon now available.

Medical measurement can be divided into two broad categories of techniques: active and passive. Passive techniques measure energy that is transmitted from the body without any direct stimulus being applied. An example of a passive medical measurement technique is thermal imaging, or even more basic, taking a temperature reading with a thermometer. Active techniques require that energy be applied to the body and then the body's reaction to that energy measured—its transmission, re-emission, reflection, etc. Examples of active techniques include X-rays, ultrasound, and MRI. The major contemporary medical imaging modalities are all active procedures.

Medical measurement can be further categorized by the degree of invasiveness. Techniques range from the totally invasive—cutting the patient open and looking—to the completely non-invasive, where there is no physical contact between the imaging device and the patient. Invasive techniques have higher risk, discomfort, and cost than non-invasive techniques and in many cases would cause more damage to the patient's quality of life than the pathology to be studied. Thus, it is desirable to develop and improve non-invasive measurement techniques. Many valuable techniques fall in a category that might be called "pseudo-non-invasive," where the imaging itself is conducted non-invasively but a contrast agent is injected subcutaneously to improve the image quality.

Medical imaging has several applications. These include asymptomatic screening, diagnosis, surgical planning, intra-operative guidance, treatment monitoring, treatment development (i.e., determine efficacy of a treatment), and research on etiology, development, histopathology, etc. Thus, imaging helps

find treatable conditions before they manifest clinically, provides or confirms diagnosis of conditions, makes surgery more precise, accurate, and efficient, helps to tailor treatments to an individual patients disease progression, and provides major support for research on how diseases and conditions work.

For medical technology to be useful it must be clinically and economically viable. That is, the risk/benefit and cost/benefit analyses of the physician, patient, and sponsoring institution must indicate that the system is worth using. The four major criteria in these decisions are:

- 1) Functionality (how well does it work)
- 2) Safety (to patient and staff)
- 3) Cost (to patient and institution)
- 4) Comfort (for patient and staff)

Metrics

Metrics are parameters that attempt to quantify the efficacy of a modality so that different imaging modalities can be compared. These measures of value can come from the engineering or the clinical realm. Some of the most important measures of value are:

1. Sensitivity
2. Specificity
3. Throughput
4. Signal to Noise Ratio (SNR)
5. Contrast and Contrast to Noise Ratio (CNR)

Sensitivity

Sensitivity is a measure of how subtle of an abnormality can be detected—the precision of the modality. It is defined conceptually as the percentage of total abnormalities detected, i.e., if a hundred patients with a particular type of tumor a scanned and the scans indicate that ninety-five of the patients have tumors then the scanner has a sensitivity of 95%. Similarly, if a scan of a single patient with 100 lesions indicates only 95 lesions then sensitivity is 95%. Although a very important statistic, sensitivity does not communicate how accurate an imaging modality is.

Specificity

Specificity is a quantitative measure of the accuracy of an imaging modality, i.e., how many times the modality says that there is an abnormality when there really isn't (false-positive) and how many times the modality says that there is not an abnormality when there really is (false-negative). Qualitatively this translates into a measure of how unambiguously the modality can indicate the precise nature of a given pathology—i.e., can it tell different diseases and conditions apart. For example, suppose a scan

detects two tumors, one malignant and the other benign, but both of them appear as white spots on the image. The modality does not provide specific information about the tumors, just the facts of their existence and location. If the tumors were in different patients (and in the absence of other information) then one of the patients would receive an inaccurate diagnosis. Specificity is related to sensitivity in that if a modality has a low sensitivity (i.e., does not detect abnormalities that are really there) then it will have a high false-negative rate.

Throughput

Throughput is simply the number of patients an imaging modality can image per unit time while maintaining acceptable sensitivity, specificity, etc. Throughput is important for patient comfort and economic cost effectiveness.

Signal, Noise, and Systematic Error

Sensitivity, specificity, and throughput are primarily clinical measures of value. They derive from the inherent functionality of the imaging modality and engineering measures of image quality such as signal amplitude and its magnitude relative to adjoining signals, noise, and error. The observed signal in a non-dynamic imaging modality (i.e., a modality that images non-moving objects), $S(r)$, is a function of the position, r , of the tissue that originates the signal for given imaging parameters. It consists of three parts:

1. Energy that contains useful information
2. Non-random systematic errors
3. Random errors (noise)

Therefore, even if there is no useful signal there might still be some signal that fluctuates randomly about some non-zero value. Noise, $n(t)$, is a time-variant fluctuation in the signal caused by random, unpredictable processes. The major source of noise is random thermal motion of molecules in the sample and the measuring equipment. Careful, and usually more costly construction, can reduce some of the noise arising from the equipment. The magnitude of noise depends on inherent characteristics of an imaging technique and the sample or patient to be imaged. Since noise is random, its expectation value is zero,

$$\langle n(t) \rangle = 0 \quad (1)$$

Since noise is unpredictable it is difficult to model. Its magnitude is often expressed as the first standard deviation of some "representative out of bandwidth" signal, whose distribution is assumed to be Gaussian. For a digitized signal with a set of data points, D , and Gaussian probability distribution function, $p(n(t))$, the noise is calculated as:

$$\sigma_n = \sqrt{\sum_D [n(t) - \langle n(t) \rangle]^2 p(n(t))} \quad (2)$$

Although much noise can be removed from a signal in post-processing, noise exerts a fundamental limitation on the amount of information that is available in a signal. Post-processing can make the image look better but it cannot add information that was obscured by noise in the signal acquisition. Systematic error includes errors that arise from predictable (non-random) phenomena. The expectation values of systematic errors are therefore non-zero. They arise from limitations in manufacturing precision and experimental design flaws. Since systematic errors are predictable some of them can be corrected through careful experimental or hardware design or modeled and then removed in post-processing.

Signal to Noise Ratio (SNR), Contrast, and Contrast to Noise Ratio (CNR)

One of the most important engineering measures of value is the signal to noise ratio (SNR), which is usually defined as the magnitude of the signal divided by the standard deviation of the noise signal as defined above.

$$SNR = \frac{|S(r)|}{\sigma_n} \quad (3)$$

SNR is limited by intrinsic features of the imaging modality, which determine the maximum possible signal magnitude and the smallest possible noise. A high SNR adds confidence to the interpretation of the image since the possibility of some noise obscuring information and thus leading to some erroneous conclusion is reduced. Therefore, increased SNR corresponds potentially to increased sensitivity. However, high SNR does not necessarily translate into greater clinical value, as inadequate contrast could still obscure important information.

Contrast is defined as the difference between the magnitude of the useful signal, $S(r)$, and the non-useful signal, $S_{nu}(r)$. This non-useful signal can be due to systematic error or signal from surrounding tissue. To illustrate the significance of contrast, consider a scanner that assigns a grayscale value of 0.8 to edematous tissue and 0.75 to normal tissue. Even if the SNR were high enough that we could neglect random errors it would still be virtually impossible to distinguish between the pathological and normal tissue. The contrast to noise ratio (CNR) provides a useful measure of contrast between the useful and non-useful signal and the noise:

$$CNR = \frac{|S(r) - S_{nu}(r)|}{\sigma_n} \quad (4)$$

Every imaging system has a human at the interpretation level and often at several other levels. This introduces random and systematic errors and tempers the usefulness of quantitative measures of value. The skill of the radiologist at interpretation can shift the relative importance of SNR and CNR.

Imaging Modalities

There are several different ways of imaging the body non-invasively or pseudo-non-invasively. Some of the most prevalent techniques include computerized X-ray tomography (CT), ultrasonography, nuclear imaging, and magnetic resonance techniques. X-ray CT has high spatial resolution, low-cost, high throughput but it uses ionizing radiation, has a low temporal response, and low soft-tissue contrast. Ultrasound provides low-cost, safe, repeatable, high throughput imaging, but it has relatively low image quality, and is limited by acoustic windows. Nuclear techniques provide metabolic and tissue viability information and functional imaging but use ionizing radiation, are very expensive, and are contraindicated for many patients. MRI provides precise 3D information, high soft tissue contrast, and uses no ionizing radiation. However, it is relatively expensive, has a spatial resolution that is lower than CT's, is contraindicated or uncomfortable for some patients, and has a low throughput.

Conclusion

Medical imaging provides valuable information that increases the effectiveness of medical practice. There are many different imaging modalities available with varying sensitivity, specificity, and throughput. SNR and CNR are important measures of value to consider when trying to improve medical imaging from the engineering perspective. Magnetic Resonance Imaging (MRI) offers precise 3D images with high soft tissue contrast.

CHAPTER III

MAGNETIC RESONANCE IMAGING

Introduction

Magnetic Resonance Imaging (MRI) creates images based on the response of certain atoms, usually Hydrogen, to static and dynamic magnetic fields. The underlying principles for MRI were discovered independently in 1946 by Bloch (Bloch, 1946) and Purcell, Torrey, and Pound (Purcell et al., 1946). Under the name Nuclear Magnetic Resonance (NMR) these principles contributed and continue to contribute valuable information in physics and chemistry. In 1973 Lauterbur demonstrated a technique for creating images with NMR (Lauterbur, 1973). In the early 1980's clinical application of this imaging technique began in earnest and has since experienced explosive growth, becoming the major imaging modality for many pathologies. In the clinical imaging context it is called Magnetic Resonance Imaging (MRI) to alleviate public concerns about all things nuclear. Other than the spatial localization necessary for imaging and MRI's focus on single resonances and not the whole spectrum, there is no fundamental difference between NMR and MRI. In this chapter I will review briefly the underlying principles of magnetic resonance (MR) and imaging, various MR techniques such as T_1 , T_2 , and proton density weighting, MR clinical applications—particularly diagnosis, and general hardware considerations.

MR Physics

I will give a superficial overview of the relevant physics. A detailed analysis is beyond my understanding and unnecessary for the purposes of this thesis. The principle sources for my overview are a monograph by Abragam and a textbook by Nishimura (Abragam, 1961; Nishimura, 1996).

Magnetic Moments

Atoms with an odd number of protons and/or an odd number of neutrons possess “spin angular momentum,” which gives rise to a magnetic dipole moment, $\mu = \gamma \hbar \mathbf{I}$, where \mathbf{I} is the spin operator, a dimensionless vector from quantum mechanics that takes integer or $1/2$ -integer values, $\hbar = 1.06 \text{ E}^{-34}$ [Joule seconds], is Planck's constant divided by 2π , and γ is the gyromagnetic ratio, which is a constant for a given nuclear species with units of frequency/magnetic flux density. Interactions of this magnetic dipole moment with externally applied static and dynamic magnetic fields give rise to magnetic resonance phenomena.

Magnetization and Precession

From a classical viewpoint, if a static external magnetic field, \mathbf{B}_0 , is applied to a sample containing atoms with magnetic moments, μ , these atoms will tend to align with the external field, thus generating a magnetization vector, $\mathbf{M} = \sum \mu$. However, quantum mechanics indicate that some of the atoms will align parallel to \mathbf{B} and some anti-parallel. The anti-parallel configuration is a higher energy state and so most of the atoms will tend to the parallel alignment. However, even at thermal equilibrium, thermal energy is sufficient to cause some atoms to align anti-parallel. Thus \mathbf{M} can be conceived as the sum of two magnetization vectors arising from a population of parallel atoms, n_+ , and anti-parallel atoms, n_- . The relative proportions of the populations at equilibrium is given by the Boltzmann distribution as $n_-/n_+ = e^{-\Delta E/kT}$ where $\Delta E = \gamma \hbar B_0$ is the energy difference between the parallel and anti-parallel states, $k = 1.38 \text{ E-}23$ [Joules/Kelvin] is Boltzmann's constant, and T is the temperature in Kelvin. At thermal equilibrium \mathbf{M} and \mathbf{B} are collinear and $|\mathbf{M}| = M_0$. If \mathbf{M} is caused to move out of alignment with \mathbf{B} then, again, using the classical model, there is a torque applied to \mathbf{M} , given by:

$$\frac{d\mathbf{M}}{dt} = \mathbf{M} \times \gamma \mathbf{B} \quad (5)$$

The solution of equation [5] is for \mathbf{M} to nutate about the axis of \mathbf{B} with a frequency known as the Larmor frequency, $\omega_L = \gamma |\mathbf{B}|$. The fact that in a magnetic field an atom can assume more energy states (i.e., the parallel and anti-parallel configurations) is called Zeeman splitting after Pieter Zeeman (1865–1943), the Dutch physicist who first observed it in 1896. The Larmor frequency is named after Joseph Larmor (1857–1942), an English physicist. Applying a radio-frequency (RF) electromagnetic pulse, \mathbf{B}_1 , orthogonal to \mathbf{B} with duration Δt and frequency equal to the Larmor frequency of the target atoms will cause \mathbf{M} to move out of alignment with \mathbf{B} by an angle $\alpha = \gamma \Delta t B_1$ by altering the proportion of the parallel and anti-parallel populations.

Relaxation: The Bloch Equation

After perturbation by an RF pulse, \mathbf{M} will tend to realign itself with \mathbf{B} . The phenomenological description of the realignment was given by Bloch (Bloch, 1946) as:

$$\frac{d\mathbf{M}}{dt} = \mathbf{M} \times \gamma \mathbf{B} - \frac{M_x \mathbf{i} + M_y \mathbf{j}}{T_2} - \frac{(M_z - M_0) \mathbf{k}}{T_1} \quad (6)$$

where M_0 is the equilibrium magnetization, i , j , and k are orthogonal unit vectors in the x , y , and z directions (by convention, B is along the z -axis), and T_1 and T_2 are time constants. After RF perturbation the component of M along the z -axis, M_z , grows with time constant T_1 . The transverse component, M_{xy} , shrinks with time constant T_2 . The energy stored in the system by the RF pulse is originally manifested as the higher energy state of the non-aligned M . This energy flows into other facets of the system as M realigns with B . There are, in general, two independent exponential pathways for this energy flow from the magnetized spins: spin-lattice, longitudinal, or T_1 relaxation and spin-spin, transverse, or T_2 relaxation. T_1 is the time constant of for the perturbed spins to reach thermal equilibrium with the surrounding system or lattice. T_2 is the time constant of energy transfer between spins. Since the atoms are close together and each has their own magnetic field, each atom experiences a magnetic field that is a combination of the external field and the fields from its neighbors. Since each atom experiences a different field each has a slightly different Larmor frequency and thus the transverse magnetization vector loses coherence as each atom's magnetization vector dephases with the surrounding magnetization vectors. T_1 and T_2 are different for various tissues. These differences are the primary source for contrast in conventional magnetic resonance imaging.

Detection of MR Signal

According to Faraday's law, a changing magnetic flux, Φ , will induce an electromotive force in a conducting coil that is proportional and opposite in sign to the rate of change of the magnetic flux. Since M is precessing about the z -axis it will induce a time varying current in an appropriately positioned conducting receiving coil. This induced current will have the same frequency as the precessing magnetization and the current's magnitude will be proportional to the magnitude of the magnetization. This current signal can then be processed using electrical methods. This signal is an exponentially decaying sinusoid called a Free Induction Decay (FID). In the process of generating, amplifying, transmitting, and processing the MR signal there are various factors that will scale its magnitude linearly. When modeling signal intensity these factors are usually lumped together into a system constant, K .

Spatial Localization

By applying spatially varying magnetic fields it is possible to associate frequency with the location of a small cubic region in the region of interest (ROI). Each cubic region is called a voxel. Through Fourier transformation it is possible to convert the time-varying signal to a spatially varying signal. Through appropriate pulse sequencing this can be used to generate 3D images—usually as a series of planar images.

MR Formats

There are two broad categories for MR application: spectroscopy and imaging. Spectroscopy collects signal from the entire sample and observes changes in resonant frequency for atoms in various configurations. Spectroscopic methods are an important tool in the chemistry and physics laboratory for differentiating between different compounds and studying the conformations of molecules. In this application it is usually called NMR spectroscopy and sometimes magnetic resonance spectroscopy (MRS). As indicated earlier, imaging involves correlating signals with spatial locations—making pictures. Magnetic resonance imaging (MRI) creates images based on the variations in signal intensity from a single nuclear species, usually Hydrogen. Magnetic resonance spectroscopic imaging (MRSI) provides the information of NMR spectroscopy together with spatial localization.

All three general approaches, MRS, MRSI, and MRI, have important clinical applications and are areas of active research. The MRI format, however, has had the most extensive application due, among several other factors, to its much greater resolution and relative ease of interpretation. As indicated above, MRI images derive contrast from the relative signal intensities from the Hydrogen atoms in each voxel. Changing the imaging parameters modifies the intensity variation and thus the contrast basis. Using different contrast bases makes MRI a more robust diagnostic tool, since some pathologies are invisible to some contrast bases. Commonly used approaches are quantitative T_1 and T_2 imaging, T_1 and T_2 weighted imaging, and magnetization transfer imaging (MTI). T_1 and T_2 , as explained previously, are tissue-specific parameters that describe how fast a perturbed system returns to equilibrium. A conceptually simple approach to MR imaging is to calculate the values for T_1 or T_2 for each voxel in the region of interest (ROI). However, it is relatively difficult and time consuming to make precise quantitative measurements of T_1 or T_2 and, as will be discussed later, the clinical value is limited. It is much easier to make images that emphasize the relative differences between tissues in one of these parameters. For example, in the spin-echo pulse sequence the signal is proportional to several factors:

$$\text{Signal} \propto M_0 \left(1 - e^{-TR/T_1}\right) e^{-TE/T_2} \quad (7)$$

where TE and TR are adjustable sequence parameters. If we make TR very long with respect to all of the T_1 values in the ROI, i.e., $TR \approx 5T_1$, then the signal reduces to a function of the T_2 relaxation and the differences in signal intensities between pixels in the image will depend solely on the differences in T_2 in the corresponding voxels. Thus, we have created a T_2 -weighted image. A conceptually similar approach can be used to create T_1 weighted images.

Diagnosis with MRI

MRI is primarily useful for its contribution to diagnosis of diseases and conditions. I will review briefly the history, approaches, and some of the factors affecting MRI's efficacy as a diagnostic modality.

The Diagnostic Problem

To diagnose a disease or condition we need measurable parameters that are different in pathological and normal substrates. To be a "stand-alone" diagnostic parameter that can indicate the diagnosis without any other tests the parameter for pathological tissue needs to exceed the range of the parameter for the normal tissue with high statistical significance—there should be no overlap between the parameter values for normal tissue and pathological tissue. Furthermore, the parameter should enable us to differentiate between different pathologies and abnormalities—for example, between benign and malignant tumors. For non-invasive imaging diagnostic modalities there are two basic approaches—what might be called the quantitative and qualitative approaches. The quantitative approach is the most desirable. It measures parameters quantitatively and then compares the results to known values for normal and pathological tissue, which are distinctly separated. Diagnosis then becomes the simple procedure of making the measurement and looking up the significance of the result in a table. The qualitative approach looks for changes in time or in space that might indicate pathology. On an image this would mean a "spot" that changed shape, position, or intensity in serial images or a spot where normal anatomy would not predict one. The relative approach is not as specific, in theory, as the quantitative approach. However, the heterogeneity of pathology and anatomy in a population and within an individual patient make the relative approach much more practical and reliable.

History and Efficacy of Diagnosis with MR

In their 1987 review, Bottomley et al indicate that Hazlewood et al were the first to report MR measurements that indicated differences between normal and pathological tissues (Bottomley et al., 1987). They reported significant differences in the line widths of dystrophic muscle and normal muscle (Hazlewood et al., 1969). Very soon thereafter Damadian published differences in T_1 and T_2 of excised cancerous rat tissue versus normal tissue (Damadian, 1971). However, further observation showed that for most tissues and pathologies there was too much overlap in parameter ranges for specific diagnosis based on simple quantitative analysis of MR parameters (Bottomley et al 1987). Various approaches have been and are still being explored that would allow simple, quantitative analyses that gave specific diagnoses. Examples include the malignancy index (Goldsmith et al., 1977; Goldsmith et al., 1978; Koutcher et al., 1978) and magnetization transfer ratios (Gass et al., 1994; Phillips et al., 1998; van Waesbergh et al., 1998).

The advent of MR imaging greatly improved the diagnostic utility of MR techniques. With imaging it became possible to identify focalized abnormalities such as tumors, lesions, and tears without having to rigorously define a "normal" condition. The clinician could look for "spots" where a localized pathology had altered the MR signal intensity relative to the adjacent tissue. Although the sensitivity and specificity are still limited, this application of MR technology to diagnosis has had a major impact on research and clinical medicine. Hutchison et al reported the first *in vivo* human T_1 measurements and images (Hutchison et al., 1980; Edelstein et al., 1980).

Conclusion

Magnetic Resonance Imaging creates images based on the variable response of tissue atoms to static and dynamic magnetic fields and radio-frequency pulses. It is a relatively new technique with the physical principles being discovered in the 1940's and clinical application beginning in earnest in the early 1980's. It has since experienced explosive growth in clinical application to become one of the principal paraclinical imaging tools.

CHAPTER IV

RELAXOMETRY WITH PREPOLARIZED MRI

Introduction

The original nuclear magnetic resonance experiment with liquids was conducted with a magnetic field strength between 0.165 T and 0.22 T (Bloch et al., 1946). The first successful experiment with solids was at a field strength of 0.7 T (Purcell et al., 1946). Since then the general trend of research and technology development has been on stronger and stronger field strengths because of the generally higher spatial resolution, thinner image slices, greater contrast, shorter acquisitions, and specific high-field applications. It appears that the main thrust of future development will also follow the high-field approach (Bradley, 1996). Currently, most clinical MRI scanning is done at 1.5 T and some research is conducted with field strengths as high as 45 T (for example, NHFML, 2001).

However, low-field's lower cost, easier maintenance, smaller space requirements, and ability to examine some unique low-field phenomenon have kept it in the research "picture." The literature has various classifications of field strength such as ultra-low, low, intermediate, etc. For the present article I will define "low-field" to mean $B_0 < 1.0$ T. A great deal of research has been done on improving MRI techniques at low-fields and developing applications that are specific to low-field imaging. Among the developments are field cycling (FC) and relaxometry.

Field Cycled MR

MR studies that utilize two or more magnetic field strengths are called field-cycled (FC) experiments. Conventional MR imaging, i.e., that which has achieved the broadest commercial distribution and the most research attention, uses a single, fixed-value magnetic field to create images. Noack and Kimmich have published reviews on FC (Noack, 1986; Kimmich, 1980). The sample is placed in a polarizing magnetic field to achieve magnetization, the field is then switched to an evolution field strength for the sample to relax, and finally, the field is switched to a readout value. Each of the three fields is optimized for noise considerations. The amplitudes of the fields can be changed to create dispersion profiles. Packard and Varian appear to be the first to use a prepolarized technique (Packard and Varian, 1954) followed quickly by Bloom and Mansir (Bloom and Mansir, 1954). Béné and his group in Geneva have made significant contributions, which have been continued by Borcard and others (for example, Béné, 1980; Borcard, 1987). Noack references several other groups that have published field-cycling studies or built FC hardware (Noack, 1986). Bratton et al conducted the first dispersion studies of

human tissue in 1965 (Bratton et al., 1965). Knispel et al were the first to report on the frequency dispersion of pathological tissue with their 1974 study of mammary adenocarcinomas implanted in mice (Knispel et al., 1974). Several groups have made recent contributions toward bringing FC techniques to the hospital. These include Carlson, who focused on the potential clinical value of relaxometry (Carlson and Crooks et al., 1992; Carlson and Goldhaber et al., 1992), Macovski and Conolly, who focused FC as a way to increase SNR and reduce cost (Macovski and Conolly, 1993; Morgan et al., 1995; Morgan et al., 1996a-c; Morgan, 1999; Conolly et al., 1994), and Lurie, who developed field cycled proton-electron double-resonance imaging (PEDRI; Lurie et al., 1988, 1989, 1998) and have worked with FC-MRI (Baras et al., 1999). Koenig and Brown, among other contributions to the field, have recently provided a review and a theoretical understanding of relaxometry (Koenig et al., 1993; Koenig and Brown, 1991; Koenig, 1995).

Relaxometry

FC is used to (1) increase SNR for a given field strength and (2) measure the effect of field strength on the signal. A graph of relaxation time (T_1 or T_2) or relaxation rate ($1/T_1$ or $1/T_2$) versus field strength is called a dispersion profile. The study of the field strength dependence of relaxation is also called relaxometry, although the terms FC and relaxometry are sometimes used interchangeably. Relaxometry has been suggested for a variety of applications (Rinck et al., 1988; Carlson and Goldhaber et al., 1992b). FC relaxometers would provide a convenient stage to evaluate and optimize the field dependence of intravenously injected contrast agents (for example, Kormano et al., 1988; Muller et al., 1988; Rinck et al., 1988). Contrast between some pathologies and normal tissue and between different types of tissue, such as gray and white matter, is also field dependent and is optimized at frequencies from 10 to 25 MHz (Rinck et al., 1988; Fischer et al., 1990). A clinical relaxometer could be adjusted to provide optimum contrast depending on the tissues to be imaged. Also, in some cases the dispersion profile appears to provide diagnostic information. For example, preliminary indications are that relaxometry might be able to indicate the level of necrosis in glioblastomas (Spiller et al., 1995) or differentiate between secretory and non-secretory pituitary adenomas (Spiller et al., 1997). Other pathologies are being explored (for example, Lundbom et al., 1990; Spiller et al., 1994).

Prepolarized MRI (PMRI)

Prepolarized MRI (PMRI) is a low-cost implementation of FC techniques in imaging format (Macovski and Conolly, 1993). Carlson called the technique Switched Field MRI (Carlson and Crooks et al., 1992a) and Lurie's group called it Field Cycled MRI (Baras et al., 1999). As mentioned earlier, Packard and Varian appear to be the first to use a prepolarized technique (Packard and Varian, 1954) followed quickly by Bloom and Mansir (Bloom and Mansir, 1954). The early literature refers to this technique as the "earth's field technique" and the prepolarizing pulse as the "soak field" (Noack, 1986).

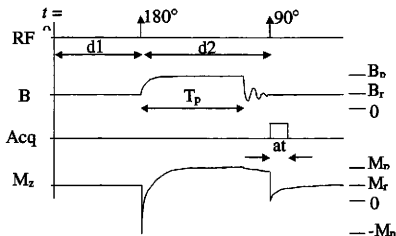


Figure 1: Two-pulse PMRI Sequence and Magnetization. Acq is the acquisition timing, M_z is the z-magnetization, B_p is the prepolarizing field strength, B_r is the readout field strength, M_p and M_r are the equilibrium magnetizations corresponding to B_p and B_r , respectively. The 180° pulse inverts the magnetization to $-M_p$, which then grows toward M_p with time constant T_p . When the prepolarizing pulse is turned off the magnetization decays toward M_r with time constant T_{1r} until the 90° pulse moves the magnetization vector into the transverse plane to be read out.

The PMRI technique utilizes two magnetic fields: a static readout field, B_0 , and a pulsed polarizing field, B_p . An example of a prepolarized pulse sequence is shown in Figure [1]. The prepolarizing field is pulsed for a time, T_p , and then turned off and the signal is readout at the main field strength, B_0 .

Effect of Prepolarization

To more fully illustrate the prepolarizing effect I will apply a slightly more rigorous treatment to the pulse sequence shown in Figure [Error: Reference source not found.] for a homogeneous sample with a "perfect" 90° tip angle and uniform fields, B_0 and B_p , aligned along the z-axis, i.e.,

$$\mathbf{B}_0 = B_0 \mathbf{a}_z \quad , \quad \mathbf{B}_p = B_p \mathbf{a}_z \quad (8)$$

As mentioned earlier, magnetization and relaxation are governed by the Bloch equation (Bloch, 1946):

$$\frac{d\mathbf{M}}{dt} = \mathbf{M} \times \gamma \mathbf{B} - \frac{M_x \mathbf{a}_x + M_y \mathbf{a}_y}{T_2} - \frac{(M_z - M_0) \mathbf{a}_z}{T_1} \quad (9)$$

M_o is the value of magnetization in the sample at equilibrium under the influence of B . Solving the Bloch equation, equation [9], for the z-axis magnetization under these conditions for a given field strength, B , in the rotating frame yields

$$M_z(t, B) = M_z^i e^{-t/T_1(B)} + [M_o(B)](1 - e^{-t/T_1(B)}) \quad (10)$$

where M_z^i is the initial value of the magnetization along the z-axis. Magnetization is related to magnetic field strength by the magnetic susceptibility, κ_m . Since M_o and T_1 are both dependent on field strength and the prepolarized pulse has two field strengths there are two values of each:

$$M_o(B_r) = \kappa_m B_r = M_{or} \quad , \quad M_o(B_p) = \kappa_m B_p = M_{op} \quad (11)$$

$$T_1(B_r) = T_{1r} \quad , \quad T_1(B_p) = T_{1p} \quad (12)$$

If we assume that the sample has reached equilibrium magnetization in the static field before we turn on the prepolarizing pulse at time $t = 0$, then the z-axis magnetization will grow from M_{or} to M_{op} with time constant T_{1p} .

$$M_z(t) = M_{or} e^{-t/T_{1p}} + M_{op} (1 - e^{-t/T_{1p}}) \quad (13)$$

If we turn off the pulse at time, $t = T_p$, immediately apply a perfect 90° pulse, and ignore any non-idealities such as ramp down time, ringing, etc., then the z-axis magnetization will go to zero and then grow back to M_{or} with time constant, T_{1r} .

$$M_z(t) = M_{or} (1 - e^{-(t-T_p)/T_{1r}}) \quad (14)$$

Homogeneity of B_p and B_r

Conventional MRI requires a very homogenous magnetic field since inhomogeneity decreases the phase coherence of the precessing spins and thus destroys the signal quality and the ability to do spatial localization for imaging. The homogeneity sensitive or limited part of the imaging is the acquisition, so the readout field, B_r , must be very homogeneous, while the magnetizing or polarizing part of the imaging can tolerate more inhomogeneity.

Consider a sample in the classical view of MRI with one magnetization vector per voxel. If the sample is magnetized with a pulsed, temporally uniform but somewhat spatially inhomogeneous prepolarizing field along the z-axis and allowed to come to steady state then the magnetization vectors will vary in magnitude from voxel to voxel due to the spatial inhomogeneity but will all be aligned with the z-axis. Therefore, when the prepolarizing pulse is turned off and some component of the magnetization vectors are tipped into the xy-plane, which causes the vectors to nutate, the vectors will be in phase. Since the readout field is very homogeneous there will be little dephasing during readout. The variations in magnetization vector amplitude caused by inhomogeneity in the prepolarizing pulse manifest themselves as slight intensity shading in the final image. Macovski and Conolly report that prepolarizing field variations of up to 20% can be tolerated (Macovski and Conolly, 1993). Morgan et al present calculations for the required homogeneity of the readout field for a given receiver bandwidth and field of view (Morgan et al., 1996).

Strength of B_p and B_1 and SNR

A high readout field, B_1 , increases the sensitivity to inhomogeneity, susceptibility errors, and chemical shift distortion, so it is advantageous to keep B_1 small (Macovski and Conolly, 1993; Scott et al., 1994). Following arguments presented by Morgan et al we can estimate the effect of B_p on SNR in FMRI (Morgan et al., 1996). The traditional formula for SNR applied to PMRI yields (Hoult and Lauterbur, 1979; Edelstein et al., 1986):

$$SNR \propto \frac{\omega B_1 B_p \Delta V \sqrt{T_{acq}}}{\sqrt{T_s R_s(\omega) + T_c R_c(\omega)}} \quad (15)$$

where B_1 is the receiver coil sensitivity, ΔV is the voxel size, T_{acq} is the total imaging time, T_s and T_c are the sample and receiver coil temperatures, and R_s and R_c are the sample and receiver coil resistances. We ignore here noise introduced by other parts of the circuitry. The inductive sample resistance and coil resistances are frequency dependent: $R_s \propto \omega^2$ and $R_c \propto \sqrt{\omega}$ (Hoult and Lauterbur, 1979). When the sample noise dominates the coil noise, i.e., $T_s R_s(\omega) \gg T_c R_c(\omega)$, equation [15] reduces to

$$SNR \propto \frac{B_p \Delta V \sqrt{T_{acq}}}{\sqrt{T_s}} \quad (16)$$

Thus, SNR is proportional to the polarizing field strength and is independent of the readout field strength. If the readout strength is B_r , for a given prepolarized value of B_p , PMRI offers a factor of B_p/B_r increase in SNR over doing conventional MRI imaging. The increase of SNR with B_p has been verified experimentally (Morgan et al., 2000; Carlson and Crooks et al., 1992).

Implementing PMRI at medium or high fields would make the technical and the bioeffect issues much more significant and would detract from the cost and SNR improvement benefits (Carlson and Goldhaber et al., 1992). Switching at high fields requires a great rate of change in the field strength, dB/dt , which can cause magnetophosphenes and nerve stimulation (Marg E, 1991; Cohen et al., 1989). Also, the marginal increase in SNR for a given B_p decreases—in order to achieve a similar percent change in field strength as a low-field PMRI system requires significantly more power, since in a resistive magnet field strength is proportional to current, $B_p \propto I$, and power dissipation is proportional to the square of the current, $P = I^2R$.

Cost of PMRI

One of the most striking outcomes from this discussion on homogeneity and SNR in PMRI is that it enables the PMRI scanner to be built with low-cost components. Although the B_r magnet needs to be homogeneous its field strength requirements are low and can be satisfied by a relatively low-cost, low-field permanent or resistive magnet. Although B_p needs to have a strong field its homogeneity requirements are low, so it can be a smaller, lower cost, resistive magnet. Thus, PMRI can be much less expensive than the high-field superconductive MRI scanners currently popular for clinical scanning in the U.S. Some factors that determine the cost of MRI and PMRI scanners are:

- 1) Initial Hardware—magnet and controller.
- 2) Shielding/Housing/Installation
- 3) Maintenance/Support—Cooling, power supply, environmental control, repairs, upgrades.
- 4) Personnel to position the patient, conduct the scan, interpret the results.

MRI hardware is expensive—typically between \$500,000 and \$2.5 million for conventional units and between \$2.5 and \$10 million for specialized, higher-field units. Although hardware prices have decreased (Hisashiga, 1994) the initial capital outlay remains high. Initial cost follows field strength and magnet type, with resistive or permanent magnets being much cheaper than super-conducting magnets. The construction of a PMRI system requires a whole body magnet, an imaging console, an electromagnet (~ \$10,000), power supply (~ \$20,000), pulsing circuitry (~ \$5,000), and software, installation, and training (~ \$25,000). If we assume that a low-field system with a whole-body magnet and a console can be acquired for \$500,000 (for example, a GE Medical Systems Profile/o 0.2 T dedicated scanner, GE Medical

Systems, 2001) then the conversion to PMRI requires approximately a 12% increase in system cost. The normal trade-off in MR equipment cost evaluation is SNR and special techniques versus cost. With PMRI the SNR reduction is much less significant. Also, if special techniques such as quadrupole dip imaging prove useful then this will reduce the tradeoff loss further.

To install an MRI or PMRI system requires dedication and preparation of an imaging environment. This includes preparing a floor that can support the weight of the system and an imaging area free of electromagnetic interference and devices that would be susceptible to interference from the magnet. Higher field systems are more sensitive to chemical shift susceptibilities and therefore require greater shielding. Superconducting magnets create a field with an air return path and thus require more floor and room space. In resistive and permanent magnets the return path is through the frame of the magnet so the fringe fields do not extend far from the magnet. There are also costs associated with transporting the magnet and calibrating and configuring the system. One author gives a range of installation costs as \$50,000 to \$1 million, with the more expensive higher-field and superconductive magnets requiring the more expensive installations. Again, since PMRI is a resistive and permanent magnet system it avoids costlier installation outlays. Superconductive magnets require cryogenic cooling, which adds a major maintenance cost. Permanent magnets are sensitive to ambient temperature and thus require air conditioning. Resistive magnets require large power supplies. In the PMRI system the resistive magnet is pulsed, which reduces the power requirements and since most hospitals in the U.S. are climate controlled anyway, maintaining the PMRI magnet in a constant ambient temperature and supplying it with power are much less expensive than keeping a superconducting magnet cooled. Clinical personnel to perform and interpret the scans are a significant cost, to be sure, but they do not vary significantly between low field, high field, or prepolarized MR systems.

Pulse sequence for T_1 Relaxometry with PMRI

Relaxometry can be implemented with PMRI by changing the magnitude of the prepolarizing pulse. Morgan and Nam have demonstrated the design and construction of appropriate, low-cost pulsing circuitry (Nam et al., 2000). The construction PMRI is potentially a cost-effective way to implement clinical relaxometry imaging. Because of the disadvantages of larger aperture pulsed magnets, it is probably going to be most effective for head and extremity imaging or possibly, with surface field coils, heart imaging (Carlson and Goldhaber et al., 1992). As will be discussed in later chapters, this could provide valuable diagnostic and monitoring information.

PMRI Pulse Sequence Constraints

To implement T_1 relaxometry with PMRI in a clinical setting we must select a pulse sequence that is:

- 1) Adaptable to PMRI

- 2) Robust at low fields
- 3) Robust with imperfect tip angles
- 4) Relatively quick
- 5) Precise and accurate

The presence of the prepolarizing pulse introduces several challenges to the task of selecting a pulse sequence. Since the prepolarizing pulse is very inhomogeneous it would be very difficult to achieve acceptable SNR and contrast if the RF pulses were applied while the prepolarizing pulse were on. This is overcome by switching the prepolarized pulse off and reading out in the homogeneous static field. There are two main difficulties: (1) we want to measure the MR parameters of the sample at the prepolarizing field strength and (2) there might be residual effects from the prepolarizing field inhomogeneity and errors induced in the switching. Other relaxometry techniques have had control over the readout field strength (for example, Kimmich, 1980; Noack, 1986). PMRI does not have that luxury.

As described earlier, the electromagnet inhomogeneity will cause the magnitude of the magnetization vector in each voxel to be slightly different. But, for pulse time, T_p , long relative to T_1 , all of the magnetization vectors will be aligned with the z-axis at the end of the pulse and thus will be in phase immediately after the tip angle. Therefore, prepolarizing pulse inhomogeneity has no impact on the RF pulse calibration, except perhaps for variations caused by small differences in susceptibility and the microscopic magnetic field magnitude that are small enough to average out over the voxel volume.

Much more serious issues are total prepolarized pulse length, ramp time, and ringing after the prepolarizing pulse. The shorter the pulse is the more likely that the actual magnetic field strength has not reached the final pulsed value, which could make measurements of T_1 at a particular field impossible since the T_1 will change with the changing field strength. The faster the prepolarizing pulse is ramped down the more likely it is to “ring”—fluctuate around the final value in a similar fashion as an underdamped second order system. To allow for ringing to die down we could lengthen the time gap between the prepolarizing pulse and the RF pulse, but this increases the effects of T_2 and T_2^* decay. Tip angle miscalibration decreases the SNR and increases the variance in measured values. These observations argue for a long prepolarizing pulse and a T_1 measurement scheme that is robust to tip angle errors.

For the experimental phase imaging time is not a major consideration. However, in clinical application since two values are required for each data point the sequence will take twice as long as simple T_1 mapping, so the pulse sequence needs to be adaptable to some sort of fast imaging sequence.

T₁ Measurements

There is no shortage of options for T_1 measurement schemes. The earliest MR observations included an awareness of T_1 (Bloch, 1946). In 1978 a calculated T_1 image created with a progressive saturation technique (Freeman and Hill, 1971) was published for the first time (Pykett and Mansfield, 1978). In the mean time descriptions of inversion recovery and spin echo techniques had been published (Hahn, 1949; Hahn, 1950) as had been others (for example, Look and Locker, 1970). Since then there have been numerous strategies published including such improvements as adiabatic pulsing (Conolly et al., 1990), echo-planar imaging (Gowland and Mansfield, 1993), and shaped pulses, such as a hyperbolic-secant pulse (Gowland et al., 1989), not to mention the proliferation of lots of dandy acronyms (POLODA). Kaldoudi and Williams provide an overview of T_1 measurement history and techniques (Kaldoudi and Williams, 1993).

These pulse sequences can be classified as single-shot or multiple-shot imaging techniques. In single-shot MRI several measurements are made for each excitation (shot). In multiple-shot techniques there are several excitations (shots), each followed by a single measurement. One-shot techniques have a lower imaging time than multi-shot techniques, which is attractive for PMRI. A common single-shot technique is the Look and Locker method (LL) (Look and Locker, 1970), which uses a 180° inversion pulse followed by multiple small-angle pulses that sample the recovery of longitudinal magnetization. Crawley and Henkelman reviewed LL and the method of stimulated echoes (ST) and compared them to the inversion recovery (IR) and saturation recovery (SR) methods (Crawley and Henkelman, 1988). They found that IR and LL had comparable T_1 SNR and that both were superior to ST and SR methods and concluded that since LL provides a significantly faster imaging time than IR it should be the method of choice. More recent work has improved the sequence (Gowland and Mansfield, 1993) and described its optimization (Kay and Henkelman, 1991).

Possible Pulse Sequence Development Strategies

The main assumptions about a PMRI pulse sequence, as described above, are (1) T_1 has a non-linear dependence on field strength, so it is non-trivial to predict $T_1(B_p)$ for a changing B_p , which is the case as the prepolarizing pulse ramps up (2) the prepolarizing pulse is too inhomogeneous to attempt to make any measurements or apply any RF pulses while it is on, and (3) although we have to allow time for ramping down and ringing in the sequence, this time is small enough that it can be ignored in calculations of signal intensity. Through proper sequence design, however, it might be possible to minimize or account for the irregularities inherent in these assumptions. This leads me to three main approaches to single-shot, quantitative T_1 pulse sequence design:

- 1) Assume (1) and (2) are valid and place RF pulses, evolution, and readout only in the readout field (Non-Modeled, Inhomogeneous Prepolarizing Pulse)
- 2) Assume (2) but not (1) is valid and place RF pulses and readout in the readout field and evolution in the prepolarizing pulse (Modeled, Inhomogeneous Prepolarizing Pulse)
- 3) Assume (1) but not (2) is valid and place RF pulses and evolution in the prepolarizing pulse and readout in the readout field (Non-Modeled, Homogeneous Prepolarizing Pulse)

In this discussion of pulse sequence design considerations I will use FC field terminology—prepolarizing, evolution, and readout fields. In particular, the evolution field is the field in which magnetization “evolves” after RF perturbation. It is the T_1 of the evolution field that is measured. The approaches I describe below are meant to be illustrative of the general principle. It is not my intent to develop rigorous or ingenious sequences—I will merely analyze in general terms the requirements to generate reliable FIDs.

T₁ Measurement with Non-Modeled, Inhomogeneous Prepolarizing Pulse

For this approach we assume that the prepolarizing pulse is too inhomogeneous for reliable RF pulses or magnetization evolution and that it ramps up in such a way that reliable measurements can only be taken when it has reached equilibrium. Of the three options I have presented, this is the most constrained, and therefore, intuition would say should be the most accurate. However, it does not work. If we allow the magnetization to come completely to equilibrium, i.e., $T_p \gg T_1(B_p)$, and don't apply any RF pulses during the prepolarization we remove the T_{1p} dependence from equation [13]. Thus, no matter how we further manipulate the sequence and torture the data we cannot extract T_{1p} .

Modeled, Inhomogeneous Prepolarizing Pulse

For this approach we assume that we ramp up effects of the prepolarized pulse are negligible or can be modeled accurately. For the pulsing circuitry at the MRS/L, the prepolarizing magnet ramps up with a time constant of ≈ 60 ms and is quenched in ≈ 11 ms (Nam et al., 2000). For cross-linked BSA gels in physiological concentration ranges, which are good models of tissue (Koenig et al., 1993), T_1 varies between ≈ 130 ms to ≈ 220 ms in the frequency range of interest (Jiao and Bryant, 1996). So, the prepolarized pulse ramping time constant is approximately half of the fastest T_1 we will want to measure. If we assume that ramping effects are negligible we will overestimate the magnitude of magnetization in the sample at a given time (before it has reached equilibrium at the pulsed field strength). Thus, our estimates of T_1 at the pulsed field strength will be longer than the actual T_1 . Ramping error will be less the longer the prepolarizing pulse is on. However, dynamic range decreases if we only make measurements after the pulse has been on for a time $> T_{1p}$. Furthermore, inherent in this approach is error arising from

allowing magnetization evolution in an inhomogeneous field. The varying magnetic field will induce magnetization with different T_1 and will mimic RF pulse miscalibration errors, which will make precise T_1 measurements difficult to impossible.

A simple way to measure T_1 based on these assumptions is to measure the magnitude of the magnetization at equilibrium in the prepolarizing pulse, M_p' , and then allow the sample to come to equilibrium magnetization in the readout field, M_p , apply a 90° pulse followed by a prepolarizing pulse with length, $T_p \sim T_1$, followed immediately by another 90° pulse and signal acquisition. With system constant, K , and tip angle, $\theta \approx 90^\circ$, the signal intensity is:

$$M(T_p) = K \sin(\theta) M_p e^{-T_p/T_1} + K \sin(\theta) M_p' (1 - e^{-T_p/T_1}) \quad (17)$$

$$M_p' = K \sin(\theta) M_p \quad (18)$$

Taking the ratio of two intensities above and assuming that the M_p' term is ≈ 0 yields:

$$R = \frac{M(T_p)}{M_p'} = \frac{K \sin(\theta) M_p e^{-T_p/T_1} + K \sin(\theta) M_p' (1 - e^{-T_p/T_1})}{K \sin(\theta) M_p} \approx 1 - e^{-T_p/T_1} \quad (19)$$

Algebraic manipulation yields T_{1p} to be:

$$T_{1p} = \frac{-T_p}{\ln(1 - R)} \quad (20)$$

Observe that since $M_p' > M(T_p)$, R is always less than 1, so the expression above yields values that are defined and positive. Perhaps a more robust procedure would be to make several measurements with varying T_p and thus map out the exponential increase in magnetization and then use a three-parameter fit to determine T_{1p} (Kowalewski et al., 1977; Kingsley et al., 1998; Granot, 1983). Dynamic range could be increased by applying a prepolarizing pulse until the sample reaches equilibrium magnetization, turning off the pulse, applying a 180° RF pulse, and then reapplying the prepolarizing pulse of length T_p . A possible way to reduce ramp up effects is to use two counter-driven electromagnets with the same ramp up time constant. If both magnets are turned on at the same time, with one (the primary) oriented along $+z$ with magnitude B_p and the other (the secondary) oriented along $-z$ with magnitude B_s , then the effective magnetic field will be B_r . If, after both magnets have reached equilibrium, the secondary is quenched in 11

ms, the effective magnetic field will grow from B_x to B_y in the +z direction in 11 ms and thus greatly reduce the ramp up problem.

Non-Modeled, Homogeneous Prepolarizing Pulse

The last approach of the three I have suggested is to treat the ramp up time as a significant source of error but assume that the prepolarizing pulse homogeneity is sufficient to apply RF pulses during the prepolarization. The attraction for this approach is that it is the simplest for which to transfer MRI pulse sequences to PMRI sequences—the prepolarizing pulse is simply turned on and left on until readout while the pulse sequence proceeds as normal. This reduces the triggering and switching requirements and limits the effects of ramping. The weaknesses are that since the prepolarizing pulse might last longer heating of the magnet could be an issue and the inhomogeneity of the magnet will cause variable T_1 evolution. Robustness to RF inhomogeneities (or RF errors due to ringing from the prepolarized pulse) might be found in strategies such as (Weiss and Ferretti, 1985ab; Venkatesan et al., 1998).

As above, a simple way to illustrate such a pulse sequence is to turn on the prepolarizing magnet for time $T \gg T_m$ and $T \gg T_{1p}$, where T_m is the ramp up time constant for the magnet. Then, without changing the value of the prepolarizing pulse, apply a 90° RF pulse, wait time T_p , turn off the prepolarizing magnet, allow for ring down, and then apply another 90° RF pulse. Using the same conventions as above, the signal is:

$$M(T_p) = K \sin(\theta) M_p \left(1 - e^{-T_p/T_m} \right) \quad (21)$$

If we divide by M_p , equation [18] we obtain equations [19] and [20], which can be used to calculate T_{1p} or we can map out the magnetization growth and then apply a parameter fit.

Conclusion

Prepolarized MRI is potentially a low-cost platform for high SNR clinical relaxometry studies. The major difficulty in implementing such a system is the development of pulse sequences that can deal with the inhomogeneity, ramping times, and ringing inherent in the pulsed system.

CHAPTER V

RELAXOMETRY OF PROTEIN SYSTEMS

Introduction

Since the solids content of most tissues is mostly protein and water is biologically ubiquitous, to understand *in vivo* MR studies we must understand the magnetic resonance behavior of hydrated protein systems. As presented earlier, relaxometry is the study of the field dependence of the relaxation rate of a sample. Protein relaxometry provides us valuable insight into the magnetic resonance interactions and, through ^{14}N - ^1H quadrupole dip imaging, could also provide us valuable diagnostic information in the frequency range of 2.5 to 3.5 MHz.

Relaxation in Tissues and Protein Gels

Most MR imaging focuses on the hydrogen atom, with the signal intensity being directly related to the water-proton relaxation time. In hydrated protein systems, such as tissues and protein gels, coupling between the protein protons and the water protons decreases the spin-lattice relaxation time of water protons (Daszkiewicz, 1963). This is a frequency dependent effect (Koenig and Schillinger, 1969). Koenig and Brown have reviewed relaxation of protein solutions and tissues and developed quantitative theoretical analyses of hydrated protein system relaxation (Koenig and Brown, 1993; Koenig et al., 1993; Koenig, 1995; Koenig and Brown, 1991). They report that there are two classes of protein-water interactions that contribute to relaxation rate:

- 1) Hydrodynamic interactions that influence solvent motion
- 2) Cross relaxation interactions between solute and solvent nuclei

Early work on hydrated protein relaxation rates focused on a "two-site" model in which water molecules were bound to the protein long enough to sense the rotational motion of the protein but with sufficiently rapid exchange to communicate the relaxation rate of bound protons to the bulk solvent (Daszkiewicz, 1963). This model proved to be inadequate to explain measured results, however (Koenig et al., 1975), and it is now known that there are at least four classes of water binding sites at the protein-water interface at which significant energy transfer takes place between the water-protons and protein protons. These sites correspond to the number of hydrogen bonds formed by a proton on a water molecule at that site—four, three, two, or one—with bond lifetimes, τ_m , 1×10^{-6} s, 2×10^{-8} s, 4×10^{-10} s, and 8×10^{-12} s, respectively. Note that τ_m is short compared to T_1 for water protons for all site classes. The four-bond sites dominate the protein-water relaxation even though they occupy at most 1% of the protein-water

interface (Koenig, 1995). An unbound liquid water proton “senses” the thermal energy of the surrounding lattice through the dipolar magnetic field of surrounding atoms, which fluctuates rapidly due to Brownian rotation and translation—so rapidly, in fact, that the interaction is essentially averaged out. This leads to the relatively long T_1 values for unbound water. If the water molecule is attached to a protein for a sufficiently long τ_m , however, its rotational correlation time, τ_c , is greatly increased, which decreases the averaging effect and allows the atom to come to thermal equilibrium more quickly. This decrease of T_1 due to a reduction in atomic movement is called “motional narrowing” (Bloembergen et al., 1948; Solomon, 1955).

The hydrodynamic interaction has two consequences: it alters the relaxation rate through motional narrowing and it affects the rate at which cross-relaxation takes place. We can conceptually conceive of cross-relaxation as being the thermodynamically driven transfer of magnetization energy across the solvent-protein interface under non-equilibrium conditions. In an external magnetic field after an RF perturbation, the protein protons relax much quicker than the water protons due to motional narrowing and energy transfer to the protein backbone. Thus, protein protons return to their equilibrium energy level while the water protons are still perturbed. By the second law of thermodynamics, energy flows from the higher energy non-relaxed protons to the lower-energy relaxed protons in the form of magnetic flux. Thus, the protein protons act as an energy sink to the water protons and decrease the spin-lattice relaxation time of the water protons (Koenig et al., 1978; Koenig and Brown, 1991). The transfer of energy through cross-relaxation can occur by intermolecular magnetic dipolar and electric quadrupolar interactions of solvent nuclei.

Although there is some ambiguity and variance of interpretation of the data, it appears that in immobilized proteins the hydrodynamic contribution to the overall relaxation rate becomes small compared to cross-relaxation effects (Koenig and Brown, 1991, p. 521; Bottomley et al., 1984; Wolff and Balaban, 1989; Grad et al., 1990; Grad and Bryant, 1990). Temperature increase increases net efficiency of cross-relaxation between water and immobilized proteins but not very much over the range of physiological temperatures (Hinton and Bryant, 1996; Conti, 1986b; Bottomley et al., 1984). Some authors have reported a correlation between relaxation rate and water content (for example, Lundbom et al., 1990; Fischer et al., 1990). However, many other reviews and studies find no such correlation (Spiller et al., 1994; Spiller et al., 1995; Englund et al., 1986; Koenig et al., 1984; Bottomley, 1987). Despite the variance in results, it seems clear that the degree of water does affect the measured relaxation rate (Fatouros et al., 1991), so whether the effect is hydrodynamic or cross-relaxant, the amount of water is significant.

Measured Relaxation Rates

In almost all cases the water-protons and not the protein-protons are the source of signal in MR experiments because the protein-protons relax more quickly than most systems can detect or there is an intentional delay used to remove the protein-proton signal (Koenig and Brown, 1991). The measured relaxation rate is a combination of the protein proton relaxation rate, R_p , the water proton relaxation rate, R_w , and the rate of transfer of magnetization between the water and protein systems, R_{wp} . I will consider four, two, and one-parameter models of relaxation, described below.

Koenig and others studied the relaxation rate dispersion for *in vitro* tissue and protein solutions with a heuristic four-parameter least-squares curve-fitting procedure. This form is derived from what is known as the "Cole-Cole fit", which was developed to describe dielectric dispersion (Cole and Cole, 1941; Koenig and Schilling, 1969; Hallenga and Koenig, 1976). The function, which has been verified for tissues and protein solutions (Conti, 1986a; Koenig and Brown, 1984; Koenig et al., 1984; Fischer et al., 1990), is given as:

$$R = R_w + D + \frac{A}{1 + (\nu/\nu_c)^B} \quad (22)$$

where ν is the Larmor frequency in MHz, R_w is the relaxation rate of pure water (0.23 s^{-1} at 37°C), and D , A , and B are constants. D and A are proportional to the solute concentration and ν_c is proportional to the inverse of the rotational correlation time of the protein, τ_c (Hallenga and Koenig, 1976; Conti, 1986). Equation [22] is a heuristic model with no *a priori* validity—it is just a mathematical expression that describes the data very well and is not based on any particular theoretical formulation on the molecular interactions. For theoretical purposes it is therefore only useful as a way to describe and catalog the data and is subject to the criticism, as Bottomley points out, that given enough parameters success is almost guaranteed in fitting a monotonic, smoothly varying function (Bottomley et al., 1984).

For a homogeneous protein gel Lester and Bryant report the bi-exponential longitudinal relaxation rate of a protein gel as:

$$R_{\pm} = \frac{1}{2} \left[R_w + R_p + R_{wp} \left(1 + \frac{1}{F} \right) \pm \sqrt{\left(R_w + R_p + R_{wp} \left(1 + \frac{1}{F} \right) \right)^2 + \frac{4R_{wp}^2}{F}} \right] \quad (23)$$

where R_+ and R_- are the fast and slow proton relaxation rates, respectively, and F is the ratio of equilibrium magnetization of the protein protons to that of water protons (Lester and Bryant, 1991). F can be calculated as the ratio of exchangeable water protons to exchangeable protein protons and is constant for a sample except for a slight pH dependence that is negligible within physiologic range and the frequency range of interest (Conti, 1986a; Zhou and Bryant, 1994). Due to machine limitations or by design, R_+ is allowed to decay and then R_- is the measured relaxation rate. In the limit that the cross-relaxation rate, R_{wp} , is rapid compared to the water proton relaxation rate, R_w , i.e., $R_{wp} \gg R_w$, which is generally the case for fields greater than 1 MHz, the slow relaxation rate, R_- , becomes the average of the water and protein proton relaxation rates weighted by their respective proton populations.

$$R_- = \frac{R_w + FR_p}{1 + F} \quad (24)$$

Furthermore, for $R_p \gg R_w$ small, which is increasingly true for decreasing magnetic field, R_- becomes directly proportional to R_p .

$$R_- \propto R_p \quad (25)$$

It would be equivalent to say that the protein relaxation rate dominates all other relaxation rates in tissue dispersion profiles. Both of these conditions hold in immobilized hydrated protein systems at room temperature for Larmor frequencies between 2.5 and 3.5 MHz, which is the frequency range of interest for the present work (Lester and Bryant, 1991). The protein proton spin-lattice relaxation rate, R_p , is modeled by Kimmich and Winter (Kimmich and Winter, 1985) as

$$R_p \propto \cos[B \tan^{-1}(2\pi\nu\tau_c)] \frac{\tau_c^B}{(1 + 4\pi^2\nu^2\tau_c^2)^{B/2}} \quad (26)$$

Where B is a constant, ν is the proton Larmor frequency, and τ_c is the rotational correlation time of the protein. When τ_c is large, i.e., when the protein is immobilized and spins slowly or not at all, equation [26] reduces to a model presented by Kimmich, Winter, and others (Kimmich and Doster, 1976; Kimmich and Winter, 1985; Kimmich et al., 1986):

$$R_p = A\nu^{-B} \quad (27)$$

where A and B are constants and ν is the proton Larmor frequency. Then, applying equation [25] to equation [27] with A still a constant (but not necessarily the same value as before) yields:

$$R = A \nu^{-B} \quad (28)$$

Bottomley et al used this two-parameter model to fit dispersion data in an extensive review of normal and pathological tissues. They found that A and B are constants dependant on tissue type with $B \approx 1/3$, and that equation [28] worked very well within relatively wide tolerances (standard deviation of 20% from fitted curve), which they attributed to systematic errors of the different teams and equipment used to collect the data that were independent of species, temperature, age differences, time after excision, or *in vivo* or *in vitro* status (Bottomley et al., 1984; Bottomley et al., 1987). Zhou and Bryant (1994) found that for completely water saturated, rotationally immobilized protein gels $B = 0.5$ fit the data well and was stable to variations in other parameters and that A was a constant for a given sample. Except for deviations caused by quadrupole dips, equation [23] has been verified for homogeneous protein gels between 0.01 and 30 MHz by Bryant's group (Lester and Bryant, 1991; Zhou and Bryant, 1994; Bryant et al., 1991). Thus, in an immobilized, hydrated protein system at room temperature for Larmor frequencies between 1 and 30 MHz, with $R_w \gg R_w$ and $FR_p \gg R_w$, the relaxation rate is given by:

$$R = \left(\frac{FA}{1+F} \right) \nu^{-B} \Rightarrow R = A \nu^{-0.5} \quad (29)$$

Again, note that A does not necessarily have the same value in the two equations. This is similar to a model proposed by Escanyé et al: $R = A \nu^{-0.5} + B$, (Escanyé et al., 1982). The fact that equation [27] is based on some degree of a theoretical framework instead of a heuristic fitting equation is intellectually satisfying. However, the present work deals with clinical application and thus precision is more important than theoretical viability. Two studies have found that equation [22] provides a better fit to measured data over a wide frequency range than does equation [27], especially in the ultra-low field case ($\nu < 1$ MHz) and the high field case ($\nu > 40$ MHz) (Fischer et al., 1990; Henriksen et al., 1993). However, in the frequency region of interest for the present work, 2.5 – 3.5 MHz, the two-parameter and four parameter models are in close agreement.

To evaluate the feasibility of using the one-parameter model, equation [29], we can use Fischer's fit parameters for excised human white matter for equation [22] to calculate a "measured" value for R at

some frequency not on the quadrupole dip, say $\nu = 3.3$ MHz (Fischer et al., 1990). Using this R and ν we can estimate the A for the one-parameter model, $A = R\nu^{0.5}$, and then create the one-parameter relaxation dispersion profile over the range 2.5–3.5 MHz. Fischer et al's parameters were: $D = -1.38 \text{ s}^{-1}$, $A = 18.25 \text{ s}^{-1}$, $\nu_c = 0.165$ MHz, $B = 0.291$. With these parameters $R(\nu=3.3 \text{ MHz})$ is calculated to be 4.23 s^{-1} and A is estimated as 7687. Graphs of equations [28] and [22] with Fischer's parameters (Fischer et al., 1990) and equation [29] with parameter calculated as described are shown in Figure 2.

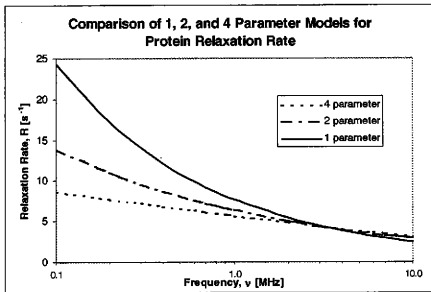


Figure 2: Comparison of 1, 2, and 4 parameter fits of relaxation rates in proteinated systems in frequency range of interest. Parameters for two-parameter fit, equation [28], and four-parameter fit, equation [22] are from Fischer et al (1990). Parameter for one-parameter fit, equation [29], is calculated as described above.

As Fischer observed, the one- and two-parameter fits break down below 1 MHz. However, over the frequency range 2.5 – 3.5 MHz all three fits agree well. With A in the one-parameter model estimated with $\nu = 3.3$ MHz, the largest percent difference between the one- and four-parameter models in this frequency range is 6.8 %.

Conclusion

For the present work, the significance of equation [29] is that it estimates relaxation contributions for relaxation paths *other than cross-relaxation with ^{14}N* and that A and thus the dispersion profile from 2.5 to 3.5 MHz can be predicted within 7 % with a single measurement of R .

CHAPTER VI

QUADRUPOLE INTERACTIONS IN PROTEIN SYSTEMS

Introduction

A nucleus that has an ellipsoidal charge distribution is said to be quadrupole and has a nuclear electric quadrupole moment, Q , arising from the asymmetric charge distribution (Ramsey, p. 3-23). It can be shown that only nuclei with nuclear spin, $I \geq 1$ can have a quadrupole moment. Examples of quadrupolar nuclei include ^2H , ^{14}N , and ^{35}Cl . The nuclear electric quadrupole moment, Q , interacts with the local electric field gradient according to a nuclear quadrupolar coupling constant. Most clinically significant MR phenomena are dominated by magnetic dipolar interactions. However, under certain circumstances the electric quadrupole interaction exerts a significant influence on the overall behavior of the system.

Quadrupole Interaction

Quadrupole interactions have been well studied and there is plenty of literature documenting the theory and experimental measurement of the phenomenon. Schuler and Schmidt observed atomic nuclear quadrupole constants in 1935 (Schuler and Schmidt, 1935) and Kellog et al observed molecular quadrupole constants in 1936 (Kellog et al., 1936). Dehmelt and Kruger reported pure quadrupole couplings transitions in solids in 1950 (Dehmelt and Kruger, 1950). Theoretical treatments are readily available (Das and Hahn, 1958; Cohen and Reif, 1957; Klainer et al., 1982; also Lehn and Kintzinger, p. 79-161; Semin et al., p. 1-15).

If we visualize the nucleus as a volume distribution of positive charges surrounded by a negative charge cloud then there is an electrostatic potential that varies slowly over the nucleus. The electrostatic energy can be expressed in terms of superimposed moments of a monopole, quadrupole, hexadecapole, etc. The monopole term is constant and therefore not orientationally-dependent. The hexadecapole and higher pole interactions are either negligible or non-existent (Ramsey, p. 23-24). Thus, the orientationally dependent term is the quadrupole energy. Further manipulation and quantum mechanical considerations, which are beyond the scope of this project, lead to a solution of the Schrodinger equation with a multiple-level system of energies. The number of possible energy levels depends on the spin. For spin $I = 5/2$ there are two energy levels; $I = 1$ and $I = 7/2$ each yield three levels; $I = 9/2$ yields four levels, etc. (Semin, p.4-7). Irradiating a quadrupolar sample with electromagnetic energy at the proper frequency can induce transitions between the energy levels. The signal created by the quadrupole energy level transition can be

detected remotely using NMR techniques and is called nuclear quadrupole resonance (NQR) spectroscopy. Some groups call this spectroscopic technique zero-field imaging or spectroscopy because it requires no external magnetic field (for example, Liao and Harbison, 1999). Although there are non-trivial technical difficulties in NQR spectroscopy, it allows research on many nuclei that are not accessible by ordinary NMR (Harbison, 14 Feb 2001) and finds practical application in narcotic and explosive detection (Grechishkin and Sinyavskii, 1997; Yesinowski et al., 1995; Rudakov et al., 1997). NQR is an active area of research. INSPEC subject search in February 2001 for "Nuclear Quadrupole Resonance" yielded 7745 hits.

¹⁴N Nuclear Quadrupole Resonance

For ¹⁴N, with nuclear spin, $I = 1$, the quadrupole interaction gives rise to a three-level system of energies given by:

$$E_z = e^2 q Q / 2 \quad (30a)$$

$$E_x = -E_z (1 - \eta) / 2 \quad (30b)$$

$$E_y = -E_z (1 + \eta) / 2 \quad (30c)$$

where e is the elementary charge (1.602 E^{-19} Coulombs), q is the electric field gradient along the z-axis of the principal axes system, Q is the quadrupole moment (0.0155 b to 0.020 b for ¹⁴N (Lehn and Kintzinger, p. 84; CRC, 11-40)), and η is the asymmetry parameter ($\eta < 1$; typically ≈ 0.1 ; Lehn and Kintzinger, p. 86-93; Winter and Kimmich, 1982b). Transitions between these levels can be induced with oscillating magnetic fields of the proper frequencies. These frequencies are given by:

$$\nu_+ = \frac{e^2 q Q}{4h} (3 + \eta) \quad (31a)$$

$$\nu_- = \frac{e^2 q Q}{4h} (3 - \eta) \quad (31b)$$

$$\nu_d = \frac{e^2 q Q \eta}{4h} = \nu_+ - \nu_- \quad (31c)$$

Variations in chemical structure and molecular environment lead to a small spectrum of possible transition frequencies.

Quadrupole Dips

Under certain conditions the T_1 dispersion profile of substances containing quadrupolar nuclei shows a sharp decrease or "dip" at the quadrupolar transition frequencies. This "quadrupolar dip" arises from the transfer of energy from the non-quadrupolar nuclei to the quadrupolar nuclei, causing a quadrupolar energy transition. Since the quadrupolar relaxation time is generally shorter than the non-quadrupolar relaxation time this energy transfer causes the overall system to relax faster, thus decreasing T_1 . Goldman observed this phenomenon in 1958 with ^1H and ^{35}Cl and ^{37}Cl in paradichlorobenzene (Goldman, 1958). Woessner and Gutowsky made similar observations that same year with the same compound (Woessner and Gutowsky, 1958). Since the initial observations several groups have reported quadrupole dips with various species, for example, $^{137}\text{Ba}-^1\text{H}$ (McGrath and Silvidi, 1962), $\text{Cl}^{35}-^1\text{H}$, $\text{Ba}^{135}-^1\text{H}$, and $\text{Ba}^{137}-^1\text{H}$ (Nakamura and Enokiya, 1963), and $^{17}\text{O}-^1\text{H}$ (Hsieh et al., 1972). For more description and references see (Stokes et al., 1979; Abragam, 1961, p. 143).

Quadrupole Dips in $^{14}\text{N}-^1\text{H}$ Systems

Nitrogen and Hydrogen are two of the most significant elements in biology. Nitrogen is present in significant quantity in all proteins as one of the components of the amino acids that make up proteins. Of the twelve isotopes of Nitrogen, ^{14}N and ^{15}N are the only naturally occurring stable species. ^{14}N has an abundance of 99.63 %, spin $I=1+$, nuclear magnetic moment $+0.40376$ nuclear magnetons, and electric quadrupole moment 0.0155 b to 0.020 b ($b = \text{barn} = 10^{-24}$ cm; Lehn and Kintzinger, p. 84; CRC, 11-40). Hydrogen is biologically ubiquitous in all organic compounds and systems. ^1H has an abundance of 99.99 %, spin of $I = 1/2+$, nuclear magnetic moment of $+2.793$ nuclear magnetons, and electric quadrupole moment $+2.86$ mb (CRC, 11-39). ^{14}N and ^2H both have interesting and varied applications in NMR (for example, LiWang and Bax, 1997; Reif et al., 2000; Czernek et al., 2000; de Alba and Tjandra, 2000). However, their almost negligible abundance and ^{15}N 's lack of a quadrupole moment make them uninteresting for the present purposes.

As a $1/2+$, $1+$ spin system, $^{14}\text{N}-^1\text{H}$ systems display the quadrupole dip phenomenon, which indicate more efficient spin-lattice relaxation through quadrupole coupling between the protons and the nitrogen atoms (Stokes and Ailion, 1979; Westlund and Wennerström, 1985). Winter and Kimmich observed that if an external magnetic field had a low enough frequency the quadrupole coupling dominates Zeeman coupling (Winter and Kimmich, 1982b). The low-field condition for ^{14}N is $B_0 < 0.3$ T, which corresponds to $\nu < 10$ MHz, where B_0 is the flux density of the external magnetic field. Further, they observed three conditions necessary for the existence of the quadrupole dip:

- 1) ^1H Larmor frequency has to equal one of the ^{14}N quadrupole transition frequencies.
- 2) The T_1 relaxation of the ^{14}N system must be fast compared to the proton system, i.e., $T_1^{14\text{N}} \gg T_1^{1\text{H}}$.

- 3) Correlation time of the ^{14}N system must be large, i.e., it must rotate slowly or not at all and thus avoid motional averaging.

The pathway for the relaxation can be modeled as energy flow from a water-proton to an amide (NH) proton to the nitrogen to the lattice. The interaction between the water proton and the NH proton is a dipolar magnetic coupling or Zeeman coupling, which transfers some of the energy of the perturbed water proton to the protein proton as it does during "normal" relaxation. The NH proton, which is bound to the immobilized protein and is thus motionally narrowed will relax faster than the water proton, again as in "normal" relaxation in a hydrated protein system. However, if the Larmor frequency of the NH proton matches a quadrupole transition frequency of the ^{14}N , because of the small N-H distance, energy can be easily transferred from the NH proton to the nitrogen, causing the Nitrogen to move to a higher energy state and relaxing the NH proton. The nitrogen is very strongly coupled to the lattice and is very stable and relaxes this added energy very quickly. This is a much more efficient relaxation pathway than relaxation through motional narrowing of the NH proton. Thus T_1 is decreased at the quadrupole resonant frequencies (Kimmich et al., 1984; Koenig, 1988). Winter and Kimmich observed that the dip frequencies for proteinated tissues and models corresponded to the NQR frequencies reported for the amide groups of amino acids (Edmonds and Summers, 1973; Blinc et al., 1972) and thus concluded that the amide groups found in proteins are responsible for the dips (Winter and Kimmich, 1982a).

Quadrupole Dips in Proteinated Samples

Since proteins contain significant amounts of Nitrogen and water is almost completely ubiquitous in biological tissues, it stands to reason that structurally intact proteinated tissues would exhibit quadrupole dips. Quadrupole dips arising from ^1H - ^{14}N systems have been found and analyzed in various *in vitro* tissues and models. These include Bovine Serum Albumin (BSA) (Kimmich and Winter, 1980), BSA, muscle tissue, *Micrococcus luteus*, and yeast (Winter and Kimmich, 1982a), rat heart (Koenig et al., 1984), various proteins, DNA, and frog muscle (Kimmich et al., 1986), multiple sclerosis plaque (Rinck et al., 1988), bovine calf eye lens homogenate (Beaulieu et al., 1987; Koenig, 1988), egg white lysozyme (Lester and Bryant, 1990), hen egg albumen (Carlson et al., 1992), BSA (Koenig and Brown, 1993), human astrocytomas (Spiller et al., 1994), transplantable human glioblastoma (Spiller et al., 1995), and pituitary adenomas (Spiller et al., 1997).

In vivo studies of quadrupole dips are not as extensive. Kimmich et al appear to have been the first to study quadrupole dips in living specimens with their report on live *Hirudo medicinalis* (leeches) published in 1984 (Kimmich et al., 1984). Rinck et al found dips in rat muscle that were similar to dips observed in *in vitro* MS plaques (Rinck et al., 1988). Carlson et al created *in vivo* dispersion profiles of fat,

bone marrow, muscle, white matter, dark matter, and the pons of healthy volunteers in a whole body imager. The fat and bone marrow provided no significant dip structure. The muscle and all three brain tissues studied yielded clear quadrupole dipoles. In the brain, the dip magnitude increased from white matter to dark matter to the pons (Carlson et al., 1992). In 1999 Lurie published a quadrupole dip collected from his forearm and three axial images of his thighs. One of the thigh images was collected at the main dip frequency (2.77 MHz) and another was collected slightly off the dip frequency (2.45 MHz). The third image was created by subtracting the second image from the first, pixel by pixel, to yield an approximate quadrupole dip magnitude map (Lurie, 1999).

The precise location of the dip on the frequency axis can vary slightly depending on the precise chemical environment of the sample and experimental variables. For rotationally immobilized, hydrated, protonated samples, the main dip, i.e., largest magnitude and highest frequency, has been measured at 2.79 MHz (Koenig and Brown, 1991), 2.77 MHz (Carlson, Radiology 1992; Lurie, 1999), 2.84 MHz (Jiao and Bryant, 1996), etc. All three of the dipoles are between 1 and 3 MHz.

Quadrupole Dip Magnitude Proportional to Protein Concentration

If amide groups in the protein backbone are the source of the quadrupole dip then it seems intuitively reasonable that the magnitude of the quadrupole dip should be proportional to the number of amides in the sample and thus proportional to the concentration of proteins. The ratio of amides to amino acids in a protein is typically slightly greater than one. The masses of the twenty biologically significant amino acids range from approximately 75 to 190 g/mol, or a factor of 2.5 between the least massive and the greatest with a mean of 133 g/mol and a standard deviation of 28 g/mol (McMurry, 1996, p. 1058-1059). So, most of the amino acids have approximately the same mass and over the volume of a single voxel, the number of amides should be directly proportional to the mass of proteins in the voxel. Jiao and Bryant verified that the quadrupole dip magnitude is linearly related to the protein concentration using cross-linked BSA/glutaraldehyde gels (Jiao and Bryant, 1996). The modeled relaxation rate that was independent of the ^{14}N contribution as

$$R = A \nu^{-0.5} \quad (32)$$

They measured R at some "off dip" frequency, $\nu_o = 3.30$ MHz, and used this $R_o = R(\nu_o)$ to calculate A and extrapolate the value of R at the dip frequency, $\nu_d = 2.84$ MHz, $R_d = R(\nu_d)$. They then measured the value of R at the dip frequency, R_d , and took the difference to find the dip magnitude, R_w .

$$R_n = R_e - R_d = R_m \sqrt{\frac{V_o}{V_d}} - R_d \quad (33)$$

The significance of R_n is that it represents the contribution of ^{14}N to the relaxation of the system. They found that the relationship between the quadrupole dip magnitude, R_n [s^{-1}], and protein concentration, ρ [% weight], is:

$$R_n = (0.114 \pm 0.006)\rho - (0.47 \pm 0.09) \quad (34)$$

with a linear correlation coefficient of 0.99. The non-zero intercept is a concern since at zero concentration there should be no contribution from the ^{14}N atoms. They attributed the negative intercept to the impossibility of making low concentration immobilized protein gels, which shifts the line to the right. A similar argument can be made about the sensitivity of the detection system—if the signal below a certain concentration is too weak to be detected then the line will be shifted to the right.

Conclusion

Electric quadrupolar interactions between ^{14}N and ^1H create dips in the T_1 dispersion profile of samples containing rotationally immobilized proteins. These dips have been observed in a variety of *in vitro* and *in vivo* specimens, including humans. The magnitude of the dip is proportional to the protein concentration in the sample.

CHAPTER VII

QUADRUPOLE DIP IMAGING WITH PMRI

Introduction

Quadrupole Dip Imaging (QDI) is a novel imaging technique that creates images based on the magnitude of the quadrupole dip. So far as I have been able to determine, Kimmich and co-workers were the first to suggest an MR contrast mechanism based on the quadrupole interaction (Kimmich et al., 1984). In 1992 Carlson suggested that changes in the quadrupole dip caused by demyelination or muscle scarring might be diagnostically useful (Carlson et al., 1992). Jiao and Bryant demonstrated a QDI scheme that isolates the contribution of the ^{14}N to relaxation by determining the T_1 relaxation rate at the maximum of the quadrupole dip and at a point well away from the quadrupole dip and using a one-parameter model to extrapolate the ^{14}N independent relaxation at the quadrupole dip frequency and subtracting the two values (Jiao and Bryant, 1996). Furthermore, Jiao and Bryant demonstrated in the same report that the magnitude of the quadrupole dip was linearly related to the concentration of rotationally immobilized proteins in their gel and tissue sample *in vitro* (Jiao and Bryant, 1996). In an imaging format with the signal amplitude scaled by the dip magnitude, which is proportional to protein concentration, contrast would come from variations in immobilized protein concentration from voxel to voxel. Lurie has demonstrated implementation of a similar technique for quadrupole-dip based contrast *in vivo* with a human subject in a whole body scanner (Lurie, 1999).

Quadrupole Dip Imaging

As explained above, the protein concentration is estimated by measuring the magnitude of the quadrupole dip. This magnitude is defined as the difference between the measured relaxation rate and an extrapolated "non-quadrupolar" relaxation rate at the highest dip frequency, ≈ 2.84 MHz. The "non-quadrupolar" model for a highly aqueous system, i.e., the relaxation dispersion we would expect if there was no quadrupolar dip, is given as:

$$R = \frac{1}{T_1} = \frac{A}{\sqrt{\nu}} \quad (35)$$

Where R is the relaxation rate and A is a constant (Zhou and Bryant, 1994). A is determined by measuring T_1 at some frequency away from the quadrupolar dip, for example, $\nu_{\text{ref}}=3.30$ MHz.

$$A = R_m \sqrt{\nu_m} \quad (36)$$

The extrapolated relaxation rate, R_e , is then calculated with A calculated from the non-quadrupole measured T_{1m} . Thus:

$$R_e = \frac{1}{T_{1e}} = \frac{A}{\sqrt{\nu_d}} = \frac{1}{T_{1m}} \sqrt{\frac{\nu_m}{\nu_d}} \quad (37)$$

The quadrupole dip magnitude, ξ , in units of s^{-1} is the difference between the measured relaxation rate at the dip, R_d , and the extrapolated relaxation rate at the same frequency, R_e .

$$\xi = R_d - R_e = R_d - R_m \sqrt{\frac{\nu_m}{\nu_d}} \quad (38)$$

I have found no symbolic representation of the quadrupole dip magnitude in the literature. I chose ξ arbitrarily. The typical range of values for ξ is 0.5 to 2.0 s^{-1} (Jiao and Bryant, 1996). For quantitative measurements it is possible to calibrate the dip magnitude to protein concentration, ρ_p , such that:

$$\rho_p = \alpha \xi + \beta \quad (39)$$

Jiao and Bryant report ξ as a function of ρ_p with a best-fit slope of 0.114 ± 0.006 and zero-intercept as -0.47 ± 0.09 for BSA/glutaraldehyde gels between 6 and 20% concentration (Jiao and Bryant, 1996).

Flipping the axes to yield ρ_p as a function of ξ to fit the model I have described above yields $\alpha = 8.80 \pm 0.47$ and $\beta = 4.12 \pm 0.79$.

Contrast Mechanism

Contrast for MRI techniques is determined by the variable reactions of target atoms, usually Hydrogen, in different tissues to the applied magnetic fields. That is, some histological difference between tissues affects MR characteristics differently in the different tissues and is therefore detectable in the MR image. Proton density, longitudinal relaxation rate ($1/T_1$), and transverse relaxation rate ($1/T_2$) are the most common parameters examined with conventional MRI techniques. More recently developed techniques such as Magnetic Transfer and Spin Diffusion imaging obtain contrast based on the motion of water molecules in relation to the surrounding macromolecules and membranes. Quadrupole Dip Imaging (QDI)

contrast is based on the histological and histopathological differences in immobilized protein concentration among various tissues and pathologies. The quadrupole dip magnitude, which arises from electric quadrupolar interactions between ^1H and ^{14}N from amides in the protein backbones and water, is proportional to the immobilized protein concentration by weight (Jiao and Bryant, 1996). QDI contrast is similar to MT contrast in that it measures an energy-exchanging interaction between water and macromolecules, however, the energy transfer mechanism in QDI is primarily electric while MT coupling is primarily magnetic. As with all MR techniques, QDI signal intensity is proportional to the number of target atoms that contribute to the measured contrast parameter—in this case the number of hydrodynamically accessible amides in the backbones of rotationally immobilized proteins.

Field Cycled Proton-Electron Double-Resonance Imaging (PEDRI)

QDI is conceptually and practically very similar to the Field Cycled Proton-Electron Double-Resonance Imaging (PEDRI) developed by Lurie's group at Aberdeen. In fact, it appears that Lurie's group was the first to produce a full QDI image (Lurie, 1999). I will briefly describe the PEDRI technique as an introduction to the QDI technique and to indicate the source of valuable published results and experience in the development of low-cost FC components. PEDRI is a technique that images free radical concentrations by irradiating an electron paramagnetic resonance (EPR) of the free radical being studied while measuring the MRI signal (Lurie, et al., 1988). EPR is the absorption of microwave radiation by an unpaired electron in a magnetic field. Under appropriate conditions interactions between the protons detectable by MRI and the free radicals enhance the MRI image in the free radical containing regions. By collecting the EPR enhanced image and the normal image consecutively and then taking the difference of the two it is possible to map the density of the free radicals (Lurie et al., 1994). PEDRI suffers from excessive power deposition, which is overcome by field cycling—by applying the EPR irradiation at a low field strength and reading out the NMR at a higher strength. Lurie's group used a small resistive electromagnet enclosed in a larger magnet that is held at a constant strength while the smaller magnet is driven such that its field is opposite to the main magnet, thus lowering the field strength in the imaging region (Lurie et al., 1989). Lurie's group has further developed the dual magnet field-cycling technique (Lurie et al., 1991; Lurie, 1994; Baras et al., 1995; Puwanich, et al., 1999). The parallel of FC-PEDRI to QDI is obvious—two field strengths are used to create a difference image that isolates the contribution of a target atom. The hardware and pulse sequence implementation for QDI will be somewhat similar to those developed by Lurie's group.

QDI Pulse Sequences

A detailed analysis of Prepolarized pulse sequences is beyond the scope of this article (see Chapter IV for a general description of PMRI pulse sequences). However, to analyze the potential for clinical implementation we must consider constraints on the imaging sequence and verify that there are

potentially viable options. We will consider considerations for quantitative protein concentration mapping and relative concentration-weighted imaging. Lurie used field-cycled, interleaved inversion-recovery/saturation-recovery pulse sequence and an interleaved field-cycled inversion recovery imaging pulse sequence to measure T_1 quantitatively (Lurie, 1999). Quantitative T_1 mapping is also used for temperature measurements (for example, Bertsch et al., 1998; Włodarczyk et al., 1999) and the insight gained there should transfer to PMRI sequence development. Jiao and Bryant demonstrated a relative approach that is fundamentally different from the quantitative approach in that it assigns signal intensity based on the ratio of the dip and non-dip signals instead of the difference between the signals (Jiao and Bryant, 1996). This relative approach may be more useful than quantitative measurements since it can probably be implemented in faster sequences. These might include snapshot or turbo FLASH (Tong and Prato, 1994; Haase, 1990; Puwanich et al., 1999; Deichmann and Haase, 1992), Look-Locker Echo variants (Gowland and Mansfield, 1993; Kay and Henkelman, 1991), or TOMROP (Brix et al., 1990; Gowland and Leach, 1992). Other work that might prove useful includes (Carlson, Crooks et al., 1992; Bielecki et al., 1984; Anordo and Pusiol, 1996; Guiberteau and Grucker, 1996). Development of robust PMRI sequences will be an important research area. However, at present it seems safe to say that it is feasible to develop sequences that are adequate for clinical QDI.

Error, Dynamic Range, and Field Accuracy

For the T_1 measurements, precision is extremely important and accuracy marginally so. To be more specific, since we are concerned with a difference measurement, control of random error is more important than control of systematic error. If some systematic error makes the T_1 estimates inaccurate but maintains the relative separation of the extrapolated and dip values then there is no problem in the protein concentration estimate.

Dynamic Range

A major limitation of QDI with PMRI is the relative magnitude and dynamic range of values involved. In Lurie's abstract, the dip magnitude is $\approx 15\%$ of the T_1 at that point (Lurie, 1999). In Jiao and Bryant the difference was $\approx 12\%$ of T_1 for an 18.5% BSA gel (Jiao and Bryant, 1996). So, the entire dynamic range of clinically useful values is on the order of 20% of the measured values. Thus, a random 5% error in one of the T_1 measurements could propagate as a 25% error in dip magnitude and therefore signal intensity. Since signal intensity is proportional to a difference the errors in the individual measurements are additive. Thus, a 5% uncertainty in each T_1 measurements results in a 10% uncertainty in the difference and a 50% uncertainty in the signal intensity.

SNR Gain

If the readout magnet of the PMRI scanner has a field strength that is close to the quadrupole transition field strengths the SNR gains from PMRI are reduced. As described in Chapter 4, in PMRI, $SNR \propto B_p$, and the improvement in SNR over conventional imaging is simply B_p/B_z . Jiao and Bryant used a dip frequency of 2.84 MHz, and an off-dip frequency of 3.30 MHz (Jiao and Bryant, 1996). This corresponds to magnetic field strengths of 0.0667 T and 0.0775 T, respectively. If we implement QDI on the PMRI scanner at the MRSL with its readout field of 0.058 T (2.46 MHz) the PMRI SNR gains are 1.15 and 1.34, respectively—hardly anything at all. A possible solution to this problem is to develop circuitry that would enable the electromagnet to be pulsed to a large magnitude ($B_p \gg B_z$) and then quenched rapidly to some evolution field strength, B_e , before being quenched completely to B_z .

Quadrupole Dip Width

The quadrupole dip peak is relatively broad, so not being perfectly at the peak does not produce large error. In Jiao and Bryant's paper the Full Width Half Maximum (FWHM) of the major dip is approximately 300 kHz (Jiao and Bryant, 1996). The precise location of the dip on the frequency axis can vary slightly depending on factors that have yet to be precisely described. Reported values for the main dip, i.e., largest magnitude and highest frequency, include 2.77 MHz (Carlson and Goldhaber et al., 1992; Lurie, 1999), 2.79 MHz (Koenig and Brown, 1991), and 2.84 MHz (Jiao and Bryant, 1996). So, the expected peak location might vary by as much as 70 kHz. In Jiao and Bryant's data, moving away from the peak center 70 kHz resulted in a change in the T_1 estimate of less than -1.5%. However, as described above, a 1.5% error in the T_1 estimate could result in a -7.5% error in protein concentration. Furthermore, since the evolution field is inhomogeneous, the entire volume of interest will not be precisely on the dip frequency. If the inhomogeneity is significant over a voxel the measured magnitude will be less than the actual magnitude. If the inhomogeneity is over several voxels, some of the voxels will be on frequency while others are off, which decreases the validity of the protein concentration map. For all parts of the sample to be within 70 kHz of the dip frequency requires homogeneity of only 24,600 ppm.

Electromagnet Heating

The relative insensitivity of the quadrupole dip magnitude to the precision of the frequency alleviates some of the concern about magnet heating. PMRI uses a resistive electromagnet that is low-cost and can have varying field strengths. Current, I , is fed through the magnet, which generates a magnetic field whose magnitude is proportional to the magnitude of the current according to the Biot-Savart Law. However, the conducting material has a resistance, R , which causes it to dissipate power in the form of heat where the amount of heat power generated is equal to $P=I^2R$. Resistance, R , is related to resistivity, ρ , by: $R = \rho(l/a)$, where l =length and a =cross sectional area of the conductor. Resistivity is dependent on

temperature by 1st, 2nd, 5th, or ½ powers depending on the temperature range and state of the material (Dyos and Farrell, 1992). Therefore, the longer the magnet is “on” the greater amount of heat is generated and therefore the higher the resistance. The magnet is driven by voltage-controlled circuitry: it maintains the voltage at a constant value by changing the current if necessary. As the resistance increases while the voltage remains constant there is decrease in the current requirements by Ohm’s law: $V=IR$. Since the magnetic field magnitude is directly proportional to current magnitude, a change in current causes a change in field strength which changes the net magnetization of the sample, i.e., from one measurement to the next the B_p changes. For temperatures between 100–1200 K the resistivity of copper is linear (Khanna and Jain, 1974; Matula, 1979; Domenicali and Christensen, 1961). In the linear region of a pure metal resistivity is related to temperature by:

$$\rho(T) = [\rho(T_o)] [1 + \alpha(T - T_o)] \quad (40)$$

where ρ is the resistivity, T is the temperature (in °C or K), and α is the temperature coefficient of expansion (with units of °C⁻¹ or K⁻¹). Copper has a temperature coefficient of resistivity, $\alpha = 0.0039$ °C⁻¹ (The Electronics Library, 2000). For the MRSL PMRI electromagnet, a current of 23 A generates a magnetic field of 0.125T (5.32 MHz; Morgan, 1999). Thus, for frequencies of 2.84 and 3.30 MHz (0.067 T and 0.078 T), when placed in a 0.06 T magnetic field the pulsed magnet requires 1.64 A and 3.63 A, respectively. To change the field by 70 kHz (i.e., off the dip frequency of 2.84 MHz) requires a change in current of 0.3 A. For constant voltage, this requires a temperature change of 57°C. On the MRSL PMRI scanner, for $I=100$ A, the magnet heats at a rate of approximately 10 °C/min (Morgan, 1999). For QDI applications the currents required are two orders of magnitude less than this current and the time the magnet is on is on the order of hundreds of milliseconds. It is unlikely that normal usage would generate this degree of temperature change. The relatively low heating rate also alleviates concerns about structural stability of the apparatus at high temperatures and patient safety and comfort.

Voltage and Current Control

The relatively small changes in field strength require relatively precise control of voltage and current. For the MRSL magnet a 70 kHz change in field strength requires 0.3 A change in current. Therefore, the power supply should allow reliable control of current to a precision of at least 0.1 A.

Factors that Could Affect QDI Accuracy and Precision

The quadrupole dip arises from magnetically perturbed, mobile water protons binding in the vicinity of NH protons and coupling to those protons magnetically, which in turn couple to Nitrogen atoms electrically, which relax efficiently. In QDI we want to measure the number of proteins that are

rotationally immobilized, which is indicated by the magnitude of the quadrupole dip. The correlation between the magnitude of the quadrupole dip and number of rotationally immobile proteins depends on:

- 1) Degree of matching between the quadrupole transition and the Larmor frequencies of ^{14}N and ^1H
- 2) Relative speed of the ^{14}N T_1 relaxation versus the ^1H relaxation, i.e., $T_1^{1\text{H}} > T_1^{14\text{N}}$
- 3) Mobility of the water molecules
- 4) Efficiency of communication between the two H on a given H_2O molecule
- 5) Availability of NH protons for coupling
- 6) Accuracy of T_1 measurement
- 7) Total number of protons contributing to signal

Although the dip is based on a specific exchange, competing exchanges or factors that change the overall rate of exchange could affect the magnitude of the dip. For example, Ceckler showed that for ordinary protein relaxation some of these factors might include temperature, cholesterol concentration, pH, and surface chemistry (Ceckler, 1992).

Protein Motions and Concentrations

Below 10 MHz, the degree of rotational tumbling of the protein is a significant factor in quadrupole dip amplitude. In a solution a protein rotates with a frequency on the order of 1 MHz (Winter and Kimmich, 1982), which is fast enough to cause the net quadrupole interaction to average to zero (Jia and Bryant, 1996). It is this rotational dependence that provides the contrast mechanism for QDI. Side chain motions of proteins are insignificant below 10 MHz irrespective of tumbling rate of whole molecule (Winter and Kimmich, 1982).

The range of immobilized protein concentrations in tissues could affect the sensitivity of QDI studies. Protein concentration in a muscle sample is approximately 20% and in an MS plaque 7.5% (Rinck et al., 1988). Koenig et al assert that typical tissue is 20% solids by weight (Koenig et al., 1993). Brain white matter (WM) is approximately 25% myelin by wet weight and myelin proteins constitute 28% of white matter protein (Norton and Autilio, 1966). Myelin is 28-30% protein by dry weight (Svennerholm and Vanier, 1978; Norton and Autilio, 1966). By manipulation of these percentages I estimate that the approximate protein concentration of CNS white matter is 27% by weight.

$$\left(\frac{\text{WM protein}}{\text{myelin protein}} \right) \left(\frac{\text{myelin protein}}{\text{myelin}} \right) \left(\frac{\text{myelin}}{\text{wet WM}} \right) = \frac{(0.30)(0.25)}{0.28} = 0.27 \quad (41)$$

The span of quadrupole dip magnitudes covers protein concentrations from 0 to 27%. The upshot is that a relatively small change in the total solids density of the brain results in a relatively large percentage

change in the imaging scale. For example, a 3% decrease in protein concentration by wet weight of the brain results in an 11% decrease in dip magnitude. Although this train of thought indicates that QDI could be a very sensitive modality, similar reasoning applied to the dynamic range of relaxation rate values, discussed below, indicates that sensitivity might be limited.

Natural histological variations in protein distribution could affect the efficacy of QDI as a diagnostic device. In the CNS, nerve cells are approximately 80% protein by dry weight and 20% by wet weight. Monkey cerebellum white matter has a mean protein concentration of 344 g/kg dry tissue (standard deviation = 9 g/kg). Other regions of the monkey brain have concentrations ranging from 381-645 g/kg dry tissue (Friede, 1966, p. 358-359). Presuming humans have a similar distribution, because of natural variations in protein distribution, it might be difficult to observe a pathological abnormality. However, Friede observed that within a particular region the protein distribution tended to be uniform (Friede, 1966, p. 493).

Mobility and Density of Water Molecules

Some authors have reported a correlation between relaxation rate and water content (for example, Lundbom et al., 1990; Fischer et al., 1990). However, many other reviews and studies find no such correlation (Spiller et al., 1994; Spiller et al., 1995; Englund et al., 1986; Koenig et al., 1984; Bottomley, 1987). Spiller et al attributed variability in relaxometry independent of water content to histologic diversity, different rates of metabolism, differences in protein content, changes in protein conformation and organization, and compartmentalization (Spiller et al., 1995). In water/protein solutions and proteinated tissues the dispersion profile can be influenced by the mobility of the water molecules (Koenig and Brown, 1984; Spiller, et al., 1995; Fatouros, et al., 1991). This is affected by:

- 1) Brownian motion of the macromolecules and solvent
- 2) Protein/water interactions such as hydrogen bonding and protein/water collisions
- 3) Compartmentalization by membranes that alters access of water to protein

Molecular Size, Shape, and Temperature

As would be expected, dip amplitude decreases significantly with temperature decrease (35 °C vs. 5 °C) due to an increase in the viscosity of water and the slowing of the rate of exchange of protons (Koenig, et al., 1990). Temperature increase also increases the net efficiency of cross-relaxation between water and immobilized proteins (Hinton and Bryant, 1996; Conti, 1986b; Bottomley et al., 1984; Beaulieu et al., 1989). However, in the physiological range of temperature values these effects are almost negligible. Protein molecular size, shape, and side chain motions could all potentially affect the mobility of water and its access to the relaxation sites. The size affects the momentum and rate of tumbling, but if the protein is

immobilized these factors are no longer a concern. Furthermore, in a clinical imaging environment with voxel sizes on the order of millimeters, each voxel will contain many different types of proteins, so even if there is differential interaction with a particular type of protein it is likely that the effect will average out due to the large number of different proteins. As mentioned above, side chain motions of proteins are insignificant below 10 MHz irrespective of tumbling rate of whole molecule (Winter and Kimmich, 1982).

Solvent Viscosity

Solvent viscosity could have a significant effect on water proton mobility. To understand this concern we must be careful to differentiate between macroscopic and microscopic viscosity. Macroscopic viscosity refers to the bulk behavior of the fluid. Microscopic viscosity refers to the ability of individual molecules to move past each other. Although microscopic and macroscopic viscosity are obviously related to each other, in a heterogeneous fluid they are not necessarily qualitatively the same. For example, consider congealed (not clotted) blood, which although very viscous on a macroscopic level, leaves interstices too large to substantively alter the thermal motion of water on a microscopic level (Koenig and Brown, 1984). Viscosity is a concern in the case of vasogenic edema, such as in multiple sclerosis, where the edema has a high concentration of solute protein and a concomitant small increase in macroscopic solvent viscosity (Naruse et al., 1986; Brück, et al., 1997; Bloomfield et al., 1998). However, on the microscopic scale the water mobility is not significantly restricted because of the relative size of the protein molecules. A change in the concentration of smaller molecules, such as glucose, could have a more significant effect on the microscopic viscosity. CSF can have a variable composition under normal circumstances and MS can alter those concentrations (for example, Osenbruck et al., 1985).

Edema

It seems clear that the degree of edema does affect the measured relaxation rate (Fatouros et al., 1991). A significant concern with proteinaceous vasogenic edema is how it affects the validity of the one-parameter model and thus the relative dip magnitude. The assumption of the one-parameter model was that there was a population of mobile solvent molecules and rotationally immobilized protein molecules and that the relaxation of the solvent protons can be modeled as equation [3.5]. In the case of vasogenic edema there is a contribution to relaxation from mobile proteins. Consider two samples with equal masses of immobilized proteins and equal volumes of liquid, one with pure water and the other with a protein solution. Although the protein solution will have fewer molecules of water it is probably not enough to reduce the number of protons relaxed by the quadrupole relaxation sink. However, protons in the protein solution sample can be relaxed by mobile and immobile proteins (and of course other water molecules) so the relative contribution by the ^{14}N sink, and therefore the magnitude of the quadrupole dip, will be lessened. The magnitude of this effect could have important ramifications for the *in vivo* precision possible with QDI. Another concern with edema is that it changes the local volume of the tissue. Will QDI be able

to distinguish between a change in volume that leads to a lesser protein concentration reading and protein degradation that leads to a lesser concentration reading?

Compartmentalization

Compartmentalization—the confining of water populations to specific regions by membranes—does not directly interfere with the ^{14}N - ^1H relaxation. What it might do is affect the relative effect on the total signal amplitude, since it could isolate protons from the quadrupole relaxation sink and proton populations from the “relaxed” protons that communicate the relaxation efficiency of the few quadrupolar interactions to the whole population. Thus, there could be a tissue with a significant hydrated, immobilized protein concentration that is isolated from a large part of the local water population. The QDI measurement of this tissue will report low protein concentration because the relaxation will be relatively confined to the few water protons in direct communication with the proteins. There are several reasons why compartmentalization should have a minimal effect. On a microscopic scale, compartmentalization effects will be averaged out over the voxel size used for scanning. Consider two situations: (1) two water proton populations with volumes on the order of intracellular compartments in close proximity to one another, one perfectly isolated from any immobilized protein system and the other in efficient communication with an immobilized protein system, and (2) the same as the first situation, but remove the membranes that separate the populations, allowing efficient mixing of the two. In the first case the population in contact with the protein will relax quicker, i.e., have a greater relaxation rate, than the non-protein population. However, when the signals from the two populations are averaged together as part of a single voxel the enhanced relaxation is “communicated” to the isolated proton population. In the second case the relaxation is communicated to the second population mechanically, resulting in an average relaxation rate similar (though certainly not necessarily equal) to the average rate that comes about through intravoxel averaging. Koenig asserts that in most cases membranes restrict water proton mobility by at most a factor of two and are often negligible (Koenig, 1995; Koenig et al., 1990), so the assumption above of perfect isolation of the populations is weak. On a macroscopic scale compartmentalization will have a detrimental effect on accuracy. For example, at the borders of the ventricles in the brain partial volume averaging between the solid tissue and the CSF will result in spurious readings. Myelinated tissues (i.e., white matter) present an interesting and special case that will be discussed below in the section on white matter.

Natural Abundance

One concern is the natural abundance of ^{14}N and ^1H in tissue. Since ^{15}N does not have a quadrupole moment, if it was present in any significant amount in natural systems it would decrease the observed magnitude of the quadrupole dip in a sample. However, ^{15}N 's natural abundance of 0.366 % compared to the 99.634 % abundance of ^{14}N (CRC, 1-10) make this concern completely negligible. There is a similar concern for ^2H or D_2O . Since a deuteron's magnetic moment is small compared a proton's

magnetic moment (+0.857 versus + 2.793 nuclear magnetons, respectively, CRC, 11-39) the hydrodynamic relaxation interaction between the hydrogen atoms on a given water molecule are reduced to the point of being negligible (Koenig et al., 1984). Furthermore, because of their greater mass, deuterons do not exchange efficiently and thus interfere with the transfer of energy from water-protons to NH protons and significantly reduce the quadrupole dip amplitude (Koenig and Brown, 1984). But, with deuterium's natural abundance of 0.015 % (CRC, 1-10), this concern is also completely negligible.

Chemical Environment

^{14}N - ^1H coupling is not direct but involves transport of magnetic energy (spin diffusion) through at least one intervening exchangeable proton (Koenig and Brown, 1984; Koenig, 1988). Therefore, dip amplitude can be influenced by factors other than the number of ^{14}N and ^1H nuclei available for coupling, such as the ease of hydrogen bonding. Therefore, the chemical environment of the exchange could have a profound impact on relaxation efficiency. In general, proton/macromolecule interactions are pH dependent. (Kucharczyk et al., 1994) and changes in the chemical environment correlated to histological changes, such as calcification and hemorrhage, have been shown to affect relaxation and MRI contrast (Henkelman et al., 1991; Tsuruda and Bradley, 1987; Gomori et al., 1987; Thulborn et al., 1990). Changes in Sodium and Potassium concentration levels that accompany demyelination in multiple sclerosis could also have an effect. In transplantable human glioblastoma SF295 grown in athymic nude mice pH and fresh hemorrhage were not directly correlated to $1/T_1$ (Spiller et al., 1995). However, to my knowledge, the effect of these factors on quadrupole dip has not been carefully studied, so any conclusions at this point must remain tentative. It is conceivable that an increase in pH could slow the amount of hydrogen bonding and thus decrease the number of water protons relaxed by NH relaxation centers and therefore decrease the dip magnitude. However, in the physiologic pH range this is probably a relatively small effect. As before, we must consider microscopic changes in pH and macroscopic, but again as before, for a voxel with dimensions on the order of millimeters the microscopic effects should average out. Cholesterol has been shown to increase the T_1 relaxation rate of white matter (Koenig et al., 1990; Koenig, 1990). The potential effects of cholesterol on quadrupole dip magnitude will be discussed in the section on white matter.

White Matter

At typical imaging fields white matter T_1 is approximately a factor of two shorter than that of gray matter even though white matter has ~12% less water than gray matter (Koenig and Brown, 1991). Myelinated white matter has significantly different structure and chemical composition than gray matter. It is predominately composed of long, tubular axons that are ~2 microns in diameter that are bounded by a phospholipid membrane of ~60 Å, which is surrounded by a layer of extracellular water ~120 Å (~40 water molecules) thick, which is in turn surrounded by the myelin sheath. The myelin sheath is a "spiral wrapping of specialized oligodendritic cells" comprised of ~12 layers of a "repeating structure of lipid-

cytoplasm-lipid-extracellular water". The repeat distance is $\sim 150 \text{ \AA}$ and the sheath contains approximately 40% water. In myelinated white matter the majority of the water is in the intracellular cytoplasm (axoplasm) of the axons of the neurons (Koenig and Brown, 1991).

Myelin lipids do not contribute to the MRI intensity (Bottomley et al., 1984) and myelin water comprises only $\sim 15\%$ of the total water, which is too little to dominate the signal by simple partial volume averaging (Koenig and Brown, 1991). However, it is myelin waters that create the enhanced relaxation rate—cholesterol in the myelin facilitates relaxation of water protons, which then diffusively mix with the axoplasmic waters to lower the overall relaxation rate (Koenig et al., 1990; Koenig, 1991). The geometry of cholesterol in myelin creates "potholes"—depressions in the macromolecular interface that are well suited for relatively long-lived hydrogen bonding of water molecules. These potholes do, in fact, efficiently bind water molecules and thus increase their relaxation rate by slowing them hydrodynamically and facilitating magnetization transfer between the water protons and the cholesterol backbone (Koenig, 1991). Then, the relaxed water molecules communicate efficiently with the axoplasmic waters by diffusion. Even though the myelin lipid bilayer is relatively water impermeable the relatively close spacing of the successive turns of the myelin sheath makes the surface to volume ratio relatively high and consequently makes the rate constant for exchange also relatively high (Koenig et al., 1990). The rate constant of exchange is temperature dependent but the dependence is probably not large enough to be significant in the physiological range of temperatures (Koenig et al., 1990).

The concern for cholesterol-facilitated relaxation is that the quadrupole and cholesterol pathways will compete, resulting in a relative reduction in the magnitude of the quadrupole dip, i.e., for two samples with equal protein concentration but one with cholesterol, the cholesterol containing sample will have a smaller dip magnitude. White matter has a lower protein concentration than gray matter, so we would expect that the white matter dip will be smaller than the gray matter dip, with the ratio of the dip magnitudes equal to the ratio of the protein concentrations. If the white matter dip is significantly smaller than the ratio predicts then there is another competing effect, very possibly cholesterol. As an initial indicator of the magnitude of this effect, consider quadrupole dipoles published by Carlson et al (Carlson et al., 1992). Although the dip resolution and scale and lack of apparent structure makes it difficult to estimate the dip magnitude precisely, I estimate the magnitudes to be $\sim 0.3 \text{ s}^{-1}$ and $\sim 0.4 \text{ s}^{-1}$ for white matter and gray matter, respectively, which gives a gray to white matter dip ratio of ~ 1.3 . In monkey brain concentration ratios for various different parts of the brain range from 1.4 to 1.9 (Friede, 1966, p. 358-359). So, presuming that concentration ratios for human brain are similar in magnitude, the white matter dip does not appear to be minimized relative to the gray matter dip—if anything the white matter dip magnitude is enhanced. Thus, as an initial approximation, the cholesterol can be assumed to have a

negligible effect on quadrupole dip magnitude in white matter. This issue will require further research—to determine if the white matter relaxation profile can be modeled as a protein/water system as described in Chapter V and if the cholesterol has any effect on the measured quadrupole dip magnitude.

Practical Viability of a PMRI system

For medical technology to be useful it must be clinically and economically viable. That is, the risk/benefit and cost/benefit analyses of the referring physician, patient, and sponsoring institution must indicate that the system is worth using.

Safety and Comfort

There is a great deal of literature that indicates that MRI is a safe modality (for example, Shellock, 2001) and, by extension, PMRI also. Furthermore, since PMRI is a low-field technique, energy deposition in scanning and the projectile hazard are lessened. A potential concern is the rate at which the electromagnet pulses. 1.3 T/sec is a high enough dB/dt to induce retinal magnetophosphenes (Marg E, 1991). The threshold for motor nerve stimulation is approximately 60 T/s (Cohen et al., 1989). Both of these values indicate the threshold dB/dt at which the patient becomes aware of an interaction and do not indicate the safety threshold, which is much higher (Marg E, 1991). Current PMRI scanners are within these safety thresholds: Carlson's scanner had dB/dt of 6 T/s (Carlson et al., 1992), Lurie reports 3T/s (Lurie, 1999), and Morgan reports ≈ 12 T/s (Morgan et al., 2000). However, in the future the use of more rapid pulsing techniques to overcome ramping problems could increase the rate of change of the field past acceptable limits. Thus, although there is a slight concern about the changing field rate, the decision to use PMRI will be based almost entirely on economics, patient comfort, and diagnostic utility, and not on safety.

Although safe, some patients find the MRI exam to be uncomfortable and report claustrophobia, high temperature, loud noise, and long examinations as being contributors to the discomfort (McIsaac et al., 1998; MacKenzie et al., 1995). Anxiety levels ranging from apprehension to severe reactions that interfere with the performance of the test occur in approximately 4% to 30% of patients undergoing MRI (Melendez and McCrank, 1993). Around 14% of MRI patients required sedatives in order to successfully complete the examination (Murphy and Brunberg, 1997). Since PMRI is a low-field technique it could conceivably be transferred to a more patient-friendly open scanner clinical applications, which makes imaging possible for most claustrophobic patients—one study reports that 94% of patients who were unable to complete a conventional scan due to claustrophobia were able to complete the exam in an open scanner (Spouse and Gedroyc, 2000). However, the pulsed electromagnet and the receiver coil must still be placed close to the patient and might cause psychological discomfort. A particular concern is for head imaging (versus extremity imaging). Murphy and Brunberg report that the head coil seems to heighten the

claustrophobic reaction, since 16.2 % of the brain scan patients they studied required sedation while only 2.5% of the extremity patients required sedation (Murphy and Brunberg, 1997). So, although PMRI should be able to get away from the whole-body magnet claustrophobia, there are still concerns about claustrophobia induced by the head coil and magnet. Imaging time and temperature in the scanner will require further examination. The pulsed electromagnet could potentially generate enough heat to make the patient uncomfortable. Appropriate cooling strategies will potentially have to be developed. Since QDI is a difference measurement it will require twice as many data points as a regular quantitative T_1 scan. The low field nature implies low SNR, which requires that more averages be taken. The increased SNR of PMRI, presuming a prepolarized pulse and an evolution pulse, should offset this concern to some degree. QDI with PMRI will probably be a relatively lengthy examination. Loud noises due to impact between the gradient coils and their mounts caused by Lorentz forces is a significant problem (Brummet et al., 1988; Hurwitz et al., 1989; McJury, 1995). As a low-field permanent magnet system, PMRI will probably have minimum clicking (for example, Kramer et al., 1989). Although the pulsed electromagnet will also experience Lorentz forces its much larger mass relative to a gradient coil will probably prevent it from impacting its mounts and making noise.

Distribution Considerations for Clinical Implementation

The cost of PMRI includes the cost of the hardware, installation, housing preparations, maintenance, supply, and support personnel. As demonstrated earlier, PMRI is less expensive than the high-field MRI scanners currently popular for clinical imaging. Lower cost translates into lower patient cost, more frequent testing, and wider geographic availability of the testing. However, simply lowering cost is not enough. The factors that lead to medical spending decisions can be complicated and do not always limit themselves to simple free-market competition and concern for patient welfare. Government regulation, academic support, public relations concerns, and professional culture can all play significant roles (Kaufman, 1996; Passariello, 1997; Takahashi, 1997). Thus, a hospital might choose to buy a more expensive high-field imaging system, citing its higher spatial resolution, thinner image slices, greater contrast, shorter acquisitions, and specific high-field applications (Bradley WG, 1996) when in reality the motivation is public relations (i.e., "we have the biggest and bestest machine money can buy") or the research interests of some of the physicians or faculty or some other non-rigorously defensible, though not dishonorable, motivation. PMRI could be distributed in two ways:

- 1) As a complete, stand-alone PMRI system (MRI magnet, console, electromagnet, pulsing circuitry, and software) for head and extremity imaging
- 2) As an insert that converts existing MRI systems into PMRI systems (electromagnet, pulsing circuitry, and software) for head and extremity imaging

Because of the disadvantages of larger aperture pulsed magnets, PMRI is probably going to be a head and extremity imaging technique, or maybe, with a surface field coil, a heart imaging technique (Carlson and Goldhaber et al., 1992). The insert approach includes two subsets: a one-time "upgrade" of the existing scanner to a PMRI scanner or a removable insert that can be removed for normal scanner operation and inserted for the occasional QDI exam. PMRI could be marketed/presented as an improved way to do conventional MRI or as a relaxometer. Variations on the marketing strategies include:

- 1) Conventional MRI contrast imaging system with enhanced SNR (no QDI capabilities)
- 2) Dedicated QDI protein concentration mapping system
- 3) Conventional MRI contrast imaging system with enhanced SNR and QDI capabilities
- 4) Conventional MRI scanner with option for QDI capabilities

Several factors will determine the viability of distributing PMRI. These include:

- 1) Diagnostic value of QDI
- 2) Trends in MR equipment acquisition
- 3) Cost of implementation
- 4) Number of Low-field scanners currently in use and their field strengths

QDI having significant diagnostic value is neither a necessary nor a sufficient condition to ensure PMRI's clinical diffusion, but it would help. There are many other factors that will affect the spread of PMRI technology, but if there were a clear diagnostic advantage in QDI, the low-cost of PMRI would help it spread quickly. If QDI turns out to be an intellectually interesting technique with little clinical value PMRI could still achieve wide diffusion based on its low-cost and enhanced SNR. In the face of changing socioeconomic views on medical reimbursement much research and debate has focused on ways to make imaging more cost effective. Several studies show that lower-cost low-field systems are comparable to the more expensive high-field systems in diagnostic efficacy (Lee et al., 1995; Steinberg et al., 1990; Orrison et al., 1991; Parizel et al., 1997), so providing a low-cost way to improve SNR seems like a robust strategy, especially as part of a tiered network of lower-cost, lower SNR scanners feeding difficult cases to fewer, more expensive machines (Parizel et al., 1997). Some have suggested that the socioeconomic pressure will push MR acquisition strategies toward low-field and dedicated extremity systems (Pasariello, 1997). Of course, others have argued that high-field imaging provides more "bang for the buck" because of its higher spatial resolution, thinner image slices, greater contrast, shorter acquisitions, and specific high-field applications and that high-field is the trend of the future (Bradley, 1996). The argument for low-field systems is strengthened if QDI turns out to provide specific useful information.

Expending the capital outlay to purchase an MR system that only does one thing, i.e., images one part of the body with a limited range of imaging techniques, at first inspection seems like bad business.

However, the low-cost and size of dedicated low-field imaging scanners make them a viable clinical option (for example, Arbogast-Ravner et al., 1995). There are 113 dedicated scanners in Europe as of 1997, which is 8% of the total number of European MRI systems (Pasariello, 1997). From 1994 to 1997 there was a 3.1% decrease in the number of medium-low field MRI units (0.5 T or less) in Europe because of the marked increase in the diffusion of dedicated scanners. So, if QDI is diagnostically useful there is a potential market for dedicated QDI scanners.

If the PMRI apparatus is presented as an insert for existing scanners then the marginal cost, i.e., the added cost for the operating facility to acquire and maintain the system, is small. If the whole body magnet and the imaging console are already in place then the insert requires an electromagnet (~ \$10,000), power supply (~ \$20,000), pulsing circuitry (~ \$5,000), and software upgrades, installation, and training (~ \$25,000). As a rough estimate this could be done for < \$60,000, which fits reasonably well within the budget of most imaging facilities. As was described earlier, the capital outlay for a complete stand-alone PMRI system is much less than that of a high-field system and closely comparable to a low-field system.

In 1994 10% of world's MRI scanners had field strengths of less than 0.5 T and 39% had a field strength of 0.5 T (Pasariello, 1997). Furthermore, in the US in 1994 8.8% of new MRI scanners sold had field strengths between 0.21 T and 0.5 T and 16% had strengths of 0.21 T or below (Martí-Bonmati and Kormanó, 1997). So, there is a large number of scanners that could potentially receive the PMRI insert. However, the marginal return on the investment of adding PMRI capabilities to a 0.5 T scanner are much less than adding them to a < 0.5 T scanner since the relative SNR improvement decreases and the technical and the bioeffect issues much more significant since more power is required and larger fields have to be switched quickly (Carlson and Goldhaber et al., 1992). Furthermore, for scanners with field strengths greater than 0.06 T, QDI studies will require that the electromagnet field be driven in opposition to the main magnet (to achieve the quadrupole dip frequency = 0.066 T), which destroys the SNR improvement and for the medium field magnets requires significant power. Martí-Bonmati and Kormanó report that only about 200 scanners in the 0.02-0.064 T field range have been installed (Martí-Bonmati and Kormanó, 1997), so there are not many machines (of the ~ 15,000 in the world) that fit the optimal target description for a PMRI insert. Nevertheless, saying that PMRI inserts are not going to be the next cash cow of medical technology companies does not necessarily mean that it is not economically viable to produce inserts. The advent of PMRI technology could increase the demand for ultra-low field machines.

Conclusion

QDI could non-invasively provide a map of immobilized protein—an indicator of tissue integrity and the histopathological substrate of disease. When implemented with PMRI it could do so at relatively

low cost. A more detailed analysis of QDI's potential value requires that we consider specific conditions. I have chosen Multiple Sclerosis as a case study and will review it and QDI's potential advantages for its study in the next chapter. I will focus on the information value that QDI might provide and will ignore the cost benefits of implementation with PMRI and any corollary benefits.

CHAPTER VIII

QDI FOR MULTIPLE SCLEROSIS

Introduction and Background on Multiple Sclerosis

I have reviewed various elements of Multiple Sclerosis (MS) prevalence, pathology, diagnosis, and treatment in an attempt to evaluate the potential value of QDI for MS study.

Prevalence and Perniciousness

Multiple Sclerosis (MS) is an inflammatory demyelinating disease of the central nervous system (CNS) with approximately 300,000 cases in the United States (Anderson, et al., 1992) and approximately 1.1 million worldwide (Dean, 1994). Symptoms, which stem from neurological damage, can include spasticity, muscle weakness and paralysis, excretory and sexual dysfunction, loss of balance and coordination, blindness, memory loss, and depression, among others (Rosenblum and Saffir, 1998; Miller, 1998; Olek, 1999). Most patients (~85%) experience a relapse-remit illness with relatively long periods of clinical quiescence and recovery interspersed with periodic worsening. Some patients (~15%) experience progressive disease from the onset and many patients exhibit relapse-remit behavior for several years and then switch to the relentlessly progressing variant (Arnason, 1999; Hickey, 1999). In almost all cases, however, neurological damage eventually accumulates, destroying the patient's cognitive and motor abilities and rendering the patient incapacitated. Besides the human suffering and degradation in quality of life for the patient and those around them, the national annual cost of MS was approximately \$9.7 billion in 1994 (Whetten-Goldstein et al., 1996).

In his review of MS, Olek (Olek, 1999) attributes the first report on an MS case to Ollivier in 1824 (Ollivier, 1824). There was some work on MS in subsequent years but the first careful clinicopathological description and analysis was by Charcot and his students, with the seminal paper published in 1868 (Charcot, 1868). Since that time MS has been studied extensively (for example, from 1960 to 2000 Medline lists approximately 20,000 articles under the keyword "multiple sclerosis"). Unfortunately, however, its etiology remains unknown. Epidemiological studies implicate environmental and genetic factors but have been unable to elucidate those factors (Martyn and Gale, 1997; Olek, 1999). Much speculation about etiology focuses on the role of viruses in causing an autoreactive immune mediated attack (Antel, 1999).

The Central Nervous System, Myelin, and Brain Protein Concentrations

The CNS is composed of two types of cells: neurons and neuroglia, of which neurons are the majority. There are four types of neuroglia found in the CNS, which collectively fill about half of the CNS. They are: astrocytes, oligodendrocytes, microglia, and ependymal cells. Astrocytes are star shaped cells with many processes that help maintain chemical balance, help form the Blood-Brain Barrier (BBB), and provide a link between neurons and blood vessels. Oligodendrocytes are the most numerous glial cells in the CNS. They are smaller and have fewer processes than astrocytes. They produce the myelin sheath that encases neurons. Microglia are phagocytic cells that help keep things clean and healthy. Ependymal cells line ventricles, make Cerebrospinal Fluid (CSF), and assist in CSF circulation. CNS tissues are lumped into two broad classifications: White and Gray matter. White matter is aggregations of myelinated processes from many neurons. Gray matter contains unmyelinated cells (Tortora and Grabowski, 1996).

The white matter of the brain is approximately 50% myelin by dry weight (25% myelin by wet weight) and 70% water (wet weight). Myelin proteins constitute 28% of white matter protein (non-myelin tissues contribute the other 72%) (Norton and Autilio, 1966). Myelin is 28-30% protein and ~65% lipid by dry weight. Wet myelin is approximately 40% water. (Svennerholm and Vanier, 1978; Norton and Autilio, 1966). Nerve cells are approximately 80% protein by weight. Cerebellum white matter (for a monkey) has a mean protein concentration of 344 g/kg dry tissue (sd=9). Other regions of the brain have concentrations ranging from 381-645 g/kg dry tissue) (Friede, 1966, p. 358-359).

Pathological Progression and Histology

The major MS pathological feature is focalized regions of demyelination, called plaques or lesions in all regions of the brain and spinal chord, including white matter and gray matter, although most lesions are in white matter. These lesions develop over time and display different characteristics depending on their relative age. These characteristics can include demyelination, edema, gliosis, hypocellularity, axonal destruction, and remyelination. The initial event seems to include a local breakdown of the Brain Blood Barrier (BBB) (McDonald, et al., 1992). In the Charcot variant (which is the most common and has lesions that have similar characteristics as most other variants), lesions can be classified as acute, chronic-active, or chronic-inactive based on histological characteristics and how fast they grow (Hickey, 1999; Trapp, et al., 1999; Rosenblum and Saffir, 1998).

Coincident with breakdown of the BBB and continuing for some time afterward is active demyelination. These acute lesions display hyperemia, edema, myelin swelling, an abundance of macrophages and lymphocytes, endothelial cell activation, plasma cells reduction, oligodendrocyte reduction, demyelination, and possibly concurrent remyelination. If the macrophages contain myelin

protein debris then the plaque is young (2-3 weeks). If the protein debris has degraded but the macrophages are still lipid-laden then the plaque is 2-3 months old (Trapp et al., 1999). The edema associated with MS is primarily vasogenic and therefore contains large amounts of protein originating from blood serum (Brück, et al., 1997). Gliosis, the multiplication of glial processes, increases physical density and increases concentration of glial fibrillary acid protein (GFAP) in the region of the lesion.

After some period of active demyelination the lesion might progress to a secondary stage. Chronic-active lesions have a quiescent center and an active margin. The center might display remyelination and active margin has characteristics of acute lesion. It is generally expanding, although the expansion may be symmetrical or asymmetrical. Some lesions might become chronic-inactive in that there is no evidence of ongoing demyelination but there is definitively an abnormality. The chronic-inactive lesion is a "quiescent glial scar" with a sharp boundary between myelinated and demyelinated tissue. Oligodendroglial cells are markedly diminished or absent and the number of axons diminishes with plaque age. Preceding complete axonal destruction is the proliferation of axonal ovoids and the concurrent accumulation of amyloid precursor protein (APP) in the ovoids (Trapp, et al., 1999). Axonal destruction correlates to a decrease in the N-acetyl aspartate/Creatine (NAA/Cr) ratio (Fu, et al., 1998). There is eventual brain atrophy (Simon, 1999).

Some studies also detect diffuse abnormality in the normal appearing white matter (NAWM) in the immediate but normal appearing regions around plaques and in the whole brain (Simon, 1999; Adams, 1983; Blakemore and Keirstead, 1999; Christiansen et al., 1993). In some MS cases the CNS has been shown to spontaneously remyelinate. Remyelination can occur simultaneous with demyelination and after demyelination. Myelin sheaths produced by remyelination are thinner and have a shorter internodal length than the original sheaths. Remyelination is distinguished from partial demyelination by the uniformity of remyelinated sheaths (versus the tapering found in partial demyelination) (Scolding and Franklin, 1997). Approximately 40% of acute lesions exhibit remyelination over more than 10% of the lesion area during ongoing inflammation (Prineas et al., 1993; Raine and Wu, 1993). Remyelination arises from oligodendrocytes progenitor cells that were outside of the region of demyelination and corresponds to a decrease in the number of progenitor cells in the surrounding non-demyelinated white matter (Blakemore and Keirstead, 1999).

The cerebrospinal fluid (CSF) also undergoes significant change concurrent with MS progression (Lowenthal and Raus, 1987; Osenbrück et al., 1985; Glikmann et al., 1980). These include elevation of myelin basic protein (MBP) and its autoantibodies (Cohen et al., 1978; Warren and Catz, 1999), decrease of somatostatin (Roca et al., 1999), increased Immunoglobulin G and plasma cell levels (Farlow et al.,

1987), increased matrix metalloproteinase-9 levels (Leppert et al., 1998), and possibly increased nitric oxide levels (Svenningsson et al., 1999; de Bustos et al., 1999).

Heterogeneity

MS is a very diverse, heterogeneous disease. Although the hallmark feature is the presence of multiple demyelinated lesions in the CNS, there is great diversity in lesion histology, pathology, size, number, and location from patient to patient and lesion to lesion. There is also diversity in symptoms, relapse frequency, and disability progression from patient to patient and even for an individual patient (Hickey, 1999; Trapp, et al., 1999; Miller, 1998). Since it can begin at a young age and often does not kill the patient, MS can afflict individuals with a broad range in age, which means that normal development and degradation of the CNS can change the character of the lesions and the surrounding CNS. Also, lesions which appear the same in T₂-weighted images are often heterogeneous histopathologically (Simon, 1999).

MS is an umbrella classification of pathology and clinical symptomology. Various authors identify from two to six "variants" of MS with various, often with contradictory and non-mutually exclusive definitions. Each variant has a somewhat unique, although not exclusive, presentation with some histological differences in the plaques. These include Classical or Charcot MS, Acute or Primary Progressive MS (PPMS), Relapsing-Remitting MS (RRMS), Secondary-Progressive MS (SPMS), Marburg's Disease, Neuromyelitis Optica or Devic's Disease, Balo's Concentric Sclerosis, Myelinoclastic Diffuse Sclerosis (MDS) or Schilder's disease, and Massive Reversible Demyelinating Lesions of Kepes (Hickey, 1999; Whitham and Brey, 1985; Bitsch et al., 1999; Kira et al., 1993; McDonnell and Hawkins, 1996). The Charcot variant is by far the most common with a prevalence of around 85% (McDonnell and Hawkins, 1996). The Primary Progressive variant occurs in 15-20% of cases (Weinsbenker BG, 1994). The other variants have a low prevalence or are concomitant with the major presentations. The heterogeneous presentation of MS presents a tall order for clinical and laboratory study. Imaging modalities must be able to distinguish lesions that present in all shapes, sizes, and distributions and in all different types of CNS tissue, including at boundaries between tissues and at the borders near CSF. Furthermore, it also must distinguish MS lesions from other demyelinating abnormalities such as those caused by progressive multifocal leukoencephalopathy or acute disseminated encephalomyelitis,

Therapy and the Case for Early Treatment

MS is a treatable disease. Betaseron[®], Avonex[®], Rebif[®], and Copaxone[®] are immunomodulatory treatments that have been shown to be effective in the treatment of relapse-remitting MS. Attack frequency, attack severity, accumulated disease burden (number and size of lesions showing up in MRI), and disease activity are all reduced with these treatments. Accumulation of disability was reduced in some

studies but not others. Betaseron[®] can be used to treat progressive MS (Arnason, 1999; Tselis and Lisak, 1999). All of the current MS therapies focus on preventing or delaying relapse and thereby delaying the inevitable neurological deficit accumulation. None of them can permanently stop progression. Therefore, the sooner diagnosis is made and treatment begins the longer the individual will live without deficit. Also, patients in the Copaxone[®] study who had the mildest disease seemed to do the best, which suggests early intervention is advantageous (Bourdette, et al., 1999; Rudick, 1999). Further, the Medical Advisory Board of the National Multiple Sclerosis Society recently issued a statement supporting early disease modifying therapy for relapsing multiple sclerosis (R-MS) (Cohen, et al., 1999).

Even though there is an immediate therapeutic advantage for early detection, it is not like breast cancer where early detection increases treatment efficacy by fantastic amounts. To further temper the excitement about effective treatments we must remember that all of these treatments have mild to severe side effects and none of the studies were for more than five years (Arnason, 1999; Tselis and Lisak, 1999). Early detection and treatment shows promise, but the advantage of immunomodulatory therapy for individuals with a single demyelinating event has not been determined (Cohen, et al., 1999). Furthermore, quality of life degradation caused by the cost and inconvenience of treatment might offset the advantages of early treatment.

Impact and Efficacy of MRI

Since the early 1980's the use of Magnetic Resonance Imaging (MRI) has resulted in revolutionary increases in our understanding of MS and our ability to diagnose and treat it. In MS practice MRI is used to confirm diagnosis, study progression, monitor treatment efficacy in clinical trials, and guide treatment decisions on an individual level. There are several reviews on the use and impact of MRI on MS (Miller, et al., 1998; Khoury and Weiner, 1998; Cerreta, 1998; Ormerod et al., 1987; Husted, 1994; Kent et al., 1994a; Kent et al., 1994b). The consensus is that MRI is an invaluable tool in the medical battle against MS that has contributed greatly to our understanding of the disease and serves as a powerful confirmatory diagnostic tool, but it is limited by the lack of correlation between many MRI results and clinical manifestation. Conventional (i.e., T₁ or T₂ weighted) MRI is sensitive to various histopathological characteristics of MS lesions, including demyelination, axonal destruction, gliosis, edema, inflammation, hypocellularity, and necrosis but is, for the most part, unable to distinguish between them. Techniques such as Fluid attenuated inversion-recovery (FLAIR), Magnetization Transfer Imaging (MTI), Gadolinium-diethylenetriaminepentaacetic acid (Gd-DTPA) enhancement, and spectroscopy have increased or shown promise of increasing the efficacy of MS diagnosis, monitoring, and study.

Correlation of MRI with Histopathology

The first correlation of MS plaques with MRI abnormalities was in the early 1980's (Young et al., 1981; Young et al., 1983; Stewart et al., 1984). Since then the correlations between signal intensity and histopathology have been more fully explored. The references cited on pathological correlates are hardly exhaustive or seminal and are intended as examples of the conclusions presented. For more references see the reviews cited above (Miller, et al., 1998; Khoury and Weiner, 1998; Ormerod et al., 1987; Husted, 1994). Bright spots on Proton-density or T₂ weighted images correlate to MS lesions in general and more specifically to edema or inflammation (Brück et al., 1997; Gass et al., 1998). Hypointensity in T₁ weighted images correlates to inflammation, demyelination, gliosis, and axonal loss (Khoury and Weiner, 1998; Brück et al., 1997; van Walderveen et al., 1998). Gd-DTPA enhanced T₁ weighted images show hyperintensity in regions where there is BBB compromise (Brück et al., 1997; Nesbit et al., 1991).

Diagnosis

The diagnosis of MS can be complicated due to the heterogeneity of presentation. A set of criteria proposed by Schumacher (Schumacher et al., 1965) is commonly accepted as being necessary for MS diagnosis (Miller, 1998):

- 1) Age at onset between 10 and 50 years
- 2) Objective neurological signs present on examination
- 3) Neurological symptoms and signs indicative of CNS white matter disease
- 4) Dissemination in time: two or more attacks (of at least 24 hours) separated by at least 1 month
- 5) Dissemination in space: two or more noncontiguous anatomical areas involved
- 6) No alternative clinical explanation.

The advent of paraclinical tools such as MRI, CSF testing, and evoked responses testing provide valuable diagnostic support (Bartel et al., 1983; Miller, 1998; Poser et al., 1983; Rosenblum and Saffir, 1998; Laman et al., 1998) and have led to a modification of the diagnostic criteria to accommodate paraclinical evidence (Poser et al., 1983). MRI is one of the major paraclinical tools in the diagnosis, monitoring, and study of MS.

MRI has not had as profound an impact on the overall rate of diagnosis of MS as might have been expected. Poser et al found that only 3/69 MS diagnoses would have been missed without MRI between 1986 and 1990 in South Lower Saxony, Germany (Poser et al., 1991). This is most probably because the vast majority of MRI detected MS lesions are clinically silent (Arnason, 1999) and the correlation between disease burden and clinical symptoms is weak (Miller, et al., 1998; Tselis and Lisak, 1999). So, by the time a patient is being evaluated for MS the clinical evidence is already strong for diagnosis. MRI is an important adjunctive tool for MS diagnosis, but it must be emphasized that MS diagnosis remains a

clinical chore—the paraclinical tests are not yet sensitive or specific enough to supplant the clinical evaluation and diagnosis (Miller, 1998; Poser et al., 1983; Rosenblum and Saffir, 1998).

MRI is neither sensitive nor specific enough to function as a “stand-alone” diagnostic evaluation that can provide enough evidence for a diagnosis without any other information. Some studies report diagnostic sensitivity as high as 88% with a false-positive rate of about 6% (Kent and Larson, 1988). However, others have questioned their results, saying that a more reasonable figure is that for a diagnosis of probable or definite MS the sensitivity is 58% with a false-positive rate of 9% (Mushlin, et al., 1993). In Kent et al’s review they report specificity ranges in the literature from 0.75 to 1.0 and sensitivities from 70% to 90% (Kent et al., 1994). Diagnostic accuracy is increased when lesion position and size are considered (Offenbacher et al., 1993; Namer et al., 1993). Quantitative measurements of NAWM and gray matter T_1 are not diagnostically useful because of the wide variation in values. Quantitative NAWM T_2 measurements show a slight elevation over the non-MS population (94 ms vs. 89 ms) and so might prove to be useful but this has not yet found clinical application (Rinck et al., 1987). Fluid Attenuated Inversion Recovery (FLAIR) enables much more sensitive detection of lesions in the spinal cord and brain stem (de Coene et al., 1992; Thomas et al., 1993). In elderly patients diagnosis is further complicated by the appearance of “incidental” MRI abnormalities (for example, Fazekas et al., 1993).

The main difficulty with MS diagnosis by standard MRI is that the clinical relevance of lesion load is unclear. So, even with FLAIR’s improved detection of certain types of lesions, the ability to diagnose is not necessarily improved. As a side note, the added certainty and quicker diagnosis made possible by MRI can have a positive effect on patient outlook, though not necessarily (Mushlin et al., 1994).

Monitoring and Studying MS with MR

Once diagnosis has been made MR techniques are used to track disease progression in patients and as treatment trial outcomes. This longitudinal study of disease progression also provides valuable insight into the disease’s function and nature. The advent of viable treatment options has increased the necessity of effective monitoring techniques so that changes in disease progression can be identified and addressed as quickly as possible (Bourdette et al., 1999). Clinical and paraclinical evaluations are used to make treatment decisions for individual patients and as outcomes in treatment trials. The use of MR techniques for monitoring disease evolution and as treatment trial outcomes have been amply reviewed (Rovaris and Filippi, 1999; Miller, et al., 1998; Khoury and Weiner, 1998; Husted, 1994). Clinical rating scales are tests and questions that help to codify the degree of neurological dysfunction and disease progression. There are several scales available for MS evaluation, but the most common is the Expanded

Disability Status Scale (EDSS). No one scale is adequate for all needs and all are susceptible to interobserver and intraobserver variability. Imaging measures that are objective, reliable, sensitive, responsive, and valid are needed to make evaluation more effective. MRI shows promise as a surrogate measure of disease progression or treatment efficacy but, due to the low correlation of MRI measures with clinical disease progression, has not yet been demonstrated to be completely effective (Wingerchuck et al., 1997; Noseworthy, 1994; Erickson and Noseworthy, 1997; Miller et al., 1996). MRI can be used as the primary outcome measure in a preliminary clinical trial or as an entry condition for a long-term trial, but the primary outcomes in long-term studies must be clinical (Miller et al., 1996). If, however, MRI allows more rapid evaluation of prospective therapies then its clinical effect may be greatly enhanced (Kent et al., 1994; Paty and Li, 1993).

One of the most common MR surrogate markers of disease progress is T_2 lesion load, or the percentage volume of the CNS that contains sclerotic tissue as measured by a T_2 weighted scan (for example, Filippi et al., 1995). Rovaris and Filippi report that published values for correlation coefficients between T_2 lesion load and clinical disability range from 0.2 to 0.5 (Rovaris and Filippi, 1999). Partial volume effects limit the accuracy of lesion load measurements, as do repositioning errors (Firbank et al., 1999). However, decreasing the slice thickness to combat partial volume errors does not significantly increase the correlation with disability (Rovaris et al., 1998). Furthermore, measures of disease burden are dependent on human interpretation, which introduces interobserver and intraobserver variability, although proper pulse sequence selection can reduce this error (Filippi et al., 1995; Filippi et al., 1998).

Magnetic Resonance Spectroscopy

Magnetic resonance spectroscopy (MRS) involves creating NMR spectra of the body, usually of a single volume, i.e., the whole head. The imaging counterpart, magnetic resonance spectroscopic imaging (MRSI) adds spatial localization. Potentially MRSI is the most information rich imaging modality since it provides spatial distributions of various chemicals including metabolites. MRS and MRSI can detect freely mobile molecules such as choline (Ch), creatine and phosphocreatine (Cr), N-acetylaspartate (NAA), lactate (La), mobile lipids, glutamate, and glucose among others. NAA is found exclusively in neurons and neuronal processes in the normal mature brain and is thus an indicator of axonal integrity. By measuring NAA and Cr levels, MRS and MRSI studies are able to indicate degree of axonal damage in MS plaques and in the normal appearing white matter (NAWM; Rooney et al., 1997; Fu et al., 1998; Arnold, 1999) and can potentially differentiate between MS phase (acute versus chronic) and clinical form (benign versus secondary-progressive) (Falini et al., 1998).

Despite its potential, MRSI has been slow to spread into clinical application for various reasons (Allen and Thompson, 1999; Maudsley, 1999; Arnold, 1999). It is a relatively sophisticated technique and

can be time consuming. The chemicals that are being detected are in very low concentrations, so the signal is inherently weak. This compromises spatial resolution, with the typical voxel volume on the order of 1 cm^3 and a typical procedure only registering 8 to 16 voxels. The large voxel size introduces partial volume effects and signal contamination from subcutaneous lipids and water, with lipid and water suppression techniques further reducing spatial or spectral information. To increase SNR and therefore sensitivity requires higher magnetic field strengths (i.e., greater than 1.5 T), which are not typically available for broad clinical use and are very expensive. Natural variations in metabolite concentration with age, gender, lifestyle, etc., ambiguity caused by magnetic field inhomogeneity or gradient eddy currents, and overlapping metabolite resonances all combine to make interpretation difficult and reduce the specificity.

Diffusion Weighted Imaging

Diffusion weighted imaging (DWI) measures the rate, distance, and relative direction of water molecule diffusion by analyzing phase changes in MRI images (Le Bihan, 1991) and appears to offer significant clinical and research value (Filippi, 2000; Rovaris and Filippi, 2000; Lev, 2000). Diffusion techniques are sensitive to edema, expanded extracellular space, and axonal loss (Christiansen et al., 1993; Droogan et al., 1999; Wilson et al., 2001) and can detect focal abnormalities in the NAWM that precede lesion appearance and potentially distinguish between different types of lesions (Bammer et al., 2000; Rocca et al., 2000; Castriota Scanderbeg et al., 2000) and between different clinical subtypes (Nusbaum et al., 2000). Quantitative diffusion measurements can correlate with clinical presentation, i.e., disease duration and disability, and cerebral atrophy (Wilson et al., 2001). Within an MS lesion increased diffusivity seems to correlate to axonal destruction and demyelination. However, in the NAWM, correlations between diffusivity a pathological substrate are speculative as of yet (Cercignani et al., 2000).

Magnetization Transfer Imaging

Magnetization transfer imaging (MTI) measures the degree of magnetic exchange between mobile solvent protons and immobile macromolecules (Wolff and Balaban, 1989; McGowan, 1999). First the equilibrium magnetization of the sample, M_0 , is measured. Then the equilibrium magnetization of the macromolecular proton spins is selectively reduced to zero by an off-resonance RF pulse and the saturated equilibrium magnetization, M_s , is measured. Some of the magnetization from the solvent protons will transfer to the saturated macromolecular protons, thus reducing the measured magnetization of the solvent, i.e., $M_4 < M_0$. The magnitude of this ratio M_4/M_0 is the basis for MT contrast for qualitative and quantitative measurements. It depends on the density of macromolecules in the imaging volume and thus is a measure of tissue integrity. In the quantitative measurement the magnetization transfer ratio (MTR) is given as:

$$MTR = \left(1 - \frac{M_t}{M_o} \right) 100\% \quad (42)$$

In addition to the MTR there are several other MT parameters available for study (Hein et al., 1998). MT is becoming a major clinical tool in MS study (Rovaris and Filippi, 2000; Filippi, 2000; Grossman, 1999) with applications in studying disease evolution (Filippi, 1999), clinical and neuropsychological disease progression (van Buchem et al., 1999), and clinical trial monitoring (Richert and Frank, 1999). The MTR histogram may be a better measure of lesion load (LL) than T_2 weighted imaging techniques (van Buchem, 1996; Phillips et al., 1998) because it can measure diffuse changes in NAWM (Rocca et al., 1999) and changes in MS lesions (Bagley et al., 1999) and thus provide a more complete picture of the global disease burden. $^1\text{H-MRSI}$ used with MT seems to be sensitive to structural changes caused by myelin loss and the degradation products of active demyelination and thus, when used together, can detect active demyelination (Hiehle et al., 1994). MTR is correlated to demyelination and axonal loss but edema and inflammation can affect the value (Brochet and Dousset, 1999).

Implications of MS Histopathology for QDI

Below I will summarize some of the implications of the histopathology for quadrupole dip imaging.

Demyelination: Demyelination implies a decrease in immobilized protein concentration, release of degradation products, and matrix destruction. Matrix destruction changes the compartmentalization, thus affecting hydrogen diffusion anisotropy and magnetic transfer, which might affect dip amplitude.

Protein and Lipid degradation products: Immediately following demyelination protein and lipid degradation products are present in the CNS. These protein products probably are not rotationally immobilized and will therefore not be detected by QDI. However, these degradation products could increase the macroscopic viscosity of the interstitial fluid, which could affect QDI magnitude.

Chemical Environment: After demyelination the chemical environment of the neurons changes to facilitate demyelinated conduction, i.e., sodium channels are modified. The altered chemical environment might affect QDI magnitude, although the effect is probably small.

Inflammation: Invasion by phagocytic inflammatory cells concomitant to breakdown of the BBB and demyelination could increase the physical density of the tissue, i.e., there are more cells, therefore it is denser. However, the accompanying edema will tend to offset this effect. The proteins within the

phagocytic cell membranes and cytosol will be relatively immobilized, so inflammation could potentially increase QDI dip magnitude.

Edema: Edema, or an increase in the amount of interstitial fluid, decreases the density in the region of the lesion. It therefore decreases protein concentration (maintaining protein mass but increasing volume decreases density). It should not, however, increase rotational mobility of proteins that are still firmly embedded in tissues. The edema of MS is vasogenic and therefore rich in protein serum (Brück, et al., 1997; Naruse, et al., 1986), which might provide a competing relaxation pathway to the quadrupole dip relaxation pathway and skew the QDI magnitude.

Gliosis: Gliosis, the multiplication of glial processes, increases physical density and increases concentration of glial fibrillary acid protein (GFAP). It also restores a semblance of a matrix, but it is not as structured or compartmentalized as the myelin matrix.

Hypo-cellularity and necrosis: Liquification of tissue associated with necrosis should correspond to no QDI signal. Hypo-cellularity should have a small signal from the proliferation of astrocytic processes.

Axonal Destruction: Since axons contain significant amounts of protein, axonal destruction implies significant decrease in protein concentration, decreased compartmentalization, and increased diffusion anisotropy. A counter balancing process preceding complete axonal destruction is the proliferation of axonal ovoids and the concurrent accumulation of amyloid precursor protein (APP) in the ovoids. Ovoids are found in the following densities: $1/\text{mm}^3$ for NAWM, $11,000/\text{mm}^3$ in active lesions, $>3000/\text{mm}^3$ at periphery of chronic active lesions, and $875/\text{mm}^3$ in the hypocellular core of chronic active lesions (Trapp, et al., 1999).

Remyelination: In some cases the CNS spontaneously remyelinate simultaneously with and/or after demyelination. Remyelination implies an increase in protein concentration and a partial restoration of the matrix.

In summary, there are several processes that can happen in sequence or simultaneously that might affect QDI magnitude:

- 1) Decrease in immobilized protein mass due to demyelination and axonal destruction
- 2) Increase in immobilized protein mass due to remyelination, inflammation, and gliosis
- 3) Decrease in physical density due to edema, demyelination, axonal destruction, and necrosis
- 4) Increase in physical density due to gliosis and inflammation

- 5) Decrease in compartmentalization due to demyelination, axonal destruction, and hypo-cellularity
- 6) Increase in compartmentalization due to remyelination

As described in Chapter VII, the protein concentration of normal white matter is approximately 20-27% by weight. Complete demyelination in the white matter with no gliosis, remyelination, axonal destruction or other protein concentration changing processes changes the protein concentration by 28%. So, demyelination by itself can reduce the protein concentration only to 14-19%, which is much higher than a reported value of 7.5% for an MS plaque (Rinck et al., 1988). Thus, demyelination is not necessarily the dominant process and the relative magnitude and significance of these of these processes in a QDI based image will be the subject of future research.

QDI is potentially sensitive to the concentrations of myelin, axonal, and glial proteins that are still firmly a part of their respective structures. Therefore:

- 1) Early lesions with some demyelination will be slightly hypointense.
- 2) Edema (which is vasogenic in MS) will cause a slight reduction in signal intensity.
- 3) Demyelinated lesions with little gliosis will be hypointense (but not so hypointense as hypocellular lesions).
- 4) Demyelination and gliosis might counteract each other, yielding an isointense lesion.
- 5) Progressive gliosis will appear as hyperintensity.
- 6) Gliosis might be counteracted by axonal destruction, again yielding an isointense lesion.

However, I imagine this to be unlikely as gliosis proceeds much quicker than axonal destruction.

- 7) Hypocellularity without gliosis will be severely hypointense.

Conclusion—QDI and Multiple Sclerosis

Despite its many advantages, there are limitations on the utility and practicality of MRI for MS applications. These include MRI's inability to positively distinguish MS from other demyelinating diseases, its inability to directly distinguish between histopathological features, and its expense. More recently developed techniques like MRS, MTL, and DWI offer complementary information about the histopathological substrates of the disease and increased clinical relevance over conventional techniques. QDI presents itself as perhaps a source of additional, valuable information. So, the question becomes, "What can QDI provide for the study and treatment of MS that is not available from current techniques?" We must ask this question in the context of diagnosis, study, and treatment monitoring and consider constraints of sensitivity, specificity, reproducibility, cost effectiveness, safety, applicability in an outpatient setting, and ability to function without baseline readings (Laman, 1998).

If QDI implemented with PMRI is able to detect changes in protein concentration then it should be able to detect demyelination, axonal destruction, gliosis, and remyelination. If it is sensitive to these features then it can detect MS lesions and perhaps precisely characterize lesions by differentiating demyelination, axonal destruction, and gliosis from edema. In longitudinal serial studies it might also be able to distinguish between demyelination, axonal destruction, and gliosis. The cost reduction of PMRI vs. MRI could have economic and social impact by decreasing health management costs and increasing availability of diagnostic procedures.

MTI and DWI already provide measures of tissue integrity that correlate with demyelination and axonal destruction. It is improbable that QDI will be able to distinguish demyelination from axonal destruction with a single scan, nor is it likely that QDI, with its limited dynamic range, will be more sensitive to lesion presence than conventional MRI. With the current clinical acquisition focus on higher field machines, it is unlikely that dedicated QDI scanners will find broad distribution. What QDI potentially provides that is not available currently is specificity to protein distribution. MT and DWI both register exchange between any immobilized macromolecules. It is conceivable that a longitudinal study of protein distribution could indicate developmentally significant aspects of the disease. Serial QDI studies could show the progression of protein concentration changes, independent of other disease manifestations. Also, a QDI histogram analysis, similar to MTR histogram analysis, could potentially provide an insightful measure of disease burden.

So, the most likely initial advantage for QDI implemented with PMRI is as a research tool to study disease development and progression. There might also be clinical value in a QDI measure of disease burden, i.e., total immobilized protein concentration of the brain, for prognosis evaluation and treatment efficacy. The relatively low cost of PMRI would make it feasible for research institutions to purchase dedicated machines or modify existing ones. Perhaps the strongest argument for the development of QDI for MS study is the fact that, as noted before, neither the etiology nor the complete histopathological development of MS is known. Therefore, it is unwise to ignore new techniques that might provide information, even if a precise advantage cannot be identified in the new technique.

CHAPTER IX

INITIAL DEMONSTRATION OF PMRI RELAXOMETRY

Introduction

Quadrupole Dip Imaging and Prepolarized MRI are both relatively novel and unexplored techniques. To bring them “to the hospital” we must demonstrate that the hardware techniques function as expected and characterize the sensitivity and specificity of its measurements using *in vitro* models. Then we must demonstrate potential clinical relevance using animal models and finally proceed to human testing and evaluation. In this chapter I will report on initial experiments which I have conducted at the Magnetic Resonance Systems Laboratory (MRS�) that demonstrate, at least initially, that PMRI can be used for FC relaxometry. I performed experiments to measure:

1. Linearity of magnetization increase with prepolarized pulse magnitude increase
2. Shape of magnetization decay after prepolarizing pulse
3. T_1 of CuSO_4 (aq) at 0.06 T by MRI
4. T_1 of CuSO_4 (aq) at 0.16 T by PMRI
5. T_1 of 9% BSA/gluteraldehyde gel at 0.06 T by MRI
6. T_1 of 9% BSA/gluteraldehyde gel at 0.16 T by PMRI

The objective of the first two experiments was to verify the mathematical models and assumptions that have been made about PMRI functionality. The last four experiments were to demonstrate that PMRI can in fact perform T_1 measurements at different field strengths. Pending the success of these experiments, future work will focus on developing robust quantitative T_1 measurement protocols with PMRI and the detection of quadrupole dips with PMRI.

Apparatus

PMRI Scanner

The homemade prototype PMRI scanner at the MRS� consists of a whole-body MRI magnet, electromagnet, console, pulsed electromagnet controller, and RF transmit/receiver coil. The whole-body MRI magnet is 0.06 T, 60 cm bore magnet donated by IGC/Field Effects. The electromagnet was constructed by winding #8 insulated copper wire on a PVC former and is designed for optimal power dissipation. The free bore of the electromagnet is 5 cm, resistance $R = 0.6 \Omega$, inductance $L = 28$ mH, mass $m = 27$ kg. When the field strength is 0.25 T the magnet dissipates 1.1 kW with an uncooled heating rate

of about 6°C/min. At 23 A the magnetic field strength is 0.125 T (Morgan et al., October 1999). The field strength of the electromagnet increases linearly according to the relation: $B [T] = 0.0106 V [V] - 0.0165$ (Hyokwon Nam, personal communication). The electromagnet is voltage controlled by a voltage source with 0-200 V rated control in steps of 1 V. However, I found it impossible to set the voltage source to voltages from 0–5 V. The electromagnet is controlled by a homemade switching circuit (Nam, Nandi, Morgan, 2000). The electromagnet ramps up with a time constant of ~60 ms and is quenched in ~11 ms (Nam et al., 2000). I used two transmit and receive RF coils: a solenoid and a saddle coil. The solenoid coil had seven turns and was made with 16 gauge copper wire. The axial length was 2.2 cm, diameter was 1.5 cm. The coil was tuned to a standing wave ratio (SWR) between 1.002 and 1.400. I chose the solenoid coil because of its relative ease of construction, high SNR and its ability to be in very close proximity to the sample. The coil held a glass sample vial (1.5 mm × 3.5mm) snugly. The saddle coil was made with 26 gauge copper wire wrapped thirteen times around each loop of the saddle coil, which was built around a PVC former. The coil was 15 cm long and had a diameter of 2.5 cm. It was tuned to a SWR of 2.0. The saddle coil was shielded by inserting it into a PVC former and placing strips of copper axially along the outer former. The strip architecture was chosen to reduce eddy current effects. The separation between the coil and the shield was 1 cm. PVC was chosen as the former due to its low cost. It was calculated that any attenuation from the PVC were negligible in the frequency range of interest (as were the PVC quadrupole dips). All scans were controlled by a Sisco Systems console.

Phantoms

I used Copper Sulfate doped tap water, CuSO_4 (aq), and Bovine Serum Albumin/gluteraldehyde gel as tissue phantoms.

CuSO_4

Copper Sulfate, CuSO_4 , is commonly used as a dopant to decrease the T_1 relaxation time of protons in the water. Since its T_1 dispersion is well understood and documented (Bernheim, 1959; Morgan and Nolle, 1957; Morgan and Nolle, 1959; Bloembergen, 1957), I used it as a control phantom to verify the reliability of the T_1 measurements made with the MRSL PMRI scanner. CuSO_4 has a molecular weight of 159.61 g/mole and in aqueous solution dissociates to yield Cu^{2+} ions and SO_4^- anions at a ratio of 1:1:1 ($\text{CuSO}_4: \text{Cu}^{2+}: \text{SO}_4^-$). T_1 is related to temperature exponentially (Bernheim et al. 1959) and $1/T_1$ is proportional to the cation concentration of the solution (Bernheim et al, 1959; Solomon, 1955; Zimmerman, 1954; Morgan and Nolle, 1959; Laukien and Schlüter, 1956). A 10 mM CuSO_4 (aq) solution has a susceptibility of -9.6 ppm (Mihalopolou et al, 1998; Schenck, 1996). The field dependence of the Cu^{2+} is based predominately on the dipole interaction and the tumbling time of an aquated paramagnetic ion. The graph of $\log NT_1$ versus \log frequency (where N is the molar concentration) is a sigmoid with an inflection point near 12.5 MHz (Morgan and Nolle, 1959; Kraft et al, 1987; Koenig and Brown, 1984;

Laukien and Schlüter, 1956; Hausser and Noack, 1964). I used ≈ 2 mM CuSO_4 (aq). By applying the above mentioned relationships to T_1 values in the literature reported for various field strengths, concentrations, etc., I estimate that the T_1 of my sample should be in the range of 240 – 310 ms at 0.06 T and 290 – 360 ms at 0.16 T (Bernheim et al, 1959; Morgan and Nolle, 1959; Hendrick et al., 1985; Kraft et al., 1987).

BSA/Glutaraldehyde

Albumin is the most abundant type of protein in the mammalian circulatory system and contributes 80% to colloid osmotic blood pressure and seems to be responsible for maintaining blood pH (Friedli, 1996; Carter and Ho, 1994; Figge et al., 1991). Bovine Serum Albumin (BSA), i.e., albumin from cow blood, is relatively easy to obtain and prepare, widely available, low cost, and well studied (for example, Cohn et al, 1946; Cohn et al, 1947). It is a globular protein with a molecular weight of 66,296 g/mole, including 582 amino acid residues, 776 Nitrogen atoms, and approximately 4600 protons (Dayhoff, 1976). One of BSA's interesting properties is its ability to form gels either thermally or chemically (for example, Lefebvre et al, 1998; Habeeb and Hiramoto, 1968). The chemical cross linking occurs when both aldehydes in the glutaraldehyde molecule link to amines in different BSA molecules creating a scaffold of glutaraldehyde "bridges" that holds the BSA molecules together. BSA contains 59 lysine amino acids, each of which has one amine in its side chain. This chemical cross-linking phenomenon has been exploited as a surgical glue (CryoLife, 2001; Herget et al, 2001). Chemically cross-linked gels are also used extensively as tissue models for MRI dispersion studies since dispersion profiles of many tissues are indistinguishable from gel dispersion profiles (Koenig and Brown, 1991; Koenig and Brown, 1993; Zhou and Bryant, 1994; Bryant et al., 1991). Another possible gel option is agarose gel doped with CuSO_4 , which is an extremely low-cost, stable tissue model with T_1 and T_2 quasi-independently controllable (Mitchell et al, 1986). However, Mendelson et al showed that spin relaxation coupling, i.e., magnetization transfer, in proctinated tissue is more closely modeled by a BSA gel than an agarose gel (Mendelson et al, 1991).

I used a 9% weight BSA/glutaraldehyde gel with BSA/glutaraldehyde molar ratio of ≈ 100 . The gel was prepared by adding powdered BSA (96% pure, Sigma Chemicals) to distilled water in an ice bath, stirring for two minutes, then adding 25% glutaraldehyde (aq; Fisher Scientific), centrifuging the solution for two minutes, and then allowing it to come to room temperature over several hours. From reported values I estimate that the T_1 of this gel at 0.06 T should be between 370 and 400 ms; at 0.16 T the T_1 should be between 500 and 560 ms (Koenig and Brown, 1993; Zhou and Bryant, 1994).

Procedure

I used the saddle-coil for the T_1 measurement of CuSO_4 at 0.06 T. For all other measurements I used the solenoid. I centered the sample in the RF coil and centered the coil in the electromagnet such that

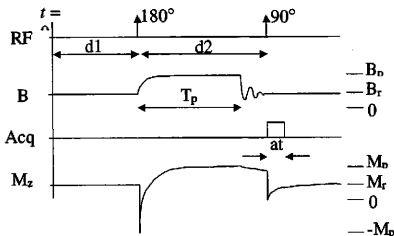


Figure 3: Two-pulse PMRI Sequence and Magnetization. Acq is the acquisition timing, M_z is the z-magnetization, B_p is the prepolarizing field strength, B_r is the readout field strength, M_p and M_r are the equilibrium magnetizations corresponding to B_p and B_r , respectively. The 180° pulse inverts the magnetization to $-M_p$, which then grows toward M_p with time constant T_p . When the prepolarizing pulse is turned off the magnetization decays toward M_r with time constant T_r until the 90° pulse moves the magnetization vector into the transverse plane to be read out.

the RF coil was also at the iso-center of the whole-body magnet. I calibrated the 90° RF pulse by applying pulses of various durations and selecting the pulse that gave the maximum signal amplitude, which was $225 \mu\text{s}$ for both coils. I assumed that the 180° pulse was twice as long, $450 \mu\text{s}$. I collected FIDs using a preprogrammed two-pulse sequence on the Sisco console as shown in Figure 3: Two-pulse PMRI Sequence and Magnetization. The pulse sequence was a magnetization recovery experiment with parameters $d1-180^\circ-d2-90^\circ$ or $d1-90^\circ-d2-90^\circ$, where $d1$ and $d2$ are delays in seconds. The electromagnet triggered off the first pulse and was on for time, T_p , which was set by a potentiometer calibrated to time. The first delay, $d1$, was set to 2.0 seconds for all measurements. By varying $d2$ and T_p I mapped out magnetization recovery or decay. To compensate for any miscalibration in the potentiometer and ringing effects I iteratively minimized $d2$ for each measurement. The acquisition spectral width was 3 kHz. There was no averaging of signals. After measuring the FIDs I transferred the data files to a PC and performed signal processing using MatLab (The MathWorks, Inc., Version 6.0). For the Fourier transform of each FID I calculated the linewidth, SNR, contrast, CNR, and peak frequency. I defined the linewidth to be the full-width half maximum (FWHM) of the peak in Hz. I calculated the other parameters as described earlier. The representative out of bandwidth noise was measured from a frequency range of thirty to fifty Hz centered approximately 150 Hz away from the peak frequency. I fit the data to models using a linear least-squares fitting routine in MatLab. For the T_1 measurements I used a three-parameter fit (Kowalewski et al, 1977; Kingsley et al, 1998; Granot, 1983). From a theoretical model, S_0 I created a parameterized

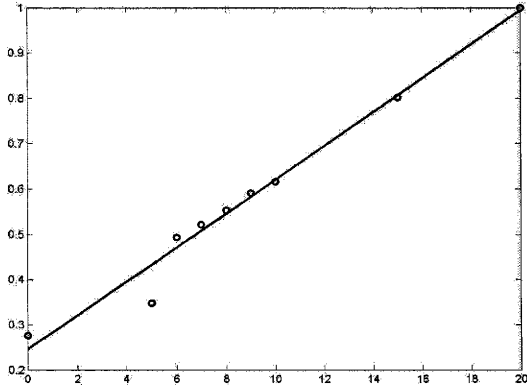


Figure 4: Magnetization versus Source Voltage in Electromagnet. The vertical axis is normalized signal intensity. The horizontal axis is voltage as read from the voltage supply. The circles are measured data points; the solid line is a linear least-squares fit. $R^2 = 0.9766$. Error bars are not shown because they are smaller than the circles.

signal model, $S_m(P, t, V)$, in terms of a parameter vector $P = [P_1, P_2, P_3]$ and with respect to time and control voltage, V . For the relaxation measurements the models were:

$$S_t = |M_z^o \cos(\theta_1) e^{-t/T_1(B_p)} + M_z^-(B_p) \cos(\theta_2) (1 - e^{-t/T_1(B_p)})| \quad (43)$$

$$S_m(P, V, t) = |P_1 e^{-t/T_2} + P_2 (1 - e^{-t/T_2})| \quad (44)$$

I then minimized the square of the difference between the model and the data, $S(d2, T_p, B_p)$, which is a function of the second delay, $d2$, the pulse time, T_p , and the pulse strength, B_p ; i.e., I minimized the function

$$\phi = |S_m - S|^2 \quad (45)$$

with respect to P . I then plotted S_m with the resultant values of P along with the measured data points. Almost all data points are presented as a normalized intensity, which I calculated for each experiment as the measured intensity of a data point divided by the maximum signal intensity in that particular experiment.

Results

The mean line width for all measurements reported here in which there was a detectable FID was 26.5 Hz with standard deviation of 6.0 Hz. After centering the center frequency of the scanner at the beginning of each day of data acquisition, the range of peak frequencies for all measurements in which there was a detectable FID was 23.5 Hz with a mean of 4.5 Hz and a standard deviation of 3.3 Hz.

Linearity of magnetization increase with prepolarized pulse magnitude increase

To verify that the switching circuitry is functioning as expected I measured the signal magnitude as a function of control voltage using the $d1-90^\circ-d2-90^\circ$ sequence with $d1=2.0$ s, $d2 = 2.1$ s, and $T_p = 2.0$ s. The results are shown below in Figure 4: Magnetization versus Source Voltage in Electromagnet. The equation of the fit line is $|S| = 0.0374V + 0.2454$, $R^2=0.9766$. The SNR also increased linearly with field strength according to $SNR = 4.195V + 31.754$, $R^2 = 0.8912$. The frequency of the center peak varied over a range of 7.5 Hz. The mean linewidth was 17.5 Hz with standard deviation of 0.5 Hz.

Shape of Magnetization Decay After Prepolarizing Pulse

To characterize the effect of ringing on signal decay I measured the signal amplitude for various $d2$ with a fixed $T_p = 1.0$ s and $d1 = 2.0$ s. The results are shown below in Figure 5: Signal Amplitude after Prepolarizing Pulse. For $d2 = 1.04$ s there was no detectable FID. The center frequency of the signal peak for each of these measurements varied over a range of 11.5 Hz with a standard deviation of 2.4 Hz. The mean FWHM line width was 25.7 Hz with standard deviation of 3.8 Hz. I applied a linear least-squares fit of the data to the equation $S = P_1 e^{-d2/R_1} + P_2 (1 - e^{-d2/R_1})$. The result is $P_1=21.07$, $P_2=0.2248$, and $P_3=0.3146$.

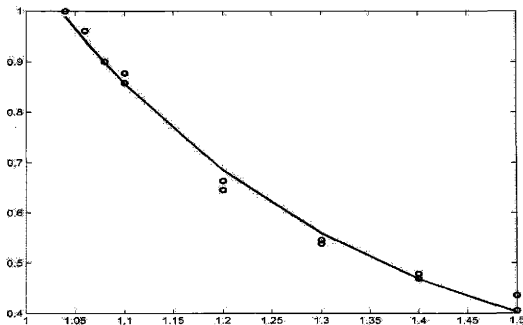


Figure 5: Signal Amplitude after Prepolarizing Pulse. Vertical scale is normalized intensity; Horizontal scale is d_2 [s] for $T_p = 1.04$ s.

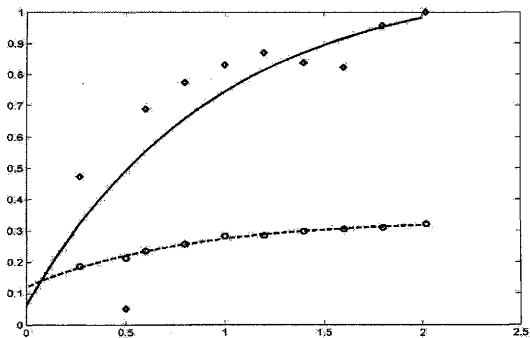


Figure 6: Inversion Recovery of CuSO_4 at 0.6 T and 0.16 T. Vertical scale is normalized signal intensity. Horizontal scale is d_2 [s]. The diamonds are the 0.16 T data points and the circles are the 0.06 T data points. The solid and dotted lines are three parameter fits with $P_1 = -0.121$, $P_2 = 0.336$, and $P_3 = 0.798$ for 0.06 T and $P_1 = -0.062$, $P_2 = 1.11$, and $P_3 = 0.946$ for 0.16 T.

T_1 of CuSO_4 (aq) and BSA/glutaraldehyde gel at 0.06 T and 0.16 T

I measured the T_1 of a ≈ 2 mM CuSO_4 (aq) solution and a 9% weight BSA/glutaraldehyde gel at 0.06 T and 0.16 T by Inversion Recovery, $d1-180^\circ-d2-90^\circ$. I varied T_p and minimized the value of $d2$ for a given T_p . For each T_p , I made the prepolarized measurement (at 0.16 T) and then disconnected the pulsing circuitry and repeated the measurement in the 0.06 T field. The timing parameters were unchanged for each pair of measurements. The results are shown in Figure 6: Inversion Recovery of CuSO_4 at 0.06 T and 0.16 T and Figure 7: Inversion Recovery of BSA at 0.06 T and 0.16 T. I fit the data to the equation,

$S_m = \left| P_1 e^{-t/T_1} + P_2 (1 - e^{-t/T_1}) \right|$. The resulting parameters for CuSO_4 were $P_1 = -0.121$, $P_2 = 0.336$, and $P_3 = 0.798$ for 0.06 T and $P_1 = -0.062$, $P_2 = 1.11$, and $P_3 = 0.946$ for 0.16 T. The resulting parameters for BSA were $P_1 = 0.0651$, $P_2 = 0.8741$, and $P_3 = 0.3751$ for 0.16 T and $P_1 = 0.1921$, $P_2 = 0.6821$, and $P_3 = 0.3080$ for the 0.06 T data.

Discussion

In all of the experiments the peak frequency was stable and the line width was reasonably narrow. The mean line width for all measurements reported here in which there was a detectable FID was 26.5 Hz

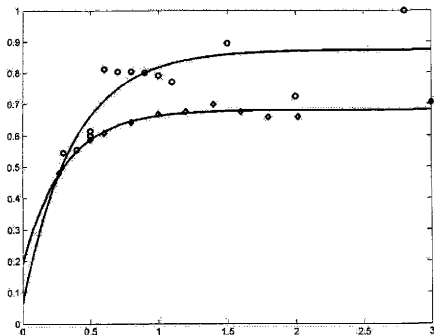


Figure 7: Inversion Recovery of BSA at 0.06 T and 0.16 T. The circles correspond to 0.16 T data points; the diamonds are for 0.06 T. Vertical axis is normalized signal amplitude; horizontal axis is $d2$ [s]. The parameters of the solid fit lines are 0.0651, 0.8741, and 0.3751 for the 0.16 T data and 0.1921, 0.6821, and 0.3080 for the 0.06 T data.

with standard deviation of 6.0 Hz. This corresponds to a line width of ≈ 11 ppm, which is too broad for techniques such as fat presaturation. However, it is sufficiently narrow to resolve the quadrupole dip effectively. After centering the center frequency of the scanner at the beginning of each day of data acquisition, the range of peak frequencies for all measurements in which there was a detectable FID was 23.5 Hz with a mean of 4.5 Hz and a standard deviation of 3.3 Hz. There is therefore no concern about frequency offset errors in QDI using PMRI since I estimated that a frequency centering error of less than 70 kHz would not cause significant error in the QD amplitude measurement.

The linearity of the signal increase and the SNR with respect to control voltage confirms that the prepolarizing mechanism functions as expected. The non-zero y-intercept is a consequence of the electromagnet being in the magnetic field of the whole-body magnet. The exponential decay of the magnetization after a prepolarizing pulse also confirms the mathematical model. Observe that the magnetization should decay with the time constant of the readout field, 0.06 T. The fit parameter time constant was 0.3146 s, which agrees reasonably well with published values for CuSO_4 at 0.06 T (240 – 310 ms; Bernheim et al, 1959; Morgan and Nolle, 1959; Hendrick et al., 1985; Kraft et al., 1987).

Because the data points for the T_1 measurements seem widely scattered and I did not collect enough data points for the three-parameter fit routine to work effectively I cannot say anything decisive or quantitative about the T_1 measurement capabilities of PMRI. The resulting parameter fit produces irreconcilable non-physical results and cannot be considered valid. However, qualitative inspection shows the procedure does indeed seem to be mapping out a T_1 recovery curve and that the curves for the different field strengths seem to have different relaxation times. Therefore, we can conclude that there is potential for PMRI as a T_1 measuring technique and therefore as a platform for QDI with the qualification that the variance in the measurements be explained and corrected.

There are four immediately apparent sources of error: tip angle miscalibration, random noise, imprecise d2 minimization, and insufficient number of data points. These four factors limit the efficacy of the fitting routine, which assumes that the magnetization is flipped to $-M_z$ and then grows through zero to M_z with time constant T_1 . Since I used a solenoid coil the RF field magnitude felt by the sample was not homogeneous across the entire sample. Therefore it is impossible to perfectly calibrate the tip angles. Each voxel relaxes from its initial condition relatively independently from the other voxels. Since the tip angle is inhomogeneous the initial condition is different from voxel to voxel. The signal amplitude, which is integral of the signal from all voxels, therefore never actually goes through zero amplitude, since there will always be some number of voxels which have not relaxed to zero or have already passed through zero on the way back to equilibrium. Random noise further complicates this fitting procedure since “zero” can

never be smaller than the noise level. Also, since the relaxation curve is relatively steep near the zero crossing if there are too few data points it will be impossible to resolve the zero crossing. Finally, I only minimized $d2$ to within 0.1 s of T_p . However, the magnetization decay experiment showed that the actual resolution of the falling edge of the pulse is less than 0.02 seconds, i.e., there is no FID for time a given T_p and $d2$ but there is a FID for a $d2$ that is 0.02 seconds longer. To quantify the possible magnitude of this error, assume that the T_1 of the sample is 300 ms and that T_p is 1.000 s. If I set $d2$ to 1.000 s I will not detect a FID. If I set $d2$ to 1.020 s I will detect a FID. However, since I am only minimizing to a resolution of 0.1 s I set $d2$ to 1.1 s, which means that the FID will decay for 0.08 s before I measure it. Therefore, the signal will decay approximately 24% of the difference between M_p and M_r . If $M_p \gg M_r$ this means a range of error of 24% . If $M_p \sim M_r$ then the error range is less but is still significant.

Conclusion

I have demonstrated experimentally that SNR and signal amplitude are linearly proportional to the control voltage of the electromagnet and that ringing in the electromagnet circuitry does not seem to be a significant concern for more than 0.02 s after the prepolarized pulse is turned off. I have also demonstrated qualitatively that PMRI is able to perform field-cycled relaxometry. Further experiments are warranted to develop a precise, quantitative PMRI procedure for T_1 FC measurements. I conclude that it is feasible to implement QDI with PMRI.

CHAPTER X

CONCLUSION

Summary

Magnetic Resonance Imaging techniques provide valuable information for the diagnosis, monitoring, and study of Multiple Sclerosis. However MRI techniques have significant specificity and sensitivity limitations. There is a need to develop low-cost methods of providing more specific information on this and other diseases. Quadrupole Dip Imaging implemented with PMRI shows promise as such a modality.

In the frequency range of 2.5 to 3.5 MHz the relaxation rate of a protein system due to non-quadrupole relaxation can be predicted with a one-parameter model. The largest ^{14}N - ^1H quadrupole dip is also in this frequency range. Its magnitude can be determined by measuring the relaxation rate at the quadrupole dip frequency and subtracting it from the non-quadrupole relaxation rate, which is extrapolated from the one-parameter model. The dip magnitude measured in this way has been shown to be proportional to rotationally immobilized protein concentration by weight. It is possible to create protein-density maps using this technique, which is called Quadrupole Dip Imaging. Prepolarized MRI is a low-cost MR technique that could conceivably be used to perform the field-cycled measurements required for QDI. However, its abilities have been characterized only initially.

I have conducted a literature review and analysis of the feasibility of developing QDI with PMRI and the motivation for doing so for application to MS study. I have also conducted initial experiments to demonstrate the feasibility of implementing the field-cycling required for QDI with PMRI.

Conclusions

My analysis indicates that there is a significant need for new MS study and imaging modalities and that QDI might potentially provide information that is not presently available and that is complementary to current techniques. This information on the protein distribution will probably be most useful for researchers studying MS development and progression. It could conceivably also have value as a disease burden monitoring modality, but this is questionable.

My analysis also indicates that there are non-trivial technical challenges for implementing QDI with PMRI. These include overcoming the inherently low signal and dynamic range of QDI

measurements, developing PMRI hardware that can switch field rapidly enough to provide reliable measurements, and developing T1 measurement protocols that are robust to the non-linearities inherent in the PMRI pulsing.

My experiments demonstrate, at least qualitatively, that PMRI can be used for field-cycled measurements, although as of yet the results are not reliable.

Future Work

The next major step is to develop robust and accurate T₁ measurement techniques for PMRI. Having accomplished that we should verify Jiao and Bryant's result of the linearity of quadrupole dip magnitude with protein concentration (Jiao and Bryant, 1996). Pending successful verification we will need to examine the sensitivity of dip magnitude to density, pH, temperature, and cholesterol content in physiological ranges.

Future work will include *in vitro* studies of protein gels and animal samples. As observed earlier, BSA gels are excellent tissue models for dispersion studies and we will continue to use them for this research. Relatively quickly in the development of these techniques we will do studies with animal models, *in vitro* or *in vivo*, to determine if the QDI can highlight any useful information.

Conclusion

It appears feasible and worthwhile to implement quadrupole dip imaging with prepolarized MRI. Further research into these techniques is warranted. The Magnetic Resonance Systems Laboratory at Texas A&M University is equipped to perform this research.

REFERENCES

- Abraham A, 1961. *The Principles of Nuclear Magnetism*. Oxford, Clarendon Press.
- Adams CWM, 1983. The general pathology of multiple sclerosis: morphological and chemical aspects of the lesions, in *Multiple Sclerosis: Pathology, Diagnosis and Management*. Ed. By Hallpike JF, Adams CWM, Tourtellotte WW. Williams and Wilkins, Baltimore. Ch. 8, p. 203-240.
- Allen PS, Thompson RB, 1999. On the localized quantification of metabolites with coupled spins. *Magnetic Resonance Materials in Physics, Biology and Medicine*. 9:159-163.
- Anderson DW, Ellenberg JG, Leventhal CM, Reingold SC, Rodriguez M, Silberberg DH, 1992. Revised estimate of the prevalence of multiple sclerosis in the United States. *Annals of Neurology*. 31(3):333-336.
- Anoardo E, Pusiol DJ, 1996. ^{14}N nuclear quadrupole dips in the proton spin-lattice relaxation dispersion in the smectic-C phase of HpAB. *Physical Review Letters*. 76(21):3983-3986.
- Antel J, 1999. Multiple sclerosis—emerging concepts of disease pathogenesis. *Journal of Neuroimmunology*. 98(1):45-48.
- Arbogast-Raviey S, Xu F, Choquet P, Brunot B, Constantinesco, 1995. Dedicated low-field MRI: a promising low cost-technique. *Medical and Biological Engineering and Computing*. 33:735-739.
- Arnason BGW, 1999. Immunologic therapy of multiple sclerosis. *Annual Review of Medicine*. 50:291-302.
- Arnold DL, 1999. Magnetic resonance spectroscopy: imaging axonal damage in MS. *Journal of Neuroimmunology*. 98(1):2-6.
- Bagley LJ, Grossman RI, Galetta SL, Sinson GP, Kotapka M, McGowan JC, 1999. Characterization of white matter lesions in multiple sclerosis and traumatic brain injury as revealed by magnetization transfer contour plots. *AJNR: American Journal of Neuroradiology*. 20(6):977-81.
- Bammer R, Augustin M, Strasser-Fuchs S, Seifert T, Kapeller P, Stollberger R, Ebner F, Hartung HP, Fazekas F, 2000. Magnetic resonance diffusion tensor imaging for characterizing diffuse and focal white matter abnormalities in multiple sclerosis. *Magnetic Resonance in Medicine*. 44(4):583-591.
- Baras P, Jutchison JMS, Lurie DJ, 1995. Development of a resistive field cycled MRI system. *Proceedings of 3rd ISMRM, 1995*, p. 692.
- Bartel DR, Markand ON, Kolar OJ, 1983. The diagnosis and classification of multiple sclerosis: Evoked responses and spinal fluid electrophoresis. *Neurology*. 33:611-617.
- Beaulieu CF, Brown III RD, Clark J, Spiller M, Koenig S, 1989. Relaxometry of lens homogenates. II. Temperature dependence and comparison with other proteins. *Magnetic Resonance in Medicine*. 10:362-372.
- Beaulieu CF, Clark JI, Brown III RD, Spiller M, Koenig SH, 1988. Relaxometry of calf lens homogenates, including cross-relaxation by crystalline NH groups. *Magnetic Resonance in Medicine*. 8:45-57.
- Béné GJ, 1980. Nuclear magnetism of liquid systems in the earth field range. *Physics Reports*. 58(4):213-267.
- Béné GJ, Denis PM, Extermann CR, 1950. Upper limit of spin-spin interaction factor. *The Physical Review*. 77:288.

- Bernheim RA, Brown TH, Gutowsky HS, Woessner DE, 1959. Temperature dependence of proton relaxation times in aqueous solutions of paramagnetic ions. *Journal of Chemical Physics*. 30(4):950-956.
- Bertsch F, Mattner J, Stehling K, Muller-Lisse U, Peller M, Loeffler R, Weber J, Meissner K, Wilmanns W, Issels R, Reiser M, 1998. Non-invasive temperature mapping using MRI: comparison of two methods based on chemical shift and T₁-relaxation. *Magnetic Resonance Imaging*. 16(4):393-403.
- Bielecki A, Murdoch JB, Weitekamp DP, Zax DB, Zilm KW, 1984. Fourier transform pure nuclear quadrupole resonance by pulsed field cycling" *Journal of Chemical Physics*. 80(5):2232-2234.
- Bitsch A, Wegener C, da Costa C, Bunkowski S, Reimers CD, Prange HW, Brück W, 1999. Lesion development in Marburg's type of acute multiple sclerosis: from inflammation to demyelination. *Multiple Sclerosis*. 5:138-146.
- Blakemore WF, Keirstead HS, 1999. The origin of remyelinating cells in the central nervous system. *Journal of Neuroimmunology*. 98(1):69-76.
- Blinic R, Mali M, Osredkar R, Prelesnik A, Seliger J, Zupančič I, 1972. *Journal of Chemical Physics*. 57:5087-5093.
- Bloch F, 1946. Nuclear Induction. *Physical Review*. 70:460-474.
- Bloembergen N, 1957. Proton relaxation times in paramagnetic solutions. *Journal of Chemical Physics*. 27(2):572-573.
- Bloembergen N, Purcell EM, Pound RV, 1948. Relaxation effects in nuclear magnetic resonance absorption. *Physical Review*. 73:679-712.
- Bloom A, Mansir D, 1954. Measurement of nuclear induction relaxation times in weak magnetic fields. *The Physical Review*. 93:941.
- Bloomfield IG, Johnston IH, Bilston LE, 1998. Effects of proteins, blood cells and glucose on the viscosity of cerebrospinal fluid. *Pediatric Neurosurgery*. 28(5):246-251.
- Borcard B, 1987. A low frequency field cycling experiment for relaxation dispersion measurements. *Helvetica Physica Acta*. 60(4):577-93.
- Bottomley PA, Foster TH, Argersinger RE, Pfeifer LM, 1984. A review of normal tissue hydrogen NMR relaxation times and relaxation mechanisms from 1-100 MHz: dependence on tissue type, NMR frequency, temperature, species, excision, and age. *Medical Physics*. 11(4):425-448.
- Bottomley PA, Hardy CJ, Argersinger RE, Allen-Moore G, 1987. A review of ¹H nuclear magnetic resonance relaxation in pathology: Are T₁ and T₂ diagnostic? *Medical Physics*. 14(1):1-37.
- Bourdette D, Antel J, McFarland H, Montgomery E Jr, 1999. Monitoring relapsing remitting MS patients. *Journal of Neuroimmunology*. 98(1):16-21.
- Bradley WG, 1996. Future cost-effective MRI will be at high field. *Journal of Magnetic Resonance Imaging*. 1:63-66.
- Bratton CB, Hopkins AL, Weinberg JW, 1965. Nuclear magnetic resonance studies of living muscle. *Science*. 147:738-739.
- Brix G, Schad LR, Deimling M, Lorenz WJ, 1990. Fast and precise T₁ imaging using a TOMROP sequence. *Magnetic Resonance Imaging*. 8:351-356.
- Brück W, Bitsch A, Kolenda H, Brück Y, Stiefel M, Lassmann H, 1997. Inflammatory central nervous system demyelination: correlation of magnetic resonance imaging findings with lesion pathology. *Annals of Neurology*. 42(5):783-793.

- Brummett RE, Talbot JM, Charuhas P, 1988. Potential hearing loss resulting from MR imaging. *Radiology*. 169:539-540.
- Bryant RG, Mendelson DA, Lester CC, 1991. The magnetic field dependence of proton spin relaxation in tissues. *Magnetic Resonance in Medicine*. 21:117-126.
- Buess ML, Garroway AN, Miller JB, 1991. NQR detection using a meanderline surface coil. *Journal of Magnetic Resonance*. 92(2): 348-62.
- Carlson JW, Crooks LE, Arakawa M, Goldhaber DM, Kramer DM, Kaufman L, 1992. Switched field magnetic resonance imaging. *SPIE Proceedings, Volume 1651, Medical Imaging VI: Instrumentation*. p. 22-27.
- Carlson JW, Goldhaber DM, Brito A, Kaufman L, 1992. MR relaxometry imaging: work in progress. *Radiology*. 184:635-639.
- Carter DC, Ho JX, 1994. Structure of serum albumin. *Advances in Protein Chemistry*. 45:153-203.
- Castriota Scanderbeg A, Tomaiuolo F, Sabatini U, Nocentini U, Grasso MG, Caltagirone C, 2000. Demyelinating plaques in relapsing-remitting and secondary-progressive multiple sclerosis: assessment with diffusion MR imaging. *AJNR American Journal of Neuroradiology*. 21(5):862-868.
- Cercignani M, Iannucci G, Rocca MA, Comi G, Horsfield MA, Filippi M, 2000. Pathologic damage in MS assessed by diffusion-weighted and magnetization transfer MRI. *Neurology*. 54(5):1139-1144.
- Cerreta E, 1998. The role of magnetic resonance imaging studies in multiple sclerosis. *Journal of Neuroscience Nursing*. 30(5):290-301.
- Charcot JM, 1868. Histologie de la sclérose en plaques. *Gazete des Hopitaux Paris 1868*. 41:554-555, 557-558, 566.
- Christiansen P, Gideon P, Thomsen C, Stubgaard M, Henriksen O, Larsson HBW, 1993. Increased water self-diffusion in chronic plaques and in apparently normal white matter in patients with multiple sclerosis. *Acta Neurologica Scandinavica*. 87:195-199.
- Cohen JA, Carter JL, Kinkel RP, Schwid SR, 1999. Therapy of relapsing multiple sclerosis. Treatment approaches for nonresponders. *Journal of Neuroimmunology*. 98(1):29-36.
- Cohen MH, Reif F, 1957. Quadrupole effects in nuclear magnetic resonance studies of solids. *Solid State Physics: Advances in Research and Applications*. Edited by Seitz F, Turnbull D. 5:321-436.
- Cohen MS, Weisskopf RM, Rzedzian RR, Kantor KL, 1989. Sensory stimulation by time-varying magnetic fields. *Magnetic Resonance in Medicine*. 14:409-414.
- Cohen SR, Brune MJ, Herndon RM, McKhann, 1978. Cerebrospinal fluid myelin basic protein and multiple sclerosis. in *Advances in Experimental Medicine and Biology*. Edited by Palo J. Plenum Press, New York. 100:513-519.
- Cohn EJ, Hughes Jr WL, Weare JH, 1947. Preparation and properties of serum and plasma proteins. XIII. Crystallization of serum albumins from ethanol-water mixtures. *Journal of the American Chemical Society*. 69:1753-1761.
- Cohn EJ, Strong LE, Hughes Jr WL, Mulfor DJ, Ashworth JN, Melin M, Taylor HL, 1947. Preparation and properties of serum and plasma proteins. IV. A system for the separation into fractions of the protein and lipoprotein components of biological tissues and fluids. *Journal of the American Chemical Society*. 68:459-475.
- Cole KS, Cole RH, 1941. Dispersion and absorption in dielectrics. I. Alternating current characteristics. *Journal of Chemical Physics*. 9:341-351.

- Conolly S, Glover G, Nishimura D, Macovski A, 1991. A reduced power selective adiabatic spin-echo pulse sequence. *Magnetic Resonance in Medicine*. 18(1):28-38.
- Conolly S, Morgan P, Scott G, Macovski A, 1994. Repolarized MRI with a periodic bias field. *Proceedings of the 2nd ISMRM*. p. 750.
- Conti S, 1986a. Proton magnetic relaxation dispersion in aqueous biopolymer systems: I. Fibrinogen solutions. *Molecular Physics*. 59(3):449-482.
- Conti S, 1986b. Proton magnetic relaxation dispersion in aqueous biopolymer systems: II. Fibrinogen gels. *Molecular Physics*. 59(3):483-505.
- Crawley AP, Henkelman RM, 1988. A comparison of one-shot and recovery methods in T₁ imaging. *Magnetic Resonance in Medicine*. 7:23-34.
- CRC Handbook of Chemistry and Physics*, 77th Edition, 1997. Edited by Lide DR. CRC Press, Boca Raton.
- Cryolife, 2001. BioGlue ®, Surgical Adhesive for vascular repair. CryoLife International, Inc. <<http://www.cryolife.com/international.htm>>. Accessed 10 March 2001.
- Czernek J, Radovan F, Sklenář V, 2000. Hydrogen bonding effects in the ¹⁵N and ¹H shielding tensors in nucleic acid base pairs. *Journal of Magnetic Resonance*. 145:142-146.
- Damadian R, 1971. Tumor detection by nuclear magnetic resonance. *Science*. 171:1151-1153.
- Das TP, Hahn EL, 1958. *Nuclear Quadrupole Resonance Spectroscopy*. New York, Academic Press. Series: *Solid State Physics, Supplement 1*.
- Daskiewicz OK, Hennel JW, Lubas B, Szczepkowski TW, 1963. Proton magnetic relaxation and protein hydration. *Nature*. 200:1006-1007.
- Daszkiewicz OK, Hennel JW, Lubas B, Szczepkowski TW, 1963. *Nature*. 200:1006-1007.
- de Alba E, Tjandra N, 2000. Protein backbone ¹⁵N relaxation rates as a tool for the diagnosis of structure quality. *Journal of Magnetic Resonance*. 144:367-371.
- de Bustos F, Navarro JA, de Andrés C, Molina JA, Jiménez-Jiménez FJ, Orti-Pareja M, Gasalla T, Tallón-Barranco A, Martínez-Salio A, Arenas J, 1999. Cerebrospinal fluid nitrate levels in patients with multiple sclerosis. *European Neurology*. 41:44-47.
- de Coene B, Hajnal JV, Gatehouse P, Longmore DB, White SJ, Oatridge A, Pennock JM, Young IR, Bydder GM, 1992. MR of the brain using fluid-attenuated inversion recovery (FLAIR) pulse sequences. *AJNR: American Journal of Neuroradiology*. 13:1555-1564.
- Dean G, 1994. How many people in the world have multiple sclerosis? *Neuroepidemiology*. 13:1-7.
- Dehmelt HG, Krüger H, 1950. Kernquadrupolfrequenzen in festem Dichloräthylen. *Naturwissenschaft*, 37(5):111-112.
- Deichmann R, Haase A, 1992. Quantification of T₁ values by SNAPSHOT-FLASH NMR imaging. *Journal of Magnetic Resonance*. 96:608-612.
- Domenicali CA, Christensen EL, 1961. Effect of transition metal solutes on the electrical resistivity of copper and gold between 4 and 1200 K. *Journal of Applied Physics*. 32:2450-2456.
- Droogan AG, Clark CA, Werring DJ, Barker GJ, McDonald WI, Miller DH, 1999. Comparison of multiple sclerosis clinical subgroups using navigated spin echo diffusion-weighted imaging. *Magnetic Resonance Imaging*. 17(5):653-661.
- Dyos GT, Farrell T, editors, 1992. *Electrical Resistivity Handbook*. Peter Peregrinus on behalf of the Institution of Electrical Engineers, London, U.K. IEE materials & devices series, vol. 10.

- Edelstein WA, Glover GH, Hardy CJ, Redington RW, 1986. The intrinsic signal-to-noise ratio in NMR imaging. *Magnetic Resonance in Medicine*. 3:604-618.
- Edelstein WA, Hutchison JMS, Johnson G, Redpath T, 1980. Spin warp NMR imaging and applications to human whole-body imaging. *Physics in Medicine and Biology*. 25:751-756.
- Edmonds DT, Summers CP, 1973. ^{14}N pure quadrupole resonance in solid amino acids. *Journal of Magnetic Resonance*. 12:134-142.
- Englund E, Brun A, Larsson EM, Györfy-Wagner Z, Person B, 1986. Tumours of the central nervous system. Proton magnetic resonance relaxation times T1 and T2 and histopathologic correlates. *Acta Radiologica Diagnostica*. 27:653-659.
- Erickson BJ, Noseworthy JH, 1997. Value of magnetic resonance imaging in assessing efficacy in clinical trials of multiple sclerosis therapies. *Mayo Clinic Proceedings*. 72:1080-1089.
- Escanyé JM, Canet D, Robert J, 1982. Frequency dependence of water proton longitudinal nuclear magnetic relaxation times in mouse tissues at 20 °C. *Biochimica et Biophysica Acta*. 721:305-311.
- Falini A, Calabrese G, Filippi M, Origgi D, Lipari S, Colombo B, Comi G, Scotti G, 1998. Benign versus secondary-progressive multiple sclerosis: the potential role of proton MR spectroscopy in defining the nature of disability. *AJNR: American Journal of Neuroradiology*. 19:223-229.
- Farlow MR, Edwards MK, Kolar OJ, Stevens JC, Yu P-I, 1987. Magnetic resonance imaging in multiple sclerosis: analysis of correlations to peripheral blood and spinal fluid abnormalities. *Neurology*. 37:1527-1530.
- Fatouros PP, Marmarou A, Kraft KA, Inao S, Schwarz FP, 1991. In vivo brain water determination by T1 measurements: effect of total water content, hydration fraction, and field strength. *Magnetic Resonance in Medicine*. 17(2):402-13.
- Fazekas F, Kleinert R, Offenbacher H, Schmidt R, Kleinert G, Payer F, Radner H, Lechner H, 1993. Pathologic correlates of incidental MRI white matter signal hyperintensities. *Neurology*. 43:1683-1689.
- Figge J, Rossing TH, Fencel V, 1991. The role of serum-proteins in acid-base equilibria. *Journal of Laboratory Clinical Medicine*. 117:453-467.
- Filippi M, 2000. The role of magnetization transfer and diffusion-weighted MRI in the understanding of multiple sclerosis evolution. *Neurological Science*. 21(4 Suppl 2):S877-S881.
- Filippi M, Campi A, Martinelli V, Rodegher M, Scotti G, Canal N, Comi G, 1995. A brain MRI study of different types of chronic-progressive multiple sclerosis. *Acta Neurologica Scandinavica*. 91:231-233.
- Filippi M, Horsfield MA, Rovaris M, Youstry T, Rocca MA, Baratti C, Bressi S, Comi G, 1998. Intraobserver and interobserver variability in schemes for estimating volume of brain lesions on MR images in multiple sclerosis. *AJNR: American Journal of Neuroradiology*. 19:239-244.
- Filippi M, Horsfield MA, Tofts PS, et al., 1995. Quantitative assessment of MRI lesion load in monitoring the evolution of multiple sclerosis. *Brain*. 118:1601-1612.
- Firbank MJ, Coulthard A, Harrison RM, Williams ED, 1999. Partial volume effects in MRI studies of multiple sclerosis. *Magnetic Resonance Imaging*. 17(4):593-601.
- Fischer HW, Rinck PA, van Haverbeke Y, Muller RN, 1990. Nuclear relaxation of human brain gray and white matter: analysis of field dependence and implications for MRI. *Magnetic Resonance in Medicine*. 16(2):317-334.
- Freeman R, Hill HDW, 1971. Fourier transform study of NMR spin-lattice relaxation by "progressive saturation." *Journal of Chemical Physics*. 54:3367-3377.

- Friede RL, 1966. *Topographic Brain Chemistry*. Academic Press, New York, 1966.
- Friedli GL, 1996. *Interaction Of Deamidated Soluble Wheat Protein (Swp) With Other Food Proteins And Metals*. Thesis, University Of Surrey. <<http://www.friedli.com/research/PhD/PhD.html?>>. Accessed 10 March 2001.
- Fu L, Matthews PM, de Stefano N, Worsley KJ, Narayanan S, Rancis GS, Antel JP, Wolfson C, Arnold DL, 1998. Imaging axonal damage of normal-appearing white matter in multiple sclerosis. *Brain*. 121:103-113.
- Gass A, Barker GJ, Kidd D, Thorpe JW, MacManus D, Brennan A, Tofts PS, Thompson AJ, McDonald WI, Miller DH, 1994. Correlation of magnetization transfer ratio with clinical disability in multiple sclerosis. *Annals of Neurology*. 36(1):62-67.
- Gass A, Filippi M, Rodegher ME, Schwartz A, Comi G, Hennerici MG, 1998. Characteristics of chronic MS lesions in the cerebrum, brainstem, spinal cord, and optic nerve on T1-weighted MRI. *Neurology*. 50(2):548-550.
- GE Medical Systems, 2001. <<http://www.gemedicalsystems.com/rad/mri/products/profile/profileo.html>>. Accessed 26 March 2001.
- Glikmann G, Svehag SE, Hansen E, Hansen O, Husby S, Nielsen H, Farrell C, 1980. Soluble immune complexes in cerebrospinal fluid of patients with multiple sclerosis and other neurological diseases. *Acta Neurologica Scandinavica*. 61(6):333-343.
- Goldsmith M, Koutcher J, Damadian R, 1977. Nuclear magnetic resonance in cancer, XII: Application of NMR malignancy index to human lung tumours. *British Journal of Cancer*. 36(2):235-42.
- Goldsmith M, Koutcher J, Damadian R, 1978. NMR in cancer. XI. Application of the NMR malignancy index to human gastro-intestinal tumors. *Cancer*. 41(1):183-91.
- Gomori JM, Grossman RI, Yu-IP C, Asakura T, 1987. NMR relaxation times of blood: dependence on field strength, oxidation state, and cell integrity. *Journal of Computer Assisted Tomography*. 11:684-690.
- Gowland PA, Leach MO, 1992. Fast and accurate measurements of T_1 using a multi-readout single inversion-recovery sequence. *Magnetic Resonance in Medicine*. 26:79-88.
- Gowland PA, Leach MO, Sharp JC, 1989. The use of an improved inversion pulse with the spin-echo/inversion-recovery sequence to give increased accuracy and reduced imaging time for T_1 measurements. *Magnetic Resonance in Medicine*. 12:261-267.
- Gowland PA, Mansfield P, 1993. Accurate measurement of T_1 in vivo in less than 3 s using echo-planar imaging. *Magnetic Resonance in Medicine*. 30:351-354.
- Grad J, Bryant RG, 1990. Nuclear magnetic cross-relaxation spectroscopy. *Journal of Magnetic Resonance*. 90:1-8.
- Grad J, Mendelson D, Hyder F, Bryant RG, 1990. Direct measurements of the longitudinal relaxation and magnetization transfer in heterogeneous systems. *Journal of Magnetic Resonance*. 86:416-419.
- Granot J, 1983. Optimization of spin-lattice relaxation-time measurements: statistical analysis by stochastic simulation of inversion-recovery experiments. *Journal of Magnetic Resonance*. 53:386-397.
- Grechishkin VS, Ya Sinyavskii N, 1997. New technologies: Nuclear quadrupole resonance as an explosive and narcotic detection technique. *Physics Uspekhi*. 40(4):393-406.
- Guiberteau T, Grucker D, 1996. EPR spectroscopy by dynamic nuclear polarization in low magnetic field. *Journal of Magnetic Resonance, Series B*. 110:47-54.

- Haase A, 1990. Snapshot FLASH MRI. Applications to T₁, T₂, and chemical-shift imaging. *Magnetic Resonance in Medicine*. 13:77-89.
- Habeeb AFSA, Hiramoto R, 1968. Reaction of proteins with glutaraldehyde. *Archives of Biochemistry and Biophysics*. 125:16-26.
- Hahn EL, 1949. An accurate nuclear magnetic resonance method for measuring spin-lattice relaxation times. *Physical Review*. 76:145-146.
- Hahn EL, 1950. Spin Echoes. *Physical Review*. 80:580-594.
- Hallenga K, Koenig SH, 1976. Protein rotational relaxation as studied by solvent ¹H and ²H magnetic relaxation. *Biochemistry*. 15:4255-4263.
- Hausser R, Noack F, 1964. Kernmagnetisch Relaxation und Korrelation in Zwei-Spin-Systemen. *Zeitschrift für Physik*. 182:93-110.
- Hazelewood CF, Nichols BL, Chamberlain NF, 1969. The physical state of water in skeletal muscle of normal and dystrophic mice of strain 129. *Muscle Diseases: Proceedings of an International Congress, Milan, 19-21 May 1969*. Editors: Walton JN, Canal N, Scarlato G. p. 279-281.
- Hein, van Waesberghe JHTM, van Buchm MA, Filippi M, Castelijn JA, Rocca MA, van der Boom R, Polman CH, Barkhof F, 1998. MR outcome parameters in multiple sclerosis: comparison of surface-based thresholding segmentation and magnetization transfer ratio histographic analysis in relation to disability (a preliminary note). *AJNR: American Journal of Neuroradiology*. 19:1857-1862.
- Hendrick RE, Newman FD, Hendee WR, 1985. MR imaging technology: maximizing the signal-to-noise ratio from a single tissue. *Radiology*. 156:749-752.
- Henkelman RM, Watts JF, Kucharczyk W, 1991. High signal intensity in MR images of calcified brain tissue. *Radiology*. 179:199-206.
- Henriksen O, de Certaines JD, Spisni A, Cortsen M, Muller RN, Ring PB, 1993. V. In vivo field dependence of proton relaxation times in human brain, liver and skeletal muscle: a multicenter study. *Magnetic Resonance Imaging*. 11:851-856.
- Herget GW, Kassa M, Nikolaus Riede U, Lu Y, Brethner L, Hasse J, 2001. Experimental use of an albumin-glutaraldehyde tissue adhesive for sealing pulmonary parenchyma and bronchial anastomoses. *European Journal of Cardio-thoracic Surgery*. 19(1):4-9.
- Hickey WF, 1999. The pathology of multiple sclerosis: a historical perspective. *Journal of Neuroimmunology*. 98(1):37-44.
- Hiehle JF, Lenkinski RE, Grossman RI, Dousset V, Ramer KN, Schnall MD, Cohen JA, Gonzalez-Scarano F, 1994. Correlation of spectroscopy and magnetization transfer imaging in the evaluation of demyelinating lesions and normal appearing white matter in multiple sclerosis. *Magnetic Resonance in Medicine*. 32:285-293.
- Hinton DP, Bryant RG, 1996. ¹H magnetic cross-relaxation between multiple solvent components and rotationally immobilized protein. *Magnetic Resonance in Medicine*. 35:497-505.
- Hoult DI, Lauterbur PC, 1979. The sensitivity of the zeugmatographic experiment involving human samples. *Journal of Magnetic Resonance*. 34:425-433.
- Hsieh Y, Koo JC, Hahn EL, 1972. Pure nuclear quadrupole resonance of naturally abundant ¹⁷O in organic solids. *Chemical Physics Letters*. 13(6):563-566.
- Hurwitz R, Lane SR, Bell RA, Brant-Zawadzki MN, 1989. Acoustic analysis of gradient-coil noise in MR imaging. *Radiology*. 173:545-548.

- Husted C, 1994. Contributions of neuroimaging to diagnosis and monitoring of multiple sclerosis. *Current Opinion in Neurology*. 7:234-241.
- Hutchison JMS, Edelstein WA, Johnson G, 1980. A whole-body NMR imaging machine. *Journal of Physics, E: Scientific Instruments*. 13:947-955.
- IFN β Multiple Sclerosis Study Group, 1993. Interferon beta-1b is effective in relapsing remitting multiple sclerosis. I. Clinical results of a multi-center, randomized, double-blind, placebo-controlled trial. UBC MS-MRI Study Group and the IFN β Multiple Sclerosis Study Group. *Neurology*. 43:655-661.
- Jiao X, Bryant RG, 1996. Noninvasive Measurement of Protein Concentration. *Magnetic Resonance in Medicine*. 35:159-161.
- Kaldoudi E, Williams SCR, 1993. Relaxation time measurements in NMR imaging. Part I: longitudinal relaxation time. *Concepts in Magnetic Resonance*. 5:217-242.
- Kaufman L, 1996. The impact of radiology's culture on the cost of magnetic resonance imaging. *Journal of Magnetic Resonance Imaging*. 6(1):67-71.
- Kay I, Henkelman RM, 1991. Practical implementation and optimization of one-shot T₁ imaging. *Magnetic Resonance in Medicine*. 22:414-424.
- Kellogg JMB, Rabi II, Zacharias JR, 1936. The gyromagnetic properties of the Hydrogens. *Physical Review*. 50:472-481.
- Kent DL, Haynor DR, Longstreth WT Jr, Larson EB, 1994. The clinical efficacy of magnetic resonance imaging in neuroimaging. *Annals of Internal Medicine*. 120(10):856-871.
- Kent DL, Larson EB, 1988. Magnetic resonance imaging of the brain and spine. *Annals of Internal Medicine*. 108:402-424.
- Kent DL, Larson EB, 1988. Magnetic resonance imaging of the brain and spine. Is clinical efficacy established after the first decade? *Annals of Internal Medicine*. 108:402-424.
- Khanna SN, Jain A, 1974. Resistivity of solid Fe, Cu, W, Nb, Ta, Mo and Pd using *t* matrix. *Journal of Physics F: Metal Physics*. 4:1982-1986.
- Khoury SJ, Weiner HL, 1998. Multiple sclerosis: what have we learned from magnetic resonance imaging studies? *Archives of Internal Medicine*. 158(6):565-573.
- Kimmich R, 1980. Field cycling in NMR relaxation spectroscopy: applications in biological, chemical, and polymer physics. *Bulletin of Magnetic Resonance*. 1(4):195-218.
- Kimmich R, Doster W, 1976. Monte Carlo study of defect fluctuations and reptations in polymer melts. *Journal of Polymer Science: Polymer Physics Edition*. 14:1671-1682.
- Kimmich R, Nusser W, Winter F, 1984. *In vivo* NMR field-cycling relaxation spectroscopy reveals ¹⁴N-¹H relaxation sinks in the backbones of proteins. *Physics in Medicine and Biology*. 29:593-596.
- Kimmich R, Winter F, 1980. ¹⁴N-¹H-groups as relaxation centers in biological systems. *Bulletin of Magnetic Resonance*. 2:349.
- Kimmich R, Winter F, 1985. Double-diffusive fluctuations and the $v^{3/4}$ -law of proton spin-lattice relaxation in biopolymers. *Progress in Colloid Polymer Science*. 71:66-70.
- Kimmich R, Winter F, Nusser W, Spohn KH, 1986. Interactions and fluctuations deduced from proton field-cycling relaxation spectroscopy of polypeptides, DNA, muscles, and algae. *Journal of Magnetic Resonance*. 68:263-282.
- Kingsley PB, Ogg RJ, Reddick WE, Steen RG, 1998. Correction of errors caused by imperfect inversion pulses in MR imaging measurement of T₁ relaxation times. *Magnetic Resonance Imaging*. 16(9):1049-55.

- Kira J, Tobimatsu S, Goto I, Hasuo K, 1993. Primary progressive versus relapsing remitting multiple sclerosis in Japanese patients: a combined clinical, magnetic resonance imaging and multimodality evoked potential study. *Journal of the Neurological Sciences*. 117:179-185.
- Klainer SM, Hirschfeld TB, Marino RA, 1982. Fourier transform nuclear quadrupole resonance spectroscopy, in *Fourier, Hadamard, and Hilbert Transforms in Chemistry*. Plenum Press, NY, p. 147-182.
- Knispel RR, Thompson RT, Pintar MM, 1974. Dispersion of proton spin-lattice relaxation in tissues. *Journal of Magnetic Resonance*. 14:44-51.
- Koenig SH, 1988. Theory of relaxation of mobile water protons induced by protein NH moieties, with application to rat heart muscle and calf lens homogenates. *Biophysical Journal*. 53:91-96.
- Koenig SH, 1995. Classes of hydration sites at protein-water interfaces: The source of contrast in magnetic resonance imaging. *Biophysical Journal*. 69:593-603.
- Koenig SH, Brown RD III, 1984. Determinants of proton relaxation rates in tissue. *Magnetic Resonance in Medicine*. 1(4):437-449.
- Koenig SH, Brown RD III, 1991. Field-cycling relaxometry of protein solutions and tissue: implications for MRI. *Progress in Nuclear Magnetic Resonance Spectroscopy*. 22:487-567.
- Koenig SH, Brown RD III, 1993. A molecular theory of relaxation and magnetization transfer: application to cross-linked BSA, a model for tissue. *Magnetic Resonance in Medicine*. 30:685-695.
- Koenig SH, Brown RD III, Adams D, Emerson D, Harrison CG, 1984. Magnetic field dependence of $1/T_1$ of protons in tissue. *Investigative Radiology*. 2:76-81.
- Koenig SH, Brown RD III, Ugolini R, 1993. A unified view of relaxation in protein solutions and tissue, including hydration and magnetization transfer. *Magnetic Resonance in Medicine*. 29(1):77-83.
- Koenig SH, Brown RD III, Ugolini R, 1993. Magnetization transfer in cross-linked bovine serum albumin solutions at 200 MHz: a model for tissue. *Magnetic Resonance in Medicine*. 29:311-316.
- Koenig SH, Bryant RG, Hallenga K, Jacob GS, 1978. Magnetic cross-relaxation among protons in protein solutions. *Biochemistry*. 17:4348-4358.
- Koenig SH, Hallenga K, Shporer M, 1975. Protein-water interaction studied by solvent ^1H , ^2H , and ^{17}O magnetic relaxation. *Proceedings of the National Academy of Science, USA*. 72:2667-2671.
- Koenig SH, Schillinger WE, 1969. Nuclear magnetic relaxation dispersion in protein solutions. *Journal of Biological Chemistry*. 244:3283-3289.
- Kormano M, Niemi P, Paajanen H, Määtänen, Katevuo K, 1988. The utility of contrast media in MRI at 0.02 T. *Investigative Radiology*. 23(S1):S289-S291.
- Korogi Y, Takahashi M, 1997. Cost containment and diffusion of MRI: oil and water? Japanese experience. *European Radiology*. 7(Suppl. 5):S256-S258.
- Koutcher JA, Goldsmith M, Damadian R, 1978. NMR in cancer. X. A malignancy index to discriminate normal and cancerous tissue. *Cancer*. 41(1):174-82.
- Kowalewski J, Levy G, Johnson LF, Palmer L, 1977. A Three-parameter non-linear procedure for fitting in version-recovery measurements of spin-lattice relaxation times. *Journal of Magnetic Resonance*. 26:533-536.
- Kraft KA, Fatouros PP, Clarke GD, Kishore PRS, 1987. An MRI phantom material for quantitative relaxometry. *Magnetic Resonance in Medicine*. 5:555-562.
- Kramer DM, Guzman RJ, Carlson JW, Crooks LE, Kaufman L, 1989. Physics of thin-section MR imaging at low field strength. *Radiology*. 173:541-544.

- Kucharczyk W, Macdonald PM, Stanisz GJ, Henkelman RM, 1994. Relaxivity and magnetization transfer of white matter lipids at MR imaging: importance of cerbrosides and pH. *Radiology*. 192:521-529.
- Laman JD, Thompson EJ, Kappos L, 1998. Body fluid markers to monitor multiple sclerosis: the assays and the challenges. *Multiple Sclerosis*. 4:266-269.
- Laukien G, Schlüter J, 1956. Impulstechnische Messungen der Spin-Gitter- und der Spin-Spin-Relaxationszeiten von Protonen in wässrigen Lösungen paramagnetischer Ionen. *Zeitschrift für Physik*. 146:113-126.
- Lauterbur PC, 1973. Image formation by induced local interactions: examples employing nuclear magnetic resonance. *Nature*. 242:190-191.
- Le Bihan D, 1991. Molecular diffusion nuclear magnetic resonance imaging. *Magnetic Resonance Quarterly*. 7(1):1-30.
- Lefebvre J, Renard D, Sanches-Gimeno AC, 1998. Structure and rheology of heat-set gels of globular proteins. I. Bovine serum albumin gels in isoelectric conditions. *Rheologica Acta*. 37:345-357.
- Lehn JM, Kintzinger JP, 1973. *Nitrogen NMR*. Edited by Witanowski M and Webb GA. Plenum Press, New York. Ch. 3, Nitrogen-14 Nuclear Quadrupole Effects. 79-161.
- Leppert D, Ford J, Stabler G, Grygar C, Lienert C, Huber S, Miller KM, Hauser SL, Kappos L, 1998. Matrix metalloproteinase-9 (gelatinase B) is selectively elevated in CSF during relapses and stable phases of multiple sclerosis. *Brain*. 121:2327-2334.
- Lester CC, Bryant RG, 1991. Water-Proton nuclear magnetic relaxation in heterogeneous systems: hydrated lysozyme results. *Magnetic Resonance in Medicine*. 22:143-153.
- Lester CC, Bryant RG, 1991. Water-proton nuclear magnetic relaxation in heterogeneous systems: hydrated lysozyme results. *Magnetic Resonance in Medicine*. 22:143-153.
- Lev MH, 2000. Diffusion-weighted MR imaging of multiple sclerosis: added clinical value or "just another pretty face?". *AJNR American Journal of Neuroradiology*. 21(5):805-808.
- Liao MY, Harbison GS, 1999. Two-dimensional nuclear magnetic resonance correlation spectroscopy at zero field. *Journal of Chemical Physics*. 111(7):3077-3082.
- LiWang AC, Bax A, 1997. Solution NMR characterization of hydrogen bonds in a protein by indirect measurement of deuterium quadrupole couplings. *Journal of Magnetic Resonance*. 127:54-64.
- Look DC, Locker DR, 1970. Time saving in measurement of NMR and EPR relaxation times. *The Review of Scientific Instruments*. 41(2):250-251.
- Lowenthal A, Raus J, eds., 1987. *Cellular and Humoral Immunological Components of Cerebrospinal Fluid in Multiple Sclerosis*. NATO ASI Series, Vol. 129. Plenum Press, New York.
- Lundbom N, Brown III RD, Koenig SH, Lansen TA, Valsamis MP, Kasoff SS, 1990. Magnetic field dependence of $1/T_1$ of human brain tumors. Correlations with histology. *Investigative Radiology*. 25:1197-1205.
- Lurie DJ, 1994. Progress toward whole-body proton-electron double-resonance imaging of free radicals. *MAGMA*. 2(3):267-271.
- Lurie DJ, 1999. Quadrupole-dips measured by whole-body field-cycling relaxometry and imaging. *Proceedings of ISMRM, 1999*, p. 653.
- Lurie DJ, Bussell DM, Bell LH, Mallard JR, 1988. Proton electron double magnetic resonance imaging of free radical solutions. *Journal of Magnetic Resonance*. 76:366-370.
- Lurie DJ, Foster MA, Partridge RS, Nicholson I, Robb FJL, 1994. EPRI and PEDRI functional imaging. In Proceedings, IEEE Colloquium on Functional Imaging, 1994. p. 5/1-5/3.

- Lurie DJ, Foster MA, Yeung D, Hutchison MS, 1998. Design, construction and use of a large-sample field-cycled PEDRI imager. *Physics in Medicine and Biology*. 43:1877-1886.
- Lurie DJ, Hutchison JMS, Bell LH, Nicholson I, Bussell DM, Mallard JR, 1989. Field-cycled proton-electron double resonance imaging of free radicals in large aqueous samples. *Journal of Magnetic Resonance*. 84:431-7.
- Lurie DJ, Nicholson I, Mallard JR, 1991. Low-field EPR measurements by field-cycled dynamic nuclear polarization. *Journal of Magnetic Resonance*. 95:405-409.
- MacKenzie R, Sims C, Owens RG, Dixon AK, 1995. Patients' perceptions of magnetic resonance imaging. *Clinical Radiology*. 50(3):137-143.
- Macovski A, 1996. Noise in MRI. *Magnetic Resonance in Medicine*. 36(3):494-7.
- Macovski A, Conolly S, 1993. Novel Approaches to low-cost MRI. *Magnetic Resonance in Medicine*. 30:221-30.
- Marg E, 1991. Magnetostimulation of vision: direct noninvasive stimulation of the retina and the visual brain. *Optometry and Vision Science*. 68:427-440.
- Marti-Bonmati L, Korman M, 1997. MR equipment acquisition strategies: low-field or high-field scanners. *European Radiology*. 7 Suppl 5:263-268.
- Martyn CN, Gale CR, 1997. The epidemiology of multiple sclerosis. *Acta Neurologica Scandinavica*. Supplement, 169:3-7.
- Matula RA, 1979. Electrical resistivity of copper, gold, palladium and silver. *Journal of Physical and Chemical Reference Data*. 8:1147-1298.
- Maudsley AA, 1999. Future prospects for in-vivo MR spectroscopy. *Magnetic Resonance Materials in Physics, Biology, and Medicine*. 9:164-166.
- McDonald WI, Miller DH, Barnes D, 1992. The pathological evolution of multiples sclerosis. *Neuropathology and Applied Neurobiology*. 18:319-334.
- McDonnell GV, Hawkins SA, 1996. Primary progressive multiple sclerosis: a distinct syndrome? *Multiple Sclerosis*. 2:137-141.
- McGowan JC, 1999. The physical basis of magnetization transfer imaging. *Neurology*. 53(5 Suppl 3):S3-7.
- McGrath JW, Silvidi AA, 1962. Quadrupolar study of barium in barium bromide dihydrate by proton magnetic resonance. *Journal of Chemical Physics*. 36:1496-1499.
- McIsaac HK, Thordarson DS, Shafran R, Rachman S, Poole G, 1998. Claustrophobia and the magnetic resonance imaging procedure. *Journal of Behavioral Medicine*. 21(3):255-268.
- McJury MJ, 1995. Acoustic noise levels generated during high field MR imaging. *Clinical Radiology*. 50:331-334.
- McMurry J, 1996. *Organic Chemistry*. 4th edition. Brooks/Cole Publishing Company, Albany, New York.
- Melendez JC, McCrank E, 1993. Anxiety-related reactions associated with magnetic resonance imaging examinations. *JAMA*. 270(6):745-747.
- Mendelson DA, Heinsbergen JF, Kennedy SD, Szczepaniak LS, Lester CC, Bryant RG, 1991. Comparison of agarose and cross-linked protein gels as magnetic resonance imaging phantoms. *Magnetic Resonance Imaging*. 9:975-978.

- Mihalopoulou E, Allein S, Luypaert R, Eisendrath H, Bezerianos A, Panayiotakis G, 1998. Comparison of computer simulated and phantom measured phase variance in the study of trabecular bone. *Magnetic Resonance Imaging*. 16(1):29-36.
- Miller A, 1998. Diagnosis of multiple sclerosis. *Seminars in Neurology*. 18(3):309-316.
- Miller DH, Albert PS, Barkhof F, Francis G, Frank JA, Hodgkinson S, Lublin FD, Paty DW, Reingold SC, Simon J, 1996. Guidelines for the use of magnetic resonance techniques in monitoring the treatment of multiple sclerosis. *Annals of Neurology*. 39:6-16.
- Miller DH, Grossman RI, Reingold SC, McFarland HF, 1998. The role of magnetic resonance techniques in understanding and managing multiple sclerosis. *Brain*. 121:3-24.
- Mitchell MD, Kundel HL, Axel L, Joseph PM, 1986. Agarose as a tissue equivalent phantom material for NMR imaging. *Magnetic Resonance Imaging*. 4:263-266.
- Morgan P, Conolly S, Scott G, Macovski A, 1996. A readout magnet for prepolarized MRI. *Magnetic Resonance in Medicine*. 36:527-536.
- Morgan P, Conolly S, Macovski A, 1996. Open access conical magnets for MRI. *Proceedings of the 4th ISMRM*. p. 1399.
- Morgan P, Conolly S, Scott G, Macovski A, 1995. A bias magnet design for prepolarized MRI. *Proceedings of the 3rd ISMRM*. p. 936.
- Morgan P, Conolly S, Scott G, Macovski A, 1996. A readout magnet for prepolarized MRI. *Proceedings of the 4th ISMRM*. p. 121.
- Morgan PN, 1999. A pulsing system for prepolarized MRI. *Proceedings of the First Joint BMES/EMBS Conference, 1999*. 2:1070.
- Morgan PN, 1999. Shielded Electromagnet Design with Restricted Volume for Prepolarized MRI, in "Proc. 7 International Society of Magnetic Resonance in Medicine", p. 474, May 1999.
- Morgan PN, Nandi S, Nam H, Spence D, 2000. Signal-to-noise ratio gain in prepolarized MRI. *Proceedings of the 8th ISMRM*. p. 338.
- Muller RN, Vander Elst L, Rinck PA, Vallet P, Maton F, Fischer H, Roch A, Van Haverbeke Y, 1988. The importance of nuclear magnetic relaxation dispersion (NMRD) profiles in MRI contrast media development. *Investigative Radiology*. 23(S1):S229-S231.
- Murphy KJ, Brunberg JA, 1997. Adult claustrophobia, anxiety and sedation in MRI. *Magnetic Resonance Imaging*. 15(1):51-54.
- Mushlin AI, Detsky AS, Phelps CE, O'Connor PW, Kido DK, Kucharczyk W, Giang DW, Mooney C, Tansey CM, Hall WJ, 1993. The accuracy of magnetic resonance imaging in patients with suspected multiple sclerosis. *JAMA*. 269(24):3146-3151.
- Mushlin AI, Mooney C, Grow V, Phelps CE, 1994. The value of diagnostic information to patients with suspected multiple sclerosis. Rochester-Toronto MRI Study Group. *Archives of Neurology*. 51(1):67-72.
- Nakamura S and Enohiya H, 1963. Detection of nuclear quadrupole resonances by means of the crossing technique. *Journal of the Physical Society of Japan*. 18(2):183-188.
- Nam H, Nandi S, Morgan PN, 2000. A Pulsed Electromagnet Controller for Prepolarized MRI. in *Proceedings of the 22nd Annual International Conference of the IEEE*. Engineering in Medicine and Biology Society, 4:2629-2631.

- Namer LJ, Yu O, Mauss Y, Dumitresco BE, Chambron J, 1993. An evaluation of the significance of areas of intense signal in the MR brain images of patients with multiple sclerosis. *Magnetic Resonance Imaging*. 11:311-317.
- Naruse S, Horikawa Y, Tanaka C, Hirakawa K, Nishikawa H, Yoshizaki K, 1986. Significance of proton relaxation time measurement in brain edema, cerebral infarction and brain tumors. *Magnetic Resonance Imaging*. 4(4):293-304.
- Nesbit GM, Forbes GS, Scheithauer BW, Okazaki L, Rodriguez M, 1991. Multiple sclerosis: histopathologic and MR and/or CT correlation in 37 cases at biopsy and three cases at autopsy. *Radiology*. 180:467-474.
- NHFML, 2001. National High Field Magnetic Laboratory, Florida State University. <<http://www.magnet.fsu.edu>>. Accessed 26 March, 2001.
- Nishimura DG, 1996. *Principles of Magnetic Resonance Imaging*. Department of Electrical Engineering, Stanford University.
- Noack F, 1986. NMR Field-cycling spectroscopy: principles and applications. *Progress in Nuclear Magnetic Resonance Spectroscopy*. 18:171-276.
- Nolle AW, Morgan LO, 1957. Frequency dependence of proton spin relaxation in aqueous solutions of paramagnetic ions. *Journal of Chemical Physics*. 26(3):642-648.
- Nolle AW, Morgan LO, 1959. Proton spin relaxation in aqueous solutions of paramagnetic ions. II. Cr^{+++} , Mn^{++} , Ni^{++} , Cu^{++} , and Gd^{+++} . *Journal of Chemical Physics*. 31(2):365-368.
- Norton WT, Autilio LA, 1966. The lipid composition of purified bovine brain myelin. *Journal of Neurochemistry*. 13:213-222.
- Noseworthy JH, 1994. Clinical Scoring Methods for Multiple Sclerosis. *Annals of Neurology*. 36:S80-S85.
- Nusbaum AO, Tang CY, Wei T, Buchsbaum MS, Atlas SW, 2000. Whole-brain diffusion MR histograms differ between MS subtypes. *Neurology*. 54(7):1421-1427.
- Offenbacher H, Fazekas F, Schmidt R, Freidl W, Flooh E, Payer F, Lechner H, 1993. Assessment of MRI criteria for a diagnosis of MS. *Neurology*. 43:662-667.
- Olek MJ, 1999. Multiple sclerosis—Part I. Overview, pathophysiology, diagnostic evaluation, and clinical parameters. *JAOA: Journal of the American Osteopathic Association*. 99(11):574-588.
- Ollivier CP. *De la Moele Epiniere et de ses Maladies*. Paris, Crevot.
- Ormerod IEC, Miller DH, McDonald WI, du Boulay EPGH, Rudge P, Kendal BE, Moseley IF, Johnson G, Tofts PS, Halliday AM, Bronstein AM, Scaravilli F, Harding AE, Barnes D, Zilkha KJ, 1987. The role of NMR imaging in the assessment of multiple sclerosis and isolated neurological lesions. *Brain*. 110:1579-1616.
- Osenbruck M, Rao ML, Quednau HD, 1985. Pattern of albumin, immunoglobulins, and glucose in cerebrospinal fluid and serum of patients with disorders of the central nervous system. *European Neurology*. 24(1):16-22.
- Packard M, Varian R, 1954. Free nuclear induction in the earth's magnetic field. *The Physical Review*. 93:941.
- Parizel PM, van Goethem JW, van den Hauwe L, de Schepper AM, 1997. Low cost MR imaging: medical and economic perspectives. *Journal of British Radiology*. 80(4):187-191.
- Passariello R, 1997. Cost containment and diffusion of MRI: oil and water? The situation in Europe. *European Radiology*. 7(Suppl. 5):S259-S262.

- Paty DW, Li DK, 1993. Interferon beta-1b is effective in relapsing remitting multiple sclerosis. II. MRI analysis of results of a multi-center, randomized, double-blind, placebo-controlled trial. UBC MS-MRI Study Group and the IFNB Multiple Sclerosis Study Group. *Neurology*. 43:662-667.
- Phillips MD, Grossman RI, Miki Y, Wei L, Kolson D, van Buchem MA, Polansky M, McGowan JC, Udupa JK, 1998. Comparison of T2 lesion volume and magnetization transfer ratio histogram analysis and of atrophy and measures of lesion burden in patients with multiple sclerosis. *AJNR American Journal of Neuroradiology*. 19:1055-1060.
- Phillips MD, Grossman RI, Miki Y, Wei L, Kolson DL, van Buchem MA, Polansky M, McGowan JC, Udupa JK, 1998. Comparison of T2 lesion volume and magnetization transfer ratio histogram analysis and of atrophy and measures of lesion burden in patients with multiple sclerosis. *AJNR: American Journal of Neuroradiology*. 19(6):1055-1060.
- Poser CM, Paty DW, Scheinberg L, et al, 1983. New diagnostic criteria for multiple sclerosis: Guidelines for research protocols. *Annals of Neurology*. 13:227-231.
- Poser S, L ur W, Bruhn H, Frahm J, Br uck Y, Felgenhauer K, 1992. Acute demyelinating disease. Classification and non-invasive diagnosis. *Acta Neurologica Scandinavica*. 86:579-585.
- Poser S, Scheidt P, Kitzke B, L ur W, Sch afer U, Nordmann B, Stichnoth FA, 1991. Impact of magnetic resonance imaging (MRI) on the epidemiology of MS. *Acta Neurologica Scandinavica*. 83:172-175.
- Purcell EM, Torrey HC, Pound RV, 1946. Resonance absorption by nuclear magnetic moments in a solid. *Physical Review*. 69:37-38.
- Purcell EM, Torrey HC, Pound RV, 1946. Resonance absorption by nuclear magnetic moments in a solid. *Physical Review*. 69:37-38.
- Puwanich P, Lurie DJ, Foster MA, 1999. Rapid imaging of free radicals *in vivo* using field cycled PEDRI. *Physics in Medicine and Biology*. 44:2867-2877.
- Pykett IL, Mansfield P, 1978. A line scan image study of a tumorous rat leg by NMR. *Physics in Medicine and Biology*. 23:961-967.
- Raine CS, Wu E, 1993. Multiple sclerosis: remyelination in acute lesions. *Journal of Neuropathology and Experimental Neurology*. 52:199-204.
- Ramsey NF, 1953. *Nuclear Moments*. John Wiley & Sons, Inc., New York.
- Reif B, Hohwy M, Jaroniec CP, Rienstra CM, Griffin RG, 2000. NH-NH vector correlation in peptides by solid-state NMR. *Journal of Magnetic Resonance*. 145:132-141.
- Rinck PA, Appel B, Moens E, 1987. Relaxationszeitmessungen der weissen und grauen Substanz bei Patienten mit multipler Sklerose [Relaxation-time measurements of the white and gray substances in multiple sclerosis patients]. *Rafo: Fortschritte auf dem Gebiete der Rontgenstrahlen und der Nuklearmedizin*. 147(6):661-663.
- Rinck PA, Fischer HW, Vander Elst L, Van Haverbeke Y, Muller RN, 1988. Field-cycling relaxometry: medical applications. *Radiology*. 168(3):843-849.
- Roca CA, Su TP, Elpern S, McFarland H, Rubinow DR, 1999. Cerebrospinal fluid somatostatin, mood, and cognition in multiple sclerosis. *Biological Psychiatry*. 46:551-556.
- Rocca MA, Cercignani M, Iannucci G, Comi G, Filippi M, 2000. Weekly diffusion-weighted imaging of normal-appearing white matter in MS. *Neurology*. 55(6):882-884.
- Rocca MA, Mastronardo G, Rodegher M, Comi G, Filippi M, 1999. Long-term changes of magnetization transfer-derived measures from patients with relapsing-remitting and secondary progressive multiple sclerosis. *AJNR: American Journal of Neuroradiology*. 20(5):821-7.

- Rooney WD, Goodkin DE, Schuff N, Meyerhoff DJ, Norman D, Weiner MW, 1997. ¹H MRSI of normal appearing white matter in multiple sclerosis. *Multiple Sclerosis*. 3:231-237.
- Rosenblum D, Saffir M, 1998. The natural history of multiple sclerosis and its diagnosis. *Physical Medicine and Rehabilitation Clinics of North America*. 9(3):537-549.
- Rovaris M, Filippi M, 1999. Magnetic resonance techniques to monitor disease evolution and treatment trial outcomes in multiple sclerosis. *Current Opinion in Neurology*. 12:337-344.
- Rovaris M, Filippi M, 2000. The value of new magnetic resonance techniques in multiple sclerosis. *Current Opinion in Neurology*. 13(3):249-254.
- Rovaris M, Rocca MA, Capra R, Prandini F, Martinelli V, Comi G, Filippi M, 1998. A comparison between the sensitivities of 3-mm and 5-mm thick serial brain MRI for detecting lesion volume changes in patients with multiple sclerosis. *Journal of Neuroimaging*. 8(3):144-147.
- Rudakov TN, Mikhaltsevich VT, Selchikhin OP, 1997. The use of multi-pulse nuclear quadrupole resonance techniques for the detection of explosives containing RDX. *Journal of Physics, D: Applied Physics*. 30:1377-1382.
- Rudick RA, et al., 1999. Cerebrospinal fluid abnormalities in a phase III trial of Avonex® (IFNβ-1a) for relapsing multiple sclerosis. *Journal of Neuroimmunology*. 93:8-14.
- Sass M, Ziessow D, 1977. Error analysis for optimized inversion recovery spin-lattice relaxation measurements. *Journal of Magnetic Resonance*. 25:263-276.
- Schenck JF, 1996. The role of magnetic susceptibility in magnetic resonance imaging: MRI magnetic compatibility of the first and second kinds. *Medical Physics*. 23:815-850.
- Schuler H, Schmidt T, 1935. *Z. Phys.* 94. 457.
- Schumacher GA, Beebe G, Kubler RF, et al, 1965. Problems of experimental trials of therapy in multiple sclerosis: Report by the panel on the evaluation of experimental trials of therapy in multiple sclerosis. *Annals of the New York Academy of Science*. 122:522-568.
- Scolding NJ, Franklin RJM, 1997. Remyelination in demyelinating disease. *Baillière's Clinical Neurology*. 6(3):525-548.
- Scott G, Conolly S, Morgan P, Macovski A, 1994. Body noise feasibility limits of PMRI. *Proceedings of 2nd ISMRM*. p. 1083.
- Semin GK, Babushkina TA, Yakobson GG, 1975. *Nuclear Quadrupole Resonance in Chemistry*. [Primenenie iadernogo kvadrupolnogo rezonansa v khimii]. Translated by A. Barouch. New York, Wiley.
- Shellock FG, 2001. *Magnetic Resonance Procedures: Health Effects and Safety*. Lewis Publishers, Inc.; See also, <<http://www.mrisafety.com/index.html>>, accessed 07 March 2001.
- Simon JH, 1999. From enhancing lesions to brain atrophy in relapsing MS. *Journal of Neuroimmunology*. 98(1):7-15.
- Singh S, Taylor CPS, Rutt BK, 1992. Application of projection presaturation to localized proton relaxometry. *Journal of Magnetic Resonance*. 98:49-61.
- Solomon I, 1955. Relaxation processes in a system of two spins. *Physical Review*. 99:559-565.
- Spiller M, Childress SM, Koenig SH, Duffy KR, Valsamis MP, Tenner MS, Kassof SS, 1997. Secretory and nonsecretory pituitary adenomas are distinguishable by 1/T₁ magnetic relaxation rates at very low magnetic fields in vitro. *Investigative Radiology*. 32(6):320-329.
- Spiller M, Kassof SS, Larsen TA, Rifkinson-Mann S, Valsamis MP, Koenig SH, Tenner MS, 1994. Variation of the magnetic relaxation rate of 1/T₁ of water protons with magnetic field strength (NMRD

- Profile) of untreated, non-calcified, human astrocytomas: correlation with histology and solids content. *Journal of Neuro-Oncology*. 21(2):113-125.
- Spiller M, Merker PC, Iatropoulos MJ, Childress SM, Williams GM, Kasoff SS, 1995. Correlation of relaxometry and histopathology: the transplantable human glioblastoma SF295 grown in athymic nude mice. *Journal of Neuro-oncology*. 25(2):113-26.
- Spouse E, Gedroyc WM, 2000. MRI of the claustrophobic patient: interventionally configured magnets. *British Journal of Radiology*. 73(866):146-151.
- Steen RG, Gronemeyer SA, Kingsley PB, Reddick WE, Langston JS, Taylor JS, 1994. Precise and accurate measurement of proton T₁ in human brain in vivo: validation and preliminary clinical application. *Journal of Magnetic Resonance Imaging*. 4:681-691.
- Stewart WA, Hall LD, Berry K, Paty DW, 1984. Correlation between NMR scan and brain slice data in multiple sclerosis. *Lancet*. 2(8399):412.
- Stokes HT, Ailion DC, 1979. Zeeman-quadrupole cross relaxation between two nuclear spin species. *Journal of Chemical Physics*. 70:3572.
- Svennerholm L, Vanier MT, 1978. Lipid and fatty acid composition of human cerebral myelin during development. *Advances in Experimental Medicine and Biology*. 100:27-41.
- Svenningsson A, Petersson A, Anderson O, Hansson GK, 1999. Nitric oxide metabolites in CSF of patients with MS are related to clinical disease course. *Neurology*. 53(8):1880-1882.
- Taylor JS, Langston JW, Reddick WE, et al., 1996. Clinical value of proton magnetic resonance spectroscopy for differentiating recurrent or residual brain tumor from delayed cerebral necrosis. *International Journal of Radiation Oncology, Biology, Physics*. 36(5):1251-1261.
- The Electronics Library, 2000. Resistance and Ohm's Law, Foundations of Electronics-Physics, Tutorials. <<http://library.thinkquest.org/10784/>>. Accessed 21 September 2000.
- Thomas DJ, Pennock JM, Hajnal JV, Your IR, Bydder GM, Steiner RE, 1993. Magnetic resonance imaging of spinal cord in multiple sclerosis by fluid-attenuated inversion recovery. *Lancet*. 341:593-594.
- Thulborn KR, Sorensen AG, Kowall NW, McKee A, Lai A, McKinstry RC, Moore J, Rosen BR, Brady TJ, 1990. The role of ferritin and hemosiderin in the MR appearance of cerebral hemorrhage: a histopathologic biochemical study in rats. *AJNR*. 11:291-297.
- Tong CY, Prato FS, 1994. A novel fast T1-mapping method. *Journal of Magnetic Resonance Imaging*. 4:701-708.
- Tortora GJ, Grabowski SR, 1996. *Principles of Anatomy and Physiology, Eighth Ed.*, Addison Wesley Longman, Inc. 1996, Menlo Park, CA. P. 332-340.
- Trapp BD, Bö L, Mörk S, Chang A, 1999. Pathogenesis of tissue injury in MS lesions. *Journal of Neuroimmunology*. 98(1):49-56.
- Tselis AC, Lisak RP, 1999. Multiple Sclerosis: Therapeutic Update. *Archives of Neurology*, 56:277-280.
- Tsuruda JS, Bradley WG, 1987. MR detection of intracranial calcification: a phantom study. *American Journal of Neuroradiology: AJNR*. 8:1049-1055.
- van Buchem MA, Udupa JK, McGowan JC, Miki Y, Heyning FH, Boncoeur-Martel M-P, Kolson DL, Polansky M, Grossman RI, 1997. Global volumetric estimation of disease burden in multiple sclerosis based on magnetization transfer imaging. *AJNR: American Journal of Neuroradiology*. 18:1287-1290.
- van Waesberghe JH, van Buchem MA, Filippi M, Castelijns JA, Rocca MA, van der Boom R, Polman CH, Barkhof F, 1998. MR outcome parameters in multiple sclerosis: comparison of surface-based

- thresholding segmentation and magnetization transfer ratio histographic analysis in relation to disability (a preliminary note). *AJNR: American Journal of Neuroradiology*. 19(10):1857-1862.
- Van Walderveen MAA, Kamphorst W, Scheltens P, van Waesberghe JHTM, Ravid R, Valk J, Polman CH, Barkhof F, 1998. Histopathologic correlate of hypointense lesions on T1-weighted spin-echo MRI in multiple sclerosis. *Neurology*. 50:1282-1288.
- Venkatesan R, Lin W, Haacke M, 1998. Accurate determination of spin-density and T_1 in the presence of RF-field inhomogeneities and flip-angle miscalibration. *Magnetic Resonance in Medicine*. 40(4):592-602.
- Voigt G, Kimmich R, 1976. Quadrupolar dip in proton relaxation dispersion of Poly(vinyl chloride). *Journal of Magnetic Resonance*. 24:149-154.
- Warren KG, Catz I, 1999. An extensive search for autoantibodies to myelin basic protein in cerebrospinal fluid of non-multiple-sclerosis patients: implications for the pathogenesis of multiple sclerosis. *European Neurology*. 42:95-104.
- Weinshenker BG, 1994. Natural history of multiple sclerosis. *Annals of Neurology*. 36:S6-S11.
- Weiss GH, Ferretti JA, 1985. The choice of optimal parameters for measurement of spin-lattice relaxation times. III. Mathematical preliminaries for nonideal pulses. *Journal of Magnetic Resonance*. 61:490-498.
- Weiss GH, Ferretti JA, 1985. The choice of optimal parameters for measurement of spin-lattice relaxation times. IV. Effects of nonideal pulses. *Journal of Magnetic Resonance*. 61:499-515.
- Westlund PO, Wennerström H, 1985. Spin-lattice relaxation of a spin- $\frac{1}{2}$ nucleus couple to a quadrupolar spin-1 nucleus. The quadrupolar dip. *Journal of Magnetic Resonance*. 63:280-286.
- Whetten-Goldstein K, Sloan F, Conover C, Viscusi K, Kulas B, Chessen H, 1996. The economic burden of multiple sclerosis. *MS Management*. 3(1):33-37.
- Whitham RH, Brey RL, 1985. Neuromyelitis optica: two new cases and review of the literature. *Journal of Clinical Neuro-ophthalmology*. 5:263-269.
- Wilson M, Morgan PS, Lin X, Turner BP, Blumhardt LD, 2001. Quantitative diffusion weighted magnetic resonance imaging, cerebral atrophy, and disability in multiple sclerosis. *Journal of Neurology, Neurosurgery, and Psychiatry*. 70(3):318-322.
- Wingerchuk DM, Noseworthy JH, Weinshenker BG, 1997. Clinical outcome measures and rating scales in multiple sclerosis trials. *Mayo Clinic Proceedings*. 72:1070-1079.
- Winter F, Kimmich R, 1982a. NMR field-cycling relaxation spectroscopy of bovine serum albumin, muscle tissue, micrococcus luteus and yeast ^{14}N - ^1H Quadrupole dipoles. *Biochimica et Biophysica Acta*, 719:292-298.
- Winter F, Kimmich R, 1982b. Spin lattice relaxation of dipole nuclei ($I = \frac{1}{2}$) coupled to quadrupole nuclei ($S = 1$). *Molecular Physics*. 45:33-49.
- Włodarczyk W, Hentschel M, Wust P, Noeske R, Hosten N, Rinneberg H, Felix R, 1999. Comparison of four magnetic resonance methods for mapping small temperature changes. *Physics in Medicine and Biology*. 44:607-624.
- Wolff SD, Balaban RS, 1989. Magnetization transfer contrast (MTC) and tissue water proton relaxation in vivo. *Magnetic Resonance in Medicine*. 10:135-144.
- Yesinowski JP, Buess ML, Garraway AN, Ziegeweid M, Pines A, 1995. Detection of ^{14}N and ^{35}Cl in cocaine base and hydrochloride using NQR, NMR, and SQUID. *Analytical Chemistry*. 67(13):2256-2263.

- Young IR, Hall AS, Pallis CA, Legg NJ, Bydder GM, Steiner RE, 1981. NMR imaging of the brain in multiple sclerosis. *Lancet*. 2:1063-1066.
- Young IR, Randell CP, Kaplan PW, Jane A, Bydder GM, Steiner RE, 1983. Nuclear magnetic resonance (NMR) imaging in white matter disease of the brain using spin echo sequences. *Journal of Computer Assisted Tomography*. 7:290-294.
- Zhou D, Bryant RG, 1994. Magnetization transfer, cross-relaxation, and chemical exchange in rotationally immobilized protein gels. *Magnetic Resonance in Medicine*. 32:725-732.

VITA

Edward Hilton Jeter

I am from Groves, Texas and am the second of eleven children born to Will and Louise Jeter. I will graduate from Texas A & M University in May 2001 with a Bachelor of Science in Electrical Engineering and plan to pursue a Masters and a Ph.D. in magnetic resonance systems engineering at Texas A&M and then get an M.D. somewhere else. My goal in this life is to have a large, happy family. In my spare time and in order to pay the bills I hope to be on the faculty of a university hospital where I will teach classes, treat patients, and conduct research.

My professional/work/research experience includes two summers as an engineering intern at the City of Groves working with Mr. Mark Sherley and George Newsome, one summer at MD Anderson Cancer Center conducting research with Dr. Lihong Wang on Ultrasound Modulated Optical Fluorescent Tomography, two years as a missionary in Brazil, and four semesters of independent study undergraduate research with Dr. Patrick Morgan at Texas A&M, including a summer in the Undergraduate Summer Research Grant Program. My undergraduate education was funded by the Minnie Stevens Piper Foundation and the Terry Foundation. My graduate education will be funded, at least the first three years, by the National Science Foundation as I am an NSF Graduate Research Fellow, class of 2001.

My hobbies include studying language and languages, literature, particularly British literature from the nineteenth century, music, and philosophy of science and religion.

My permanent address is: 5301 Garfield, Groves, TX 77619-5610.